DYNAMIC MODEL-BASED DESIGN, VALIDATION, AND CHARACTERIZATION OF A COMPACT, HIGH-INERTANCE FREE LIQUID PISTON ENGINE COMPRESSOR

By

Joel A. Willhite

Dissertation

Submitted to the Faculty of the

Graduate School of Vanderbilt University

in partial fulfilment of the requirements

for the degree of

DOCTOR OF PHILOSOPHY

in

Mechanical Engineering

December, 2010

Nashville, Tennessee

Approved:

Eric J. Barth

Michael Goldfarb

Robert Webster

Nilanjan Sarkar

George E. Cook

To my wife and parents

ACKNOWLEDGEMENTS

My deepest thanks go to Dr. Eric J. Barth, my advisor, for his guidance and mentorship during this work. His approach to the art has inspired me, both sharpening my creative instincts and strengthening my systematic scientific approach to problem solving. His direction and friendship during my time as a Ph.D. student are irreplaceable. I would also like to thank the members of my committee (Dr. Michael Goldfarb, Dr. Nilanjan Sarkar, Dr. Robert Webster, and Dr. George Cook.) Many thanks as well go to Suzanne Weiss, Myrtle Daniels, and Jean Miller for their assistance and for truly caring about the students in this department.

I want to thank my wonderful wife, Mandy, who has been encouraging and supportive always and without whom I could not have accomplished this work. I would also like to thank my parents for their example of hard work, their encouragement of my goals, and their support of my academic endeavours.

A special thanks goes to Chao Yong, who has been a great lab mate and an even better friend. My experience working in the DCES lab will always be remembered fondly because of friends like Chao, and all the other "Lab 504 guys": Jose Riofrio, Mark Hofacker, Alex Pedchenko, John Tucker, and Dave Comber.

Finally, I would like to thank the National Science Foundation (NSF) and the Center for Compact and efficient Fluid Power (CCEFP) for their financial support of this work.

TABLE OF CONTENTS

LIST OF FIGURES AND TABLES

Page

CHAPTER I

INTRODUCTION

1.0 Motivation

One of the largest obstacles impeding the advancement of untethered robotic systems with power needs in the neighborhood of 100 Watts is the inability of current power supply and actuation methods to perform human-scale mechanical work for significant durations of time [12]. The vast majority of systems are actuated by DC servo motors powered by NIMH or Li-ion batteries, due to the relative ease of servo control. With such systems, the energy density of the batteries limits the useful work of the system between re-fueling, while the bulkiness of the electromagnetic actuators limits power density. For example, the Honda P3 humanoid robot carries a 30-kg battery pack that provides only 15-25 minutes of low-power work [13].

Apart from a large leap in battery technology, other energetic domains offer opportunities to address these power density and energy density issues. One alternative to address power density is the use of linear pneumatic actuators, which possess an order of magnitude better volumetric power density and five times better mass specific power density than state of the art electric motors [14]. The use of pneumatics has recently been investigated for small scale robotics to exploit these advantages, with efforts focused on addressing two main obstacles for the realization of such systems: first, developing adequate position control for pneumatic actuators to be effective, and second, the development of on-board pneumatic power supplies that can provide useful amounts of supply air in a compact and efficient manner. Recent work by Zhu, et al [15], is an

example of work addressing the first issue, showing that the position control of pneumatic actuators can be precise enough to compete with DC servomotors in this application. The work described in this proposal is a continuation of efforts in addressing the latter obstacle.

Since storing enough compressed air for a useful duty cycle is size and weight prohibitive, effective on-board production of pressurized gas has been investigated. Goldfarb, et al [16] used catalytic decomposition of hydrogen peroxide to successfully drive pneumatic actuators directly, i.e., no storage of pneumatic potential, with measured system energy density competitive with that of batteries/motors [17].

For the goal of significantly outperforming batteries in energy storage, the use of a hydrocarbon fuel to produce a pneumatic supply is attractive due to the high specific energy density of the fuel. For example, propane has an energy density of 46,350 kJ/kg, which is more than two orders of magnitude greater than the storage potential of state-of-the-art batteries. However, the conversion process from petrochemical potential to cool compressed gas is relatively complex; conventional commercially available engines and compressors at the size scale of interest have efficiencies that are prohibitively low.

The work of Riofrio [18,19,20] addresses the need for an efficient, compact conversion of fuel to pneumatic potential by utilizing the unique dynamic characteristics of a free piston engine compressor. The term “free piston engine” is used to describe a class of positive displacement machines that lack any kinematic constraints on the piston motion. This characteristic leads to a mechanically simpler design, which is promising for small-scale applications. For example, the friction losses and extra mass associated with the slider-crank mechanism of conventional engines scale down poorly with output

power of the device, yielding poor efficiency and power density. A free piston device would have no such losses. Riofrio's Free Liquid Piston Compressor (FLPC) demonstrated the viability of such a design. This work uses the FLPC as the starting point, with the goal of addressing the limitations of Riofrio's device by developing a new engine compressor design that is a lighter weight, more efficient, more operationally robust pneumatic power source.

1.1 History of Free Piston Devices

The use of free piston engines for compressors is not a new idea. In fact, the first free piston machine designed by Pescara [1] in 1928 was used as an air compressor. Free piston engine compressors were used through the mid-twentieth century, such as the Junkers-designed compressor used in German submarines [2]. Other applications for the technology were investigated, such as gas generators for use in automobiles [3,4] and small power plants. However, the lack of adequate sensing and control technology led to the free piston engine being largely abandoned after 1960 [5]. Modern electronic controls available today have led to a second generation of free piston engine research. Most of this research, however, uses free piston engine technology for hydraulic pumps [6,7] and small-scale electrical power generators [8,9,10], not as air compressors. An extensive review of both early free-piston engine compressor and gas generator applications as well as the recent resurgence in research in free piston hydraulic pumps and linear alternators has been conducted by Mikalsen et al [11].

1.2 Organization of the Document

Chapters 2 through 4 are manuscripts accepted as conference papers that document the progression of work toward the design and dynamic modelling of the high inertance free liquid piston engine compressor (HIFLPC.) Chapters 5 and 6 are manuscripts that are to be submitted as full journal papers to the *ASME Journal of Dynamic Systems, Measurement, and Control*. In Chapter 5, *The high inertance free piston engine compressor part 1: dynamic modeling,* an inertance-based dynamic model of a liquid piston is developed and validated experimentally for a high inertance free liquid piston compressor design (HIFLPC.) A complete system dynamic model for the HIFLPC, incorporating the piston dynamics, is presented. Critical model parameters for individual components and subsystems of a proposed HIFLPC prototype are experimentally characterized, and simulation results for the proposed prototype are shown and discussed.

Chapter 6, *The high inertance free piston engine compressor part 2: design and experimental evaluation*, presents the design and operation of the HIFLPC, as well as the fabrication and evaluation of an experimental prototype of the device. Efficiency, power output, and operational characteristics of the prototype are experimentally assessed. A validation of the dynamic model developed for the HIFLPC is conducted, and model-based simulations are performed to investigate the influence on system performance of varying liquid piston dynamics.

1.3 References

[1] Pescara, R. P., (1928) “Motor Compressor Apparatus,” U.S. Patent No. 1,657,641.

[2] Nakahara, M., (2001) "Free Piston Kikai-Kouzou to Rekisi". Shinko-Techno Gihou, Vol.13, No. 25 & 26.

[3] Klotsch, P., (1959) “Ford Free-Piston Engine Development,” SAE Technical Paper Series, 590045, vol. 67, pp. 373-378.

[4] Underwood, A. F., (1957) “The GMR 4-4 ‘Hyprex’ Engine: A Concept of the Free-Piston Engine for Automotive Use,” SAE Technical Paper Series, 570032, vol. 65, pp. 377-391.

[5] Johansen, T. A.; Egeland, O.; Johannessen, E. A.; Kvamsdal, R, (2002) “Free-Piston Diesel Engine Timing and Control – Toward Electronic Cam- and Crankshaft,” IEEE Transactions on Control Systems Technology, vol. 10, no. 2, March, pp. 177 – 190.

[6] Beachley, N. H. and Fronczak, F. J., (1992) “Design of a Free-Piston Engine-Pump,” SAE Technical Paper Series, 921740, pp. 1-8.

[7] Achten, P. A., Van Den Oeven, J. P. J., Potma, J., and Vael, G. E. M. (2000) ‘Horsepower with Brains: the design of the CHIRON free piston engine,” SAE Technical Paper 012545.

[8] Aichlmayr, H. T., Kittelson, D. B., and Zachariah, M. R., (2002a) “Miniature free-piston homogenous charge compression ignition engine-compressor concept – Part I: performance estimation and design considerations unique to small dimensions,” Chemical Engineering Science, 57, pp. 4161-4171.

[9] Aichlmayr, H. T., Kittelson, D. B., and Zachariah, M. R., (2002b) “Miniature free-piston homogenous charge compression ignition engine-compressor concept – Part II: modeling HCCI combustion in small scales with detailed homogeneous gas phase chemical kinetics,” Chemical Engineering Science, 57, pp. 4173-4186.

[10] Aichlmayr, H. T., Kittelson, D. B., and Zachariah, M. R., (2003) “Micro-HCCI combustion: experimental characterization and development of a detailed chemical kinetic model with coupled piston motion,” Combustion and Flame, 135, pp. 227-248.

[11] Mikalsen, R., and Roskilly, A. P., (2007) "A Review of Free-Piston Engine History and Applications," Applied Thermal Engineering, vol. 27, pp. 2339-2352.

[12] Dunn-Rankin, D., Leal, E. M., and Walther, D. C., (2005) "Personal Power Systems". Progress in Energy and Combusion Scence, vol. 31, pp. 422–465.

[13] Hirai, K., Hirose, M., Haikawa, Y., and Takenaka, T., (1998) "The Development of Honda Humanoid Robot," Proceedings of the 1998 IEEE International Conference on Robotics & Automation (ICRA), Leuven, Belgium, pp. 1321-1326.

[14] Kuribayashi, K., (1993) "Criteria for the evaluation of new actuators as energy converters," Advanced Robotics, vol. 7, no. 4, pp. 289-37.

[15] Zhu, Y., Barth, E. J., (2008) “An energetic control methodology for exploiting the passive dynamics of pneumatically actuated hopping,”. *ASME Journal of Dynamic Systems, Measurement and Control*, vol. 130, issue 4, pp.041004-1 – 041004-11.

[16] Goldfarb, M., Barth, E. J., Gogola, M. A., and Wehrmeyer, J. A., (2003) “Design and Energetic Characterization of a Liquid-Propellant-Powered Actuator for Self-Powered Robots,” IEEE/ASME Transactions on Mechatronics, vol. 8, no. 2, pp. 254-262.

[17] Fite, K. B., and Goldfarb, M., (2006) "Design and Energetic Characterization of a Proportional-Injector Monopropellant-Powered Actuator," IEEE/ASME Transactions on Mechatronics, vol. 11, no.2, pp. 196-204.

[18] Riofrio, J.A.; Barth, E.J. (2007) “Design and analysis of a resonating free liquid-piston compressor,” ASME International Mechanical Engineering Congress and Exposition (IMECE). IMECE2007-42369, Nov. 11-15, Seattle,Wa.

[19] Riofrio, J.A.; Barth, E.J. (2008) “Design and analysis of a resonating free liquid-piston compressor,” *ASME International Mechanical Engineering Congress and Exposition (IMECE).* IMECE2007-42369, Nov. 11-15, Seattle,Wa.

[20] Riofrio, J.A. (2007) “Design, modeling, and experimental characterization of a free liquid-piston engine compressor with separated combustion chamber,” Dissertation. Vanderbilt University . Print.

CHAPTER II

MANUSCRIPT I

REDUCING PISTON MASS IN A FREE PISTON ENGINE COMPRESSOR BY EXPLOITING THE INERTANCE OF A LIQUID PISTON

Joel A. Willhite

Eric J. Barth

Department of Mechanical Engineering

Vanderbilt University

Nashville TN 37235

Accepted as a Technical Paper to the 2009 ASME Dynamic Systems and Control Conference & Bath/ASME Symposium on Fluid Power and Motion Control

2.0 Abstract

A dynamic model of a free liquid piston that exploits piston geometry to produce a high inertance was developed for use in a free piston engine compressor. It is shown that for the size scale targeted, advantageous piston dynamics can be achieved with a reduced piston mass compared to a rigid piston design. It is also shown that the viscous losses associated with the liquid piston are negligible for the application discussed. The slow dynamics achieved by the liquid piston also allow for reduced valve sizes for the compressor, creating a more energy-dense device on a systems level. Other advantages gained by this design compared to prior work are discussed, including the elimination of a separated combustion chamber, smaller (integrated) pump check valve, and the capability of more balanced operation for a single-piston compressor. A dynamic model of the proposed high inertance liquid piston is presented and simulation results are discussed.

2.1 Introduction

Energetic limitations have long plagued the development of untethered human-scale robotic systems. Typically, systems are actuated by DC servo motors powered by NIMH or Li-ion batteries. Given the low energy density of state-of-the-art rechargeable batteries, operational times of these systems in the 100W range are restrictive [1]. A second and related concern for small-scale untethered applications is the relatively low power density of electromagnetic actuators. One approach to address problems of low energy density batteries and low power density actuators is to avoid the electromechanical domain and utilize pneumatic actuation. Power supplies for pneumatic systems also need to be addressed, since portable tanks that could carry enough air for a

useful operation time would be size and weight prohibitive. Traditional air compressors are also too heavy to be used effectively as on-board air supplies for the scale of interest. Goldfarb, et al [2] have shown the viability of using catalytic decomposition of hydrogen peroxide to produce hot gas to directly drive pneumatic actuators.

Riofrio, et al [3] designed a free piston compressor specifically for a lightweight untethered air supply for actuation of traditional pneumatic cylinders and valves, using hydrocarbon fuels as an energy source. The piston, acting as an inertial load, converts the thermal energy on the combustion side of the engine into kinetic energy, which in turn compresses air into a reservoir to be used for a pneumatic actuation system.

A second device by Riofrio et al [4], a free liquid-piston compressor (FLPC), was designed using a liquid trapped between elastomeric diaphragms as a piston. The liquid piston eliminated the blow-by and friction losses of standard piston configurations [4]. This device incorporated a combustion chamber that was separated from an expansion chamber. Once the high pressure combustion gasses were vented into the expansion chamber, PV work was converted to inertial kinetic energy of the piston. The separated combustion chamber kept air/fuel injection pressure high prior to ignition for efficient combustion, and allowed for air/fuel injection that was decoupled from power and return strokes of the engine cycle. The separated combustion chamber and the high pressure injection of both air and fuel allowed for an engine devoid of intake and compression strokes.

This work continues investigation of a free liquid piston compressor power source, focusing on exploiting the geometry of the liquid piston to create a high inertance, which advantageously slows the dynamics of the system without the penalty of adding more

mass. Modeling and simulation of the high inertance free liquid piston is conducted, and implications on the performance of a free-piston engine compressor utilizing this liquid piston concept are discussed.

2.2 Liquid Piston Inertance

Consider a fluid filled pipe approximated with three regions of effective lengths L_1, L_2, and L_3, with distinct cross sectional areas and liquid masses as shown in Fig. 2-1. This configuration represents the liquid chamber between two moving seals, such as solid pistons or elastomeric diaphragms. An external force acting on either of the moving seals will cause fluid flow through the chamber.

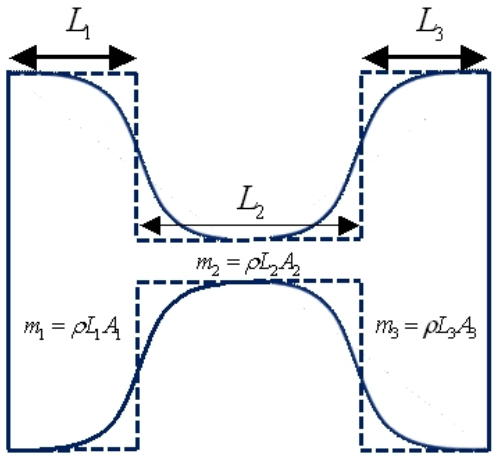

Figure 2-1: Three regions of a generic high inertance liquid piston contained by diaphragms or sliding pistons on both ends

The power flowing through the fluid filled pipe of Fig. 2-1, in response to the left and right boundaries moving, can be represented as the time derivative of the kinetic energies in each of the flow regions:

$$PQ = \frac{d}{dt}\left[\frac{1}{2}m_1\left(\frac{Q}{A_1}\right)^2 + \frac{1}{2}m_2\left(\frac{Q}{A_2}\right)^2 + \frac{1}{2}m_3\left(\frac{Q}{A_3}\right)^2\right] \tag{1}$$

where P is the pressure difference across the left and right moving boundaries, and Q is the volumetric flow rate of the piston fluid.

Substituting $m_i = \rho L_i A_i$ for the masses of liquid in each flow region, differentiating, substituting $\dot{L}_1 = -Q/A_1$, $\dot{L}_2 = 0$ and $\dot{L}_3 = Q/A_3$, and solving for pressure, we obtain Eq. 2:

$$P = \left[\frac{\rho L_1}{A_1} + \frac{\rho L_2}{A_2} + \frac{\rho L_3}{A_3}\right]\dot{Q} + \frac{\rho}{2}\left[\frac{1}{{A_3}^2} - \frac{1}{{A_1}^2}\right]Q^2 \tag{2}$$

It is interesting to note that for steady-state flow, i.e. $\dot{Q} = 0$, Eq. 2 simplifies to

$$P = \frac{\rho}{2}\left[\frac{1}{{A_3}^2} - \frac{1}{{A_1}^2}\right]Q^2 \tag{3}$$

Assuming that $A_1 >> A_3$ and solving for Q, the standard hydraulic flow equation is obtained:

$$Q = A_3\sqrt{\frac{2}{\rho}}\sqrt{\Delta P} \tag{4}$$

It follows that the relationship between pressure and flow rate of Eq. 2 consists of the steady-state term (Eq. 3) due to the area changes between regions, and the dynamic term relating P and $\dot{Q}$ through the inertance of the fluid slug. The inertance, I, of the liquid piston is therefore:

$$I = \left[\frac{\rho L_1}{A_1} + \frac{\rho L_2}{A_2} + \frac{\rho L_3}{A_3}\right] \tag{5}$$

For convenience, the steady-state term of Eq. 3 is denoted A_c:

$$A_c = \frac{\rho}{2}\left[\frac{1}{A_3^{\,2}} - \frac{1}{A_1^{\,2}}\right] \tag{6}$$

It can be seen that the second region of this configuration, termed the high inertance (HI) section, can be given a large length to area ratio L_2 / A_2 to dominate the inertance in Eq. 2. Thus, the fluid's dynamics can be made slower through piston geometry rather than by the mass of the liquid alone.

Design Implications of Slower Piston Dynamics

The FLPC described by Riofrio, et al [4], showed the viability of using a free piston compressor for use as a portable pneumatic power source for human scale robotics. The design of the FLPC does, however, have some issues that lead to either compromised performance or compromised efficiency for a compact device. The high inertance free liquid piston presented here, within the context of being incorporated into an engine-compressor (HI-FLPC) has the ability of solving three such significant issues. These issues are: 1) valve sizing, 2) complications associated with the separated combustion chamber, and 3) a balanced engine.

Valve Sizing. In a free-piston engine compressor, the check valve responsible for pump flow between the pump chamber and the reservoir has to be large enough to prevent a pressure rise in the pump chamber appreciably above the reservoir pressure (valve needs a large flow area), yet fast enough to prevent a backflow from the reservoir to the pump chamber once the pressure difference reverses at the end of the stroke (valve needs to close quickly). The speed of the piston will require a certain mass flow rate,

which can be achieved by either 1) a large flow orifice area and a small pressure difference across the valve, or 2) a small orifice area and a large pressure difference. The extreme of case 1 will cause a backflow through the valve due to the fact that a larger passive valve is slower to close. The extreme of case 2 will cause the piston to bounce against the pressure in the pump chamber before full pumping occurs. A solution that reduces the severity of this tradeoff is to reduce the required mass flow rate by slowing the overall piston motion while maintaining the same piston kinetic energy. Incorporating a liquid piston with high inertance will address this issue by achieving slower dynamics without the mass penalty of more fluid, which will allow for a smaller pump check valve, and thus a more compact and lighter weight device.

Separated Combustion Chamber. The separated combustion chamber of the FLPC [4] was necessary for holding injection pressure of the air and fuel before ignition. Flow across the combustion valve after ignition caused inefficiencies in the conversion of thermal energy to piston kinetic energy. The fixed-volume separated combustion chamber also led to scavenging problems due to the relatively large volume of spent fuel products that cannot evacuate. A piston with dynamics slow enough could allow air/fuel injection and ignition to occur before significant piston motion. This would allow a high pre-combustion pressure (equivalent to a high compression ratio in traditional 4 stroke engines) without the need for the sealed-off volume of the separated combustion chamber. The elimination of the separated combustion chamber results in a significant decrease in dead volume where spent fuel could cause scavenging problems. The lack of a separated combustion chamber also eliminates flow losses across the combustion valve.

Engine Balance. The linear configuration of the FLPC device is not self-balanced and could affect performance of an overall pneumatic system. The long, small-diameter inertance section of the HI-FLPC piston can be configured such that the combustion and compression chambers oppose each other, giving the device a more balanced operation. Coiling of the inertance tube around the compressor will also help retain a compact design, although care must be taken not to add significant pressure losses due to the configuration of the inertance section of the piston.

Dynamic Model of HI-FLPC

Whereas the previous FLPC developed dynamics for the piston using a rigid body mass-spring approach, this work will utilize Eq. 2 as the foundation of the piston model in the free-piston engine compressor. The inertial and steady-flow components can be summarized as

$$\Delta P = I\dot{Q} + A_c Q^2 \tag{7}$$

This expression will be augmented by adding viscous losses of the fluid flow, particularly in the inertance tube (region 2). Stiffness of the elastomeric diaphragms will also be included.

Viscous Losses in the Fluid. The inertance achieved by the large $\frac{L_2}{A_2}$ ratio will come at a price, namely, viscous losses of the fluid flow through the piston. This viscous loss, represented in Eq. 8 by R, relates pressure drop to volumetric flow rate:

$$\Delta P = I\dot{Q} + A_c Q^2 + RQ \tag{8}$$

A preliminary simulation of a liquid piston was conducted to investigate the magnitude of viscous losses. Equation (8) was implemented in MATLAB, with the resistance term of Eq. (9) derived from the Darcy-Weisbach equation:

$$R = \frac{8\rho}{\pi^2 d_2^{\,4}} Q \cdot f \frac{L_2}{d_2} \tag{9}$$

Where ρ is the density of the fluid (water), and L_2 and d_2 are the diameter and length of the high inertance tube, respectively. The friction factor f was taken from the Moody Chart to be 0.025, based on drawn tubing and a conservative Reynolds number calculated at the average velocity of fluid in the tube for a 40 millisecond pump stroke obtained from a dynamic simulation without losses for our scale of interest. This conservative calculation for f will help offset possible additional pressure losses associated with the oscillatory nature of the piston flow, which is not accounted for in the model. Given the chosen area ratios between region 2 to region 3 of the liquid piston, pressure losses due to the expansion of flow (Carnot-Borda losses) were estimated to be less than 5 kPa at simulated fluid velocities, and were therefore neglected.

Other physical piston parameters were chosen appropriately for the size and power range of the HI-FLPC. Most critically, the high inertance tube of the piston was modeled as 147.3 cm long (L_2) with a cross-sectional area A_2 of 1.98 cm. The initial pressure differential acting on the piston was taken to be 2.05×10^6 Pa, similar to pressures achieved from combustion in the FLPC [4]. The pressure-volume profile was similar to that used in [4]. If stiffness effects of the diaphragms are ignored, the average fluid velocity will be artificially high and therefore the viscous drag will be an upper bound.

Figure 2-2 shows results for this simulation. The total kinetic energy of the piston is seen to be more than one order of magnitude greater than the losses due to viscous effects. It is concluded that for the length and cross-sectional area used for the inertance tube in this simulation viscous losses are not significant in relation to the kinetic energy carried by the piston.

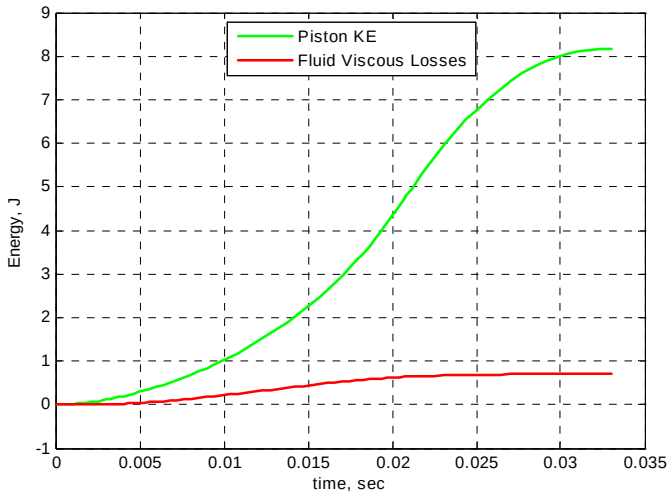

Figure 2-2. Simulation of viscous losses relative to piston kinetic energy

Diaphragm Stiffness. For the HI-FLPC design, regions 1 and 3 of the piston chamber (Fig. 1) are sealed by and mated to the combustion and pump chambers, respectively, by elastomeric diaphragms similar to those used in the FLPC, shown in Fig. 2-3. Mass of the diaphragms was neglected along with any damping effects, so that the diaphragms were modeled as stiffness only. Since the dynamic model of the piston relates pressure and volumetric flow rate, the spring stiffness derived relates pressure differential across the piston to volume displaced by the combustion chamber. Using a

diaphragm 8.55 mm thick with a 38.1 mm diameter, characterization of this stiffness was achieved experimentally, with the resultant curve:

$$\Delta P = 0.0043(V_c - V_o)^{2.344} \tag{10}$$

Adding this stiffness effect to Eq. 8 yields

$$\Delta P = I\dot{Q} + A_c Q^2 + RQ + K(V_c - V_o)^{2.344} \tag{11}$$

where $(V_c - V_o)$ is the volume sweep of the combustion chamber.

Figure 2-3. Silicone diaphragms for liquid piston

Total Dynamic Equation for the Liquid Piston. Combining the expressions for liquid inertance, viscous fluid losses, and diaphragm stiffness, and expressing the flow rate *Q* as the rate of change of combustion chamber volume, $\dot{V}_c$, the following differential equation is obtained for the piston dynamics:

$$\ddot{V}_c = \frac{1}{I}\left[\Delta P - R\dot{V}_c - A_c\dot{V}_c^{\,2} - K(V_c - V_o)^{2.344}\right] \tag{12}$$

2.3 Simulation

Computer simulation of the High-Inertance FLPC model was carried out. Control volumes for the combustion chamber and pump chamber were modeled, with the high inertance liquid piston dynamics coupling their behavior, as shown in Fig. 2-4. A control volume representing the reservoir was also incorporated. Valve dynamics and mass flows for the air/fuel intake and exhaust valves of the combustion chamber were modeled, as well as the breathe-in and pump valve for the pump chamber.

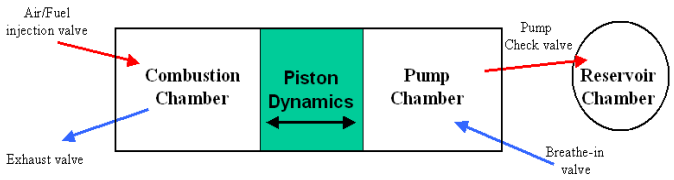

Figure 2-4. Diagram of the high-inertance FLPC

The dynamic model presented by Yong, et al, in [5] was used as a basis for the modeled components other than the piston dynamics, including combustion rate dynamics. The following represents the power balance for each j^{th} control volume (specifically, the combustion chamber, the pump chamber, and the reservoir):

$$\dot{U}_j = \dot{H}_j + \dot{Q}_j - \dot{W}_j \tag{13}$$

where $\dot{U}$ is the rate of change of internal energy, $\dot{H}$ is the net enthalpy flowing into the CV, $\dot{Q}$ is the rate of heat transfer into the CV and $\dot{W}$ is the work rate of the gas in the control volume. Each term in Eq. (13) can be expanded as follows:

$$\dot{H}_j = \sum_k \dot{m}_{j,k} \left(c_{p_{in/out}}\right)_{j,k} \left(T_{in/out}\right)_{j,k} \tag{14}$$

$$\dot{W}_j = P_j \dot{V}_j \tag{15}$$

and

$$\dot{U}_j = \dot{m}_j \left(c_v\right)_j T_j + m_j \left(c_v\right)_j \dot{T}_j = \frac{1}{\gamma_j - 1}\left(\dot{P}_j V_j + P_j \dot{V}_j\right) \tag{16}$$

where $\dot{m}$ is the k^{th} mass flow rate entering or leaving each j^{th} CV with constant-pressure specific heat $c_{p_{in/out}}$ and temperature $T_{in/out}$, P and V are the pressure and volume in the CV, c_v is the constant volume specific heat and γ is the ratio of specific heats of the gas in the CV. Equations (14-16) can be used to form the following differential equations:

$$\dot{P}_j = \frac{\left(\gamma_j - 1\right)\sum \dot{m}_j \left(c_{p_{in/out}}\right)_j \left(T_{in/out}\right)_j + \left(\gamma_j - 1\right)\dot{Q}_j - \gamma_j P_j \dot{V}_j}{V_j} \tag{17}$$

$$\dot{T}_j = \frac{\sum \dot{m}_j [\left(c_{p_{in/out}}\right)_j \left(T_{in/out}\right)_j - \left(c_v\right)_j T_j] - P_j \dot{V}_j + \dot{Q}_j}{m_j \left(c_v\right)_j} \tag{18}$$

The mass flow rates $\dot{m}_j$ for the valves are determined by the following equation [6]:

$$\begin{aligned} \dot{m}_j &= \psi_j \left(P_u, P_d\right) \\ &= \begin{cases} C_d a_j C_1 \dfrac{P_u}{\sqrt{T_u}} & \text{if} \quad \dfrac{P_d}{P_u} \le P_{cr} \\ C_d a_j C_2 \dfrac{P_u}{\sqrt{T_u}} \left(\dfrac{P_d}{P_u}\right)^{1/\gamma_u} \sqrt{1 - \left(\dfrac{P_d}{P_u}\right)^{\gamma_u - 1/\gamma_u}} & \text{if} \quad \dfrac{P_d}{P_u} > P_{cr} \end{cases} \end{aligned} \tag{19}$$

where C_d is a non-dimensional discharge coefficient of the valve, a_j is the area of the valve orifice, P_u and P_d are the upstream and downstream pressures, T_u is the upstream

temperature, γ_u is the ratio of specific heats in the upstream gas, and C_1, C_2, and P_{cr} are determined by:

$$C_1 = \sqrt{\frac{\gamma_u}{R_u}\left(\frac{2}{\gamma_u+1}\right)^{\gamma_u+1/\gamma_u-1}} \quad , \qquad C_2 = \sqrt{\frac{2\gamma_u}{R_u(\gamma_u-1)}} \quad ,$$

and

$$P_{cr} = \left(\frac{2}{\gamma_u+1}\right)^{\gamma_u/\gamma_u-1} \tag{20}$$

where R_u is the gas constant of the upstream substance.

A model of the combustion process and its influence on the pressure and temperature in the combustion chamber was taken from Yong et al [5]. All valve operation dynamics influencing each a_j were modeled as second order and tuned by experimental data from the FLPC.

Simulation Results

Two simulation models were compared to illustrate the effect of the high inertance liquid piston. The first model, representing the HI-FLPC, incorporated a high inertance piston design with an inertance tube length (L_2) of 1.473 m, and a cross-sectional area A_2 of $1.98\,cm^2$. A second simulation with no cross-sectional area change in the liquid piston was examined. All parameters excluding piston geometry and piston mass for the two models were kept the same.

Figure 2-5 shows simulation results for the pressures and volumes in the combustion, pump, and reservoir chambers for the injection, combustion, and pump phases of the HI-FLPC. Note that pumping begins at approximately 40 msec when pump chamber

pressure rises above reservoir pressure (about 25 msec after combustion). The reservoir pressure increases by approximately 20 kPa but is not visible on the scale of the figure.

Figure 2-6 shows simulation results for the simulation with no cross-sectional area change, where the piston mass was adjusted to achieve the same cycle time as the HI-FLPC. The piston mass required to achieve this similar behavior was 12.5 kg of fluid. This represents a mass 30 times that of the HI-FLPC piston mass of 0.414 kg.

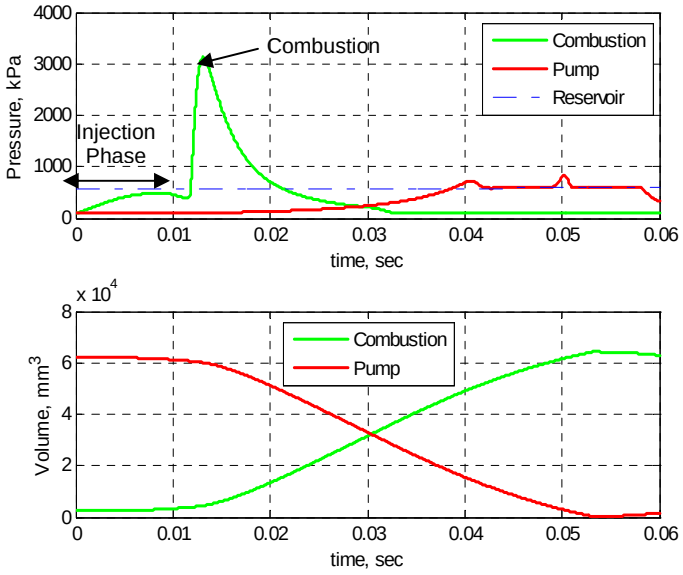

Figure 2-5. Pressures and volumes For high inertance liquid piston simulation

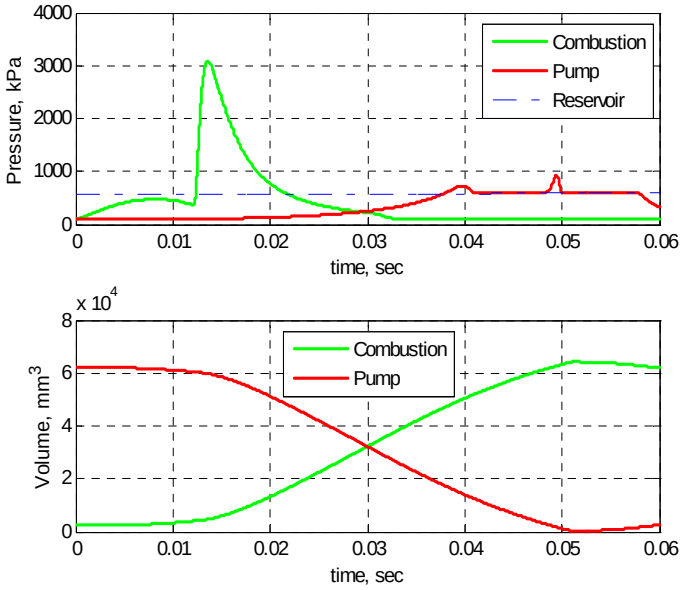

Figure 2-6. Pressures and volumes for high mass liquid piston simulation

Another point of interest in the HI-FLPC simulation is the injection phase (occurring between 0 and 11 msec in Fig. 4). Given an air/fuel valve orifice area of $1.54\,mm^2$, which is based on a valve proposed for implementation, injection pressure of air/fuel in the combustion chamber pressure is dynamically "held" by the piston long enough for good combustion, supporting the idea that the HI-FLPC does not require a separated combustion chamber.

2.4 Conclusions

A dynamic model of a high inertance free liquid piston was developed and presented. Previous work on a free-piston engine compressor revealed certain complications associated with the fast dynamics of the piston motion. Following from this motivation, the concept of inertance was exploited to slow the dynamics of the piston motion while

concomitantly reducing the mass of the piston. It was shown that a high inertance liquid piston with a mass of 0.414 kg has the equivalent dynamic response of a 12.5 kg liquid piston of uniform cross sectional area. It was also shown that the required "inertance tube" section of the high inertance liquid piston exhibits insignificant viscous losses for the geometries considered. Finally, the dynamic response of the high inertance liquid piston resolves significant issues when incorporated into a free-piston engine compressor device. These issues are: 1) valve sizing, 2) complications associated with a separated combustion chamber, and 3) a balanced engine.

2.5 References

[1] Dunn-Rankin, D., Martins, E., and Walther, D., 2005. "Personal Power Systems". *Progress in Energy and Combustion Science*, 31, August, pp. 422-465.

[2] Goldfarb, M., Barth, E. J., Gogola, M. A., and Wehrmeyer, J. A., 2003. "Design and Energetic Characterization of a Liquid-Propellant-Powered Actuator for Self-Powered Robots". *IEEE/ASME Transactions on Mechatronics*, 8(2), June, pp. 254-262.

[3] Riofrio, J. A., and Barth, E. J., 2007. "A Free Piston Compressor as a Pneumatic Mobile Robot Power Supply: Design, Characterization and Experimental Operation". *International Journal of Fluid Power*, 8(1), February, pp.17-28.

[4] Riofrio, J. A., and Barth, E. J., 2007. "Design and Analysis of a resonating Free Liquid-Piston Engine Compressor". *2007 ASME International Mechanical Engineering Congress and Exposition (IMECE)*, IMECE2007-42369, November 11-15, Seattle WA, USA.

[5] C. Yong, J. A. Riofrio and E. J. Barth. "Modeling and Control of a Free-Liquid-Piston Engine Compressor," *Bath/ASME Symposium on Fluid Power and Motion Control (FPMC 2008)*, pp. 245-257, September 10-12, 2008. Bath, U K.

[6] Richer, E., and Hurmuzlu, Y., 2000. "A High Performance Pneumatic Force Actuator System: Part 1 – Nonlinear Mathematical Model". *ASME Journal of Dynamic Systems, Measurement and Control*, 122, September, pp. 416-425.

CHAPTER III

MANUSCRIPT II

EXPERIMENTAL CHARACTERIZATION OF CRITICAL DYNAMIC MODEL PARAMETERS FOR A FREE LIQUID PISTON ENGINE COMPRESSOR

Joel A. Willhite

Eric J. Barth

Department of Mechanical Engineering

Vanderbilt University

Nashville TN 37235

Accepted as a Technical Paper to the 6th FPNI PhD Symposium,
June 15-19 2010, At Purdue University, USA

3.0 Abstract

The use of a free liquid-piston engine compressor (FLPC) as an on-board pneumatic power supply for untethered human and sub-human scale autonomous robotic systems is being investigated. The liquid piston's geometry exploits fluid inertance to achieve slower overall system dynamics than an equivalent mass solid piston so that efficient compression and pumping can occur without prohibitively large pump valve size or piston mass. A dynamic analysis, along with the traditional thermodynamic analysis, of the engine has been developed due to the engine's dynamically dominant nature. Within this dynamic model, it is important to accurately characterize the critical subsystems of the engine. This paper focuses on the measured and experimentally derived parameters of three of these subsystems—liquid piston diaphragm stiffness, injection valve capacity and dynamic response, and pump check valve dynamics. A discussion of the implications of these parameters on the overall FLPC design and performance is also presented.

3.1 Introduction

The use of pneumatic actuation for human and sub-human scale robotics has recently been investigated to address the power density limitations of battery-servomotor robotic actuation. Development of a compact pneumatic power supply that provides adequate energy density is a requirement for viable untethered pneumatic systems. A free piston engine compressor is a device that utilizes the high energy-density of hydrocarbon fuels to inertially load a piston which in turn compresses and pumps air to provide a pneumatic potential, and the lack of a kinematic linkage to the piston provides the prospect of high

overall efficiencies for small scale engine compressors. Mikalsen, et al [1], provide an excellent review of free-piston engine history and applications.

Riofrio, et al, [2] designed a Free Piston Compressor (FPC) for use in compact pneumatic systems. The design incorporated electrically actuated valving and ignition, and eliminated the need for a compression stroke by utilizing compressed reservoir air with the fuel for combustion. These attributes allow for start on demand for the engine and can eliminate the need to operate at resonance. A second device by Riofrio [3,4] addressed piston friction and blow-by losses by using a liquid piston trapped by two elastomeric diaphragms. This Free Liquid Piston Compressor (FLPC) incorporated a combustion chamber that was separated from the piston so that injection pressure could be held until ignition to avoid a compression stroke. Design of the FPC and FLPC demonstrated the importance of a dynamic model for the design of such free piston devices as compared to traditional combustion engines. Testing results of the FLPC device show the viability of such a device for portable power supplies.

Willhite, et al, [5], proposed modifications to the FLPC that could reduce and or eliminate several loss mechanisms of the FLPC to provide higher efficiency of the device. By altering the geometry of the liquid piston, fluid inertance can be dramatically increased, slowing down the dynamics of the FLPC without adding system mass. Slower dynamics can eliminate the need for the (inefficient) separated combustion chamber of the device and allow for a smaller and better performing pump check valve. A dynamic model of the “high-inertance” piston was developed and incorporated into the full FLPC model so that simulation could tune the piston dynamics to achieve optimum combustion and pump performance of the High-Inertance Free Liquid Piston Compressor (HI-FLPC).

This paper reviews experimental characterization of physical subsystems of the HI-FLPC that determine model parameters needed to optimize the effective inertia of the liquid piston. These parameters include: stiffness of the elastomeric diaphragms sealing the liquid piston, air/fuel injection valve flow area and dynamic characteristics, and compressor/pump check valve dimensions and dynamic parameters.

3.2 Liquid Piston Diaphragm Stiffness

The liquid piston of the HI-FLPC is contained (and allowed to move) by two elastomeric diaphragms, an example of which is shown in Figure 3-1. These diaphragms are considered in the dynamic model of the piston to be pure springs—mass and damping characteristics are being captured by the inertance and viscous loss lumped parameter terms. The total stiffness of the diaphragms is represented by the K_{tot} term in Equation (1), the dynamic equation for the inertance-type liquid piston as derived in Willhite, J. [6]. This term relates differential pressure across the piston as a function of volume displaced by diaphragm stretching, shown in Equation (2).

$$\Delta P = I\dot{Q} + A_c Q^2 + RQ + K_{tot}\Delta V \tag{1}$$

$$\Delta P = K_{tot}\Delta V \text{ , where } K_{tot} = f(\Delta V) \text{ and } \Delta V = \int Q \tag{2}$$

For efficient transduction of energy from combustion to the pump chamber, this stiffness should be small so that it does not store much of the combustion energy. However, some energy storage is necessary for the return stroke of the piston. Since there is no “bounce chamber” effect of the gas when full pumping is achieved, the energy stored in the diaphragms is the only driver of the return stroke of the HI-FLPC. The value of K_{tot} becomes critical in optimizing overall power output of the compressor by determining how

the combustion energy is divided between pump stroke and return stroke. For example, a higher value for K_{tot} gives a faster return stroke and therefore higher operating frequency, but less pumping energy per stroke, while a lower K_{tot} yields more pumping energy but slower return (lower frequency).

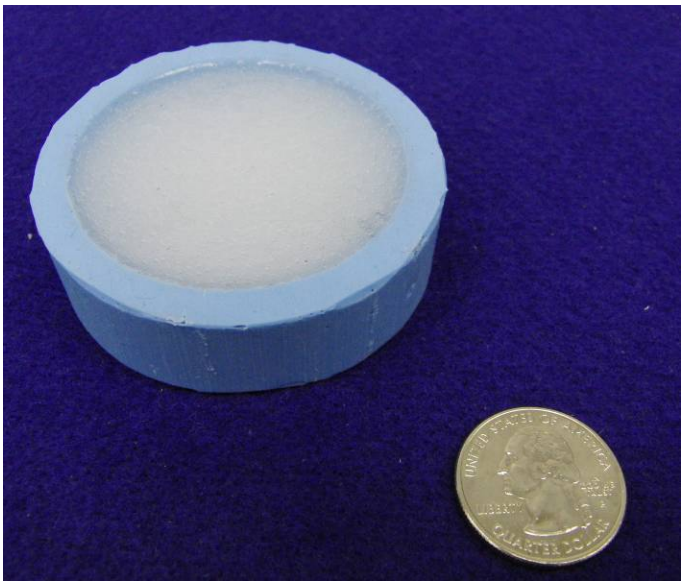

Fig. 3-1. Silicone Diaphragm for liquid piston

Diaphragm Stiffness Test

Figure 3-2 shows the test setup used. A sample diaphragm is clamped between two sealed volumes: a driving chamber and a response chamber. The driving chamber is air-filled and connected to a high-pressure air source. The response chamber is water-filled and connected to a mounted graduated cylinder, providing a column of fluid with which to measure volume displaced by the diaphragm. Both chambers are hemispherical, and the maximum displacement of the response chamber corresponds to the desired

displacement of the liquid piston in the HI-FLPC. The diaphragms tested have a displacement cross sectional radius of 25.4 mm and are 16 mm thick.

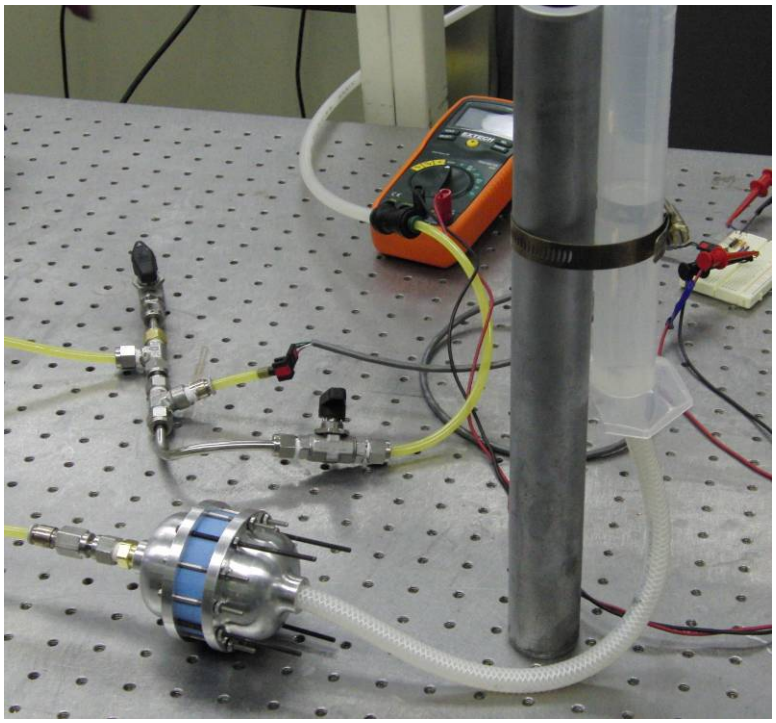

Fig. 3-2. Diaphragm Stiffness Test Setup

Figure 3-3 shows measured volume displacements for different driving pressures across the diaphragm (the height of the water column is neglected in the ΔP measurements.) An exponential least squares fit yields the curve:

$$\Delta P = K_{tot}\Delta V \text{ , where } K_{tot} = -2\times10^{-8}\Delta V + 2.7\times10^{-3} \quad (3)$$

Equation (3) represents the stiffness of a single diaphragm, which is doubled to obtain the term K_{tot}.

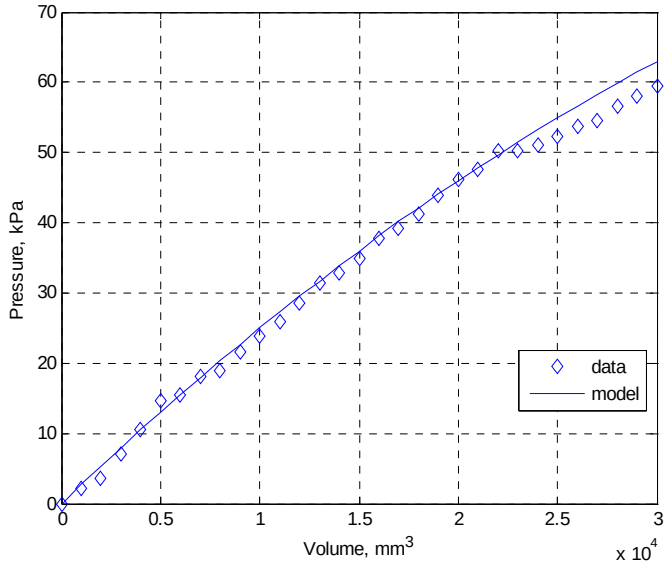

Fig. 3-3. Volume displaced by the diaphragm for given pressure differentials, and the least squares fit

With the energy storage of the piston characterized, the proper mass investment of air/fuel can be determined to compress and pump the entire charge of air in the pump chamber. Modelling of the return stroke will then indicate if this diaphragm stiffness is optimized for frequency and power output of the HI-FLPC. If needed, stiffness will be adjusted by varying the thickness and/or durometer of the diaphragms and this test will be repeated.

3.3 Air Fuel Injection and Pump Check Valve Flow Characteristics

Well-defined flow characteristics of the air/fuel injection valve are crucial for the design of the inertance piston of the HI-FLPC. The dynamics of the piston need to be slow enough to enable the proper duration of air/fuel injection (and spark) to occur before the expansion of the combustion chamber causes the air/fuel charge pressure to decrease

below the level needed for acceptably efficient engine operation. However, a piston with a larger than necessary inertance will result in lower output power potential of the device and extra heat loss due to the longer pump stroke duration.

Equations (4) and (5) collectively are a standard model used to describe isentropic mass flow through an orifice driven by upstream and downstream pressures, and are used to model the mass flow between control volumes of our model.

$$\dot{m}_j = \psi_j(P_u, P_d) \tag{4}$$

$$= \begin{cases} C_d a_j C_1 \dfrac{P_u}{\sqrt{T_u}} & \text{if} \quad \dfrac{P_d}{P_u} \le P_{cr} \\ C_d a_j C_2 \dfrac{P_u}{\sqrt{T_u}} \left(\dfrac{P_d}{P_u}\right)^{1/\gamma_u} \sqrt{1 - \left(\dfrac{P_d}{P_u}\right)^{\gamma_u - 1/\gamma_u}} & \text{if} \quad \dfrac{P_d}{P_u} > P_{cr} \end{cases}$$

where

$$C_1 = \sqrt{\frac{\gamma_u}{R_u}\left(\frac{2}{\gamma_u + 1}\right)^{\gamma_u + 1/\gamma_u - 1}} \quad , \; C_2 = \sqrt{\frac{2\gamma_u}{R_u(\gamma_u - 1)}} \quad , \quad \text{and} \quad P_{cr} = \left(\frac{2}{\gamma_u + 1}\right)^{\gamma_u/\gamma_u - 1} \tag{5}$$

Due to the short injection times necessitated by the expanding combustion chamber, the injector valve's popet response to a valve open command *u* is also modelled. The change in effective cross-sectional area a_j from closed to open is represented with the second order dynamic:

$$\frac{a_j(s)}{u(s)} = \frac{{\omega_n}^2}{s^2 + 2\xi\omega_n + {\omega_n}^2} \tag{6}$$

where ξ is assumed to be 1. A detailed treatment of how this mass flow model integrates into the total dynamic model of the HI-FLPC is presented in Riofrio, et al [3,4,5] and Willhite [6].

Fuel Injection Model Verification Test.

For the HI-FLPC air/fuel injection valve, the *Bosch 0 280 150 846 CNG* fuel injector (see Figure 3-4) is chosen due to its fast response time, adequate full-open flow rate, and specific design for gas fuel (as opposed to standard automobile liquid fuel injectors). The injector is mounted and sealed to the combustion head that will be used for the HI-FLPC prototype (see Figure 3-5). Note that two injectors are mounted to the combustion head. The reason for this configuration is to give the ability to inject twice as fast if needed, and to help mix the air/fuel charge in the combustion chamber before spark. The exhaust valve and solenoid are installed for combustion chamber sealing and to verify exhaust operation. The combustion side of the head will be mounted directly to the piston diaphragm in the final design, but for this test it seals with a fixed-volume chamber (rectangular looking block in Figure 5.) This chamber has a volume much greater than the expected volume of the combustion chamber of the FLPC at spark for combustion and serves to lengthen the injection time scale for better resolution during model validation.

Fig. 3-4. Bosch 0 280 150 846 CNG fuel injector

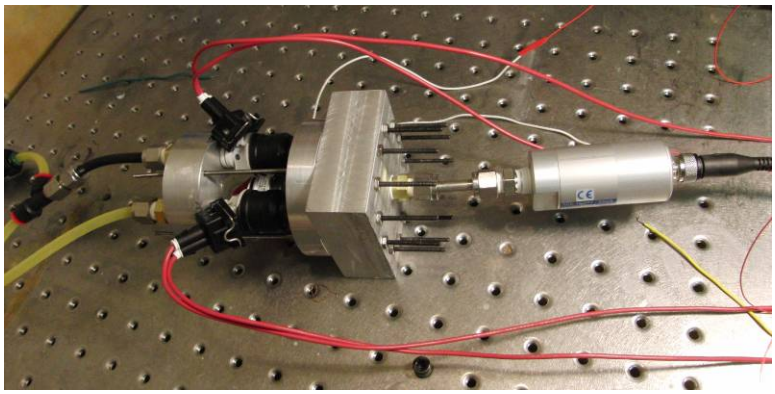

Fig. 3-5. Air/Fuel Injection Test Setup

Using the air/fuel control method described in Yong, C. [7], the proper stochiometric ratio of propane and air at 613 kPa is supplied to the injector. The valve was opened for 200 milliseconds and the pressure rise in the test chamber was recorded (expected injection time of the compressor prototype is less than 10 ms). Simulation of the injection test was performed to tune the ξ and ω_n model parameters. Figure 3-6 shows the tuned-parameter model pressure response with the measured response inside the chamber. The effective cross-sectional area of the injector is taken to be a_j = 1.82 mm^2 and the response natural frequency is determined to be ω_n =78.5 rad/sec with $\xi = 1$.

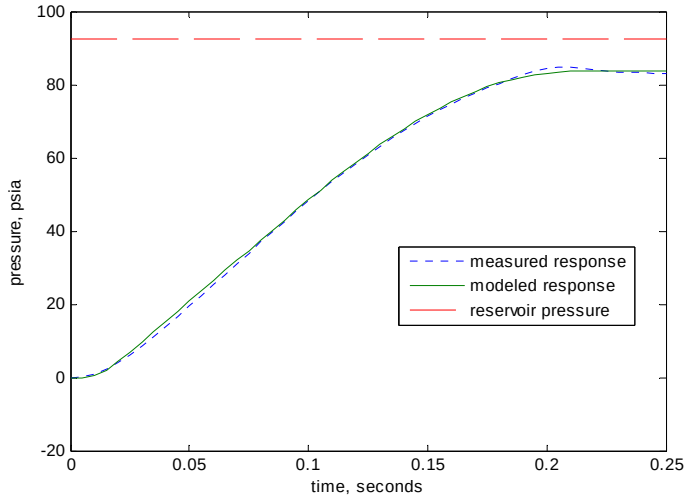

Fig. 3-6. Measured versus modelled response of the fuel injector

3.4 Pump Check Valve Parameters

In the HI-FLPC, the pump check valve is a passive valve that allows mass transfer of air from the pump chamber of the compressor to the reservoir. A larger inertance of the liquid piston reduces the $\dot{m}$ required for the same amount of pumping energy, allowing for more compact and slower valves without a loss in pumping efficiency. See Willhite [6] for a more in depth discussion of this trade-off. With this advantage, the pump check valve in the HI-FLPC compressor can be designed to be smaller than its FLPC predecessor. A piston-spring type check valve has been chosen that integrates into the pump chamber in order to minimize dead volume. Modelling of this valve will ensure that it is adequately large and fast enough for the slower pumping dynamics of the HI-FLPC.

Fig. 3-7. Pump check valve piston and spring

Like the injection valve, flow through the pump check valve is modelled by Equations (4) and (5). The a_j term is determined by the piston's open/close dynamics, which are represented as the lumped parameter second-order model as shown in Equation (7) and (8).

$$M_{ck}\ddot{x}_{ck} + b_{ck}\dot{x}_{ck} + k_{ck}(x_{ck} - x_o) = \Delta P A_{ck} \tag{7}$$

where

$$a_j = 2\pi r_{ck} x_{ck} \quad \text{and} \quad a_{j,\max} = A_v \tag{8}$$

M_{ck}, k_{ck}, and A_{ck} are directly measured from the check valve, while b_{ck} is calculated using an assumed damping ratio ξ_{ck}. When installed, the spring has an initial compression x_o. Table (1) lists values and descriptions of the parameters used in the pump check valve model.

Table 3-1. Measured pump check valve dimensions

Parameter	Value	Description
M_{ck}	0.0184 kg	Mass of check valve piston
k_{ck}	583.2973 N/mm	Spring constant for pump check valve spring
ξ_{ck}	0.05	Damping ratio for pump check valve (estimate)
r_{ck}	5.56 mm	Radius of check valve face area
A_{ck}	97.0 mm^2	Piston face area of check valve
A_v	110.84 mm^2	Maximum flow-through area of check valve piston
x_o	6.5 mm	Initial (minimum) spring compression

3.5 Conclusion

Characterization of three subsystems of the HI-FLPC for use in dynamic model simulation was presented in this work. Liquid piston diaphragm stiffness was measured for use in the liquid piston dynamic model. Mass flow and dynamic response model parameters of the air/fuel injection valve and pump check valve were determined. Accurate models of these subsystems can now be used in simulation to optimize overall system performance.

3.6 List of Notations

ΔP	Pressure Differential Across Piston	kPa
Q	Piston Fluid Volumetric Flow Rate	mm^3/sec
I	Liquid Piston Inertance	kg/mm^4
A_c	Inertance Area-Change Coefficient	kg/mm^7
R	Viscous Flow loss Coefficient in Fluid Piston	$kg/s/mm^4$
K_{tot}	Total Liquid Piston Stiffness	kPa
ΔV	Change in Volume in Chambers of Liquid Piston	mm^3
$\dot{m}_j$	Mass flow through valve	kg/s
P_u	Upstream Pressure	kPa
P_d	Downstream Pressure	kPa

T_u	Upstream Temperature	K
C_d	Valve Discharge Coefficient	-
P_{cr}	Choked-flow Threshold Pressure	kPa
a_j	Valve Orifice Cross-Sectional Area	mm^2
γ_u	Ratio of Specific Heats in the Upstream Gas	-
ω_n	Natural Frequency of Valve Popet	rad/sec
ξ	Damping Ratio of Valve	-
x_{ck}	Position of Pump Check Valve Piston Position	mm
M_{ck}	Mass of check valve piston	kg
k_{ck}	Spring constant for pump check valve spring	N/mm
ξ_{ck}	Damping ratio for pump check valve (estimate)	-
r_{ck}	Radius of check valve face area	mm
A_{ck}	Piston face area of check valve	mm^2
A_v	Maximum flow-through area of check valve piston	mm^2
x_o	Initial (minimum) spring compression	mm

3.7 References

[1] Mikalsen, R.; Roskilly, A.P. (2007). A review of free-piston engine history and application. *Applied Thermal Engineering*. Vol. 27, pp. 2339-2352.

[2] Riofrio, J.A.; Barth, E.J. (2004). Dynamic characteristics of a free piston compressor. *ASME International Mechanical Engineering Congress and Exposition (IMECE).* IMECE2005-81743, Nov. 5-11, Orlando, Fl.

[3] Riofrio, J.A.; Barth, E.J. (2005). Experimental Operation and Characterization of a Free Piston Compressor. *ASME International Mechanical Engineering Congress and Exposition (IMECE).* IMECE2004-59594, Nov. 13-19, Anaheim, Ca.

[4] Riofrio, J.A.; Barth, E.J. (2007). Design and analysis of a resonating free liquid-piston compressor. ASME International Mechanical Engineering Congress and Exposition (IMECE). IMECE2007-42369, Nov. 11-15, Seattle,Wa.

[5] Riofrio, J.A.; Barth, E.J. (2008). Design and analysis of a resonating free liquid-piston compressor. *ASME International Mechanical Engineering Congress and Exposition (IMECE).* IMECE2007-42369, Nov. 11-15, Seattle,Wa.

[6] Willhite, J.A.; Barth, E.J. (2009). Reducing piston mass in a free engine compressor by exploiting the inertance of a liquid piston. *2009 ASME Dynamic Systems and Control Conference & Bath/ASME Symposium on Fluid Power and Motion Control*. DSCC2009-2730, pp. 1-6, October 12-14, Hollywood, CA.

[7] Yong, C.; Barth, E.J. (2009). Modeling and control of a high pressure combined air/fuel injection system. *2009 ASME Dynamic Systems and Control Conference & Bath/ASME Symposium on Fluid Power and Motion Control*. DSCC2009-2769, pp. 1-8, October 12-14, Hollywood, CA.

CHAPTER IV

MANUSCRIPT III

OPTIMIZATION OF LIQUID PISTON DYNAMICS FOR EFFICIENCY AND POWER DENSITY IN A FREE LIQUID PISTON ENGINE COMPRESSOR

Joel A. Willhite

Eric J. Barth

Department of Mechanical Engineering

Vanderbilt University

Nashville TN 37235

Accepted as a Technical Paper to the Bath/ASME Symposium on Fluid Power & Motion Control (FPMC 2010), 15-17 September 2010, Bath, UK

4.0 Abstract

An optimization of piston dynamics to achieve performance goals of a High Inertance Free Liquid Piston engine Compressor (HI-FLPC) is presented in this work. The proposed HI-FLPC is a compact device that utilizes combustion of hydrocarbon fuel to provide a supply of pressurized air for use in untethered pneumatic systems. The liquid piston of this device is configured such that its geometry is exploited to produce a high inertance, which produces an advantageous (slower) dynamic response as compared to a rigid piston of equal mass. The slower dynamics achieved by the liquid piston allow for reduced valve sizes for the compressor, a direct inject-and-fire engine with no compression stroke, and the capability of more balanced operation for a single-piston device. These attributes create a more energy-dense device than developed in prior work. A review of the dynamic model of the HI-FLPC is presented along with experimental model validation of the liquid piston. Simulation studies were conducted to optimize liquid piston dynamic characteristics for overall system performance of an experimental prototype.

4.1 Introduction

The first free piston machine designed by Pescara [1] in 1928 was used as an air compressor. Free piston engines were most commonly commercially used as air compressors up to the mid-twentieth century. Other applications for the technology were investigated, such as gas generators for use in automobiles and small power plants. However, the lack of adequate sensing and control technology led to the free piston

engine being largely abandoned after 1960 [2]. Modern electronic controls available today have led to a second generation of free piston engine research, particularly for use as hydraulic pumps. Mikalsen [3] provides an extensive review of both early free-piston engine compressor and gas generator applications as well as the recent research in free piston hydraulic pumps and linear alternators.

Interest in free piston air compressors has also recently resumed for the purpose of providing a compact, energy-dense, untethered power source for pneumatically actuated autonomous human-scale robotic systems. The goal is to achieve a higher overall system-level energy and power density than current autonomous systems utilizing batteries and servomotors. Riofrio, et al [4] designed a device that incorporated a liquid trapped between elastomeric diaphragms as a piston. This free liquid-piston compressor (FLPC) addressed efficiency problems for engines of its size range (sub 1 kW) by eliminating the blow-by and friction losses of standard piston configurations. Willhite, et al [5], took advantage of the liquid piston idea by exploiting the geometry of the liquid piston of the FLPC to create a high inertance. This configuration allowed for desired (i.e., slower) piston dynamics to be achieved without the necessity of adding piston mass, thereby increasing the energy and power density of the system. This paper continues with the investigation of this High Inertance Free Liquid Piston Compressor (HI-FLPC). An experimental validation of the liquid piston dynamic model is discussed, and simulation studies of the HI-FLPC are performed to tune the dynamic characteristics of the liquid piston to optimize performance for an experimental prototype of the HI-FLPC.

Basic Operation of the HI-FLPC

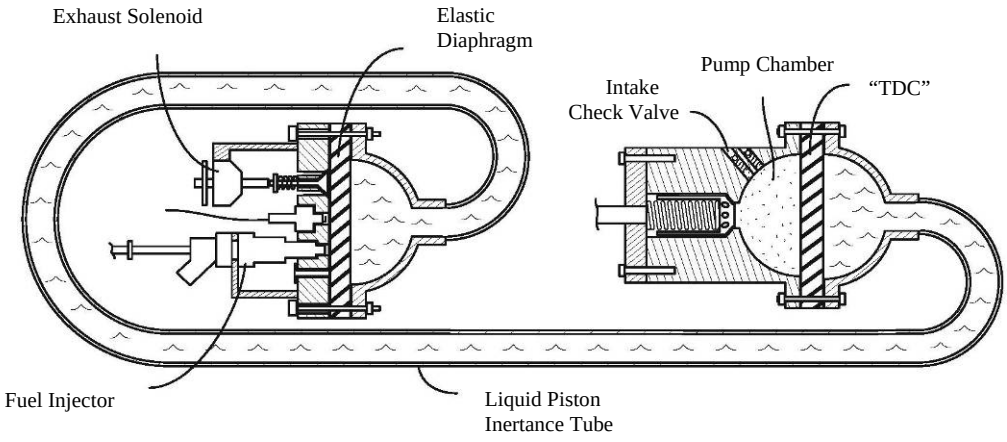

Figure 4-1. Schematic of HI-FLPC at TDC

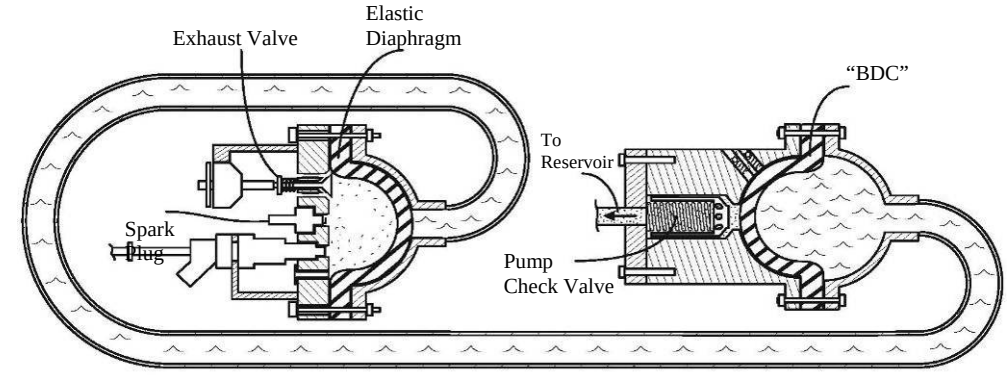

Figure 4-2. Schematic of HI-FLPC at BDC

Figure 4-1 is a representation of the HI-FLPC just before the power stroke of the engine, when the liquid piston diaphragms are relaxed. This is analogous to Top Dead Center (TDC) in conventional engines. The power stroke begins with injection of pressurized air from the system reservoir that is mixed with a hydrocarbon fuel, causing the elastic diaphragm to begin to stretch and the combustion chamber volume to increase.

The dynamic inertial load of the liquid piston limits the expansion so that injection and ignition can occur without an appreciable drop in air/fuel pre-combustion pressure. This dynamic process eliminates the need for a compression stroke. The mixture then combusts, rapidly increasing the pump chamber volume and converting the combustion energy into kinetic energy of the liquid piston. On the compressor side of the piston, this kinetic energy is used to compress and pump the air from the pump chamber. Once the pump chamber air pressure exceeds the reservoir pressure, the pump check valve opens and mass flow into the reservoir occurs. Figure 4-2 illustrates the configuration of the device at the moment pumping is completed, similar to conventional Bottom Dead Center (BDC). At this point, the combustion exhaust valve is opened and the piston diaphragms begin to relax, reversing the flow direction of the liquid piston. During this return stroke, exhaust is expelled from the combustion chamber and fresh air enters the pump chamber through a check valve. Note that diaphragm stiffness is the only driver of the return stroke. Once the piston has returned to its original TDC position, the cycle can be repeated.

The lack of a compression stroke allows the engine compressor to “fire on demand”- that is, there is no need to have a starting routing or maintain an idle cycle. This allows the HI-FLPC to operate at varying frequencies by controlling the delay between TDC and the command for air/fuel injection.

4.2 Dynamic Model

Unlike conventional IC engines, free piston engines (including the HI-FLPC) are more heavily influenced by the dynamic responses and interactions of their components.

For example, the stroke length of a conventional IC engine is kinematically defined by mechanical linkage to a crankshaft; a free piston engine's stroke length and even TDC and BDC positions are determined by the dynamic response of the piston and the dynamics of the load on each side of the piston, which includes combustion, compression/pumping and valve response rates. For this reason, a dynamic model is necessary for determination of performance and design optimization of the HI-FLPC.

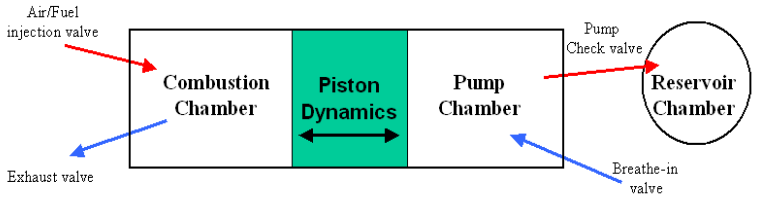

Figure 4-3. Control volumes, mass flows, and piston dynamics of the HI-FLPC model

The model developed for the HI-FLPC in sections 2.1 – 2.3 consists of three control volumes: the combustion chamber, the pump chamber, and the reservoir. The combustion and pump chamber control volumes are coupled by the liquid piston dynamics. Mass flows and valve response dynamics are modeled for the injection and exhaust valves of the combustion chamber, as well as the pump and intake check valves of the pump chamber.

Control Volume Pressure and Temperature Dynamics

The following is an overview of the derivation of the pressure and temperature dynamics of the gas in each of the model control volumes. For a more detailed treatment

of this derivation, see [4] and [6]. Equation (1) represents the power balance for each j^{th} control volume (specifically, the combustion chamber, the pump chamber, and the reservoir):

$$\dot{U}_j = \dot{H}_j + \dot{Q}_j - \dot{W}_j \tag{1}$$

where $\dot{U}$ is the rate of change of internal energy, $\dot{H}$ is the net enthalpy flowing into the control volume, $\dot{Q}$ is the rate of heat transfer into the control volume and $\dot{W}$ is the work rate of the gas. Each term in Eq. (1) can be expanded as follows:

$$\dot{H}_j = \sum_k \dot{m}_{j,k} \left(c_{p_{in/out}}\right)_{j,k} \left(T_{in/out}\right)_{j,k} \tag{2}$$

$$\dot{W}_j = P_j \dot{V}_j \tag{3}$$

$$\dot{U}_j = \dot{m}_j \left(c_v\right)_j T_j + m_j \left(c_v\right)_j \dot{T}_j = \frac{1}{\gamma_j - 1}\left(\dot{P}_j V_j + P_j \dot{V}_j\right) \tag{4}$$

where $\dot{m}$ is the k^{th} mass flow rate entering or leaving each j^{th} control volume, with constant-pressure specific heat $c_{p_{in/out}}$ and temperature $T_{in/out}$. P and V are the pressure and volume in the control volume, c_v is the constant volume specific heat and γ is the ratio of specific heats of the gas in the control volume. Equations (2-4) can be used to form the differential Equations (5) and (6), which describe the pressure and temperature dynamics of the gas in each control volume.

$$\dot{P}_j = \frac{\left(\gamma_j - 1\right)\sum \dot{m}_j \left(c_{p_{in/out}}\right)_j \left(T_{in/out}\right)_j + \left(\gamma_j - 1\right)\dot{Q}_j - \gamma_j P_j \dot{V}_j}{V_j} \tag{5}$$

$$\dot{T}_j = \frac{\sum \dot{m}_j \left[\left(c_{p_{in/out}}\right)_j \left(T_{in/out}\right)_j - \left(c_v\right)_j T_j\right] - P_j \dot{V}_j + \dot{Q}_j}{m_j \left(c_v\right)_j} \tag{6}$$

The dynamics of the combustion process of the engine are treated as a $\dot{Q}$ term of the combustion chamber control volume. A detailed description of this combustion model, is in Yong. [6].

Mass Flows

The mass flow terms $\dot{m}_j$ in Equations (5) and (6) are determined by the following equation describing isentropic flow through an orifice, from Richer and Hurmuzlu [7]:

$$\dot{m}_j = \psi_j(P_u, P_d)$$

$$= \begin{cases} C_d a_j C_1 \dfrac{P_u}{\sqrt{T_u}} & \text{if} \quad \dfrac{P_d}{P_u} \le P_{cr} \\ C_d a_j C_2 \dfrac{P_u}{\sqrt{T_u}} \left(\dfrac{P_d}{P_u}\right)^{1/\gamma_u} \sqrt{1-\left(\dfrac{P_d}{P_u}\right)^{\gamma_u - 1/\gamma_u}} & \text{if} \quad \dfrac{P_d}{P_u} > P_{cr} \end{cases} \tag{7}$$

where C_d is a non-dimensional discharge coefficient of the valve, a_j is the area of the valve orifice, P_u and P_d are the upstream and downstream pressures, T_u is the upstream temperature, γ_u is the ratio of specific heats of the upstream gas. The constants C_1, C_2, and the critical pressure for choked flow, P_{cr}, are determined by:

$$C_1 = \sqrt{\frac{\gamma_u}{R_u}\left(\frac{2}{\gamma_u + 1}\right)^{\gamma_u + 1/\gamma_u - 1}} \quad , \quad C_2 = \sqrt{\frac{2\gamma_u}{R_u(\gamma_u - 1)}} \quad , \text{ and}$$

$$P_{cr} = \left(\frac{2}{\gamma_u + 1}\right)^{\gamma_u/\gamma_u - 1} \tag{8}$$

where R_u is the gas constant of the upstream substance. The dynamic responses of valves can then be modeled as dynamically determining the orifice area. In the case of

electronically actuated valves, the lift of the valve and the subsequent revealing of a_j can be modeled as a second order response to a current. In the case of a check valve, the orifice area is the dynamic response to a differential driving pressure lifting the valve off the seat.

High-Inertance Piston Dynamics

The dynamic model of the high inertance liquid piston summarized here was developed in [5]. Consider a configuration consisting of three sections of a liquid, as shown in Figure 4-4. A power balance based on fluid flow due to the movement of the piston boundaries (in our case, diaphragms stretching and relaxing) is given by Equation 9, where *P* is the pressure difference across the left and right moving boundaries, and *Q* is the volumetric flow rate of the piston fluid.

$$PQ = \frac{d}{dt}\left[\frac{1}{2}m_1\left(\frac{Q}{A_1}\right)^2 + \frac{1}{2}m_2\left(\frac{Q}{A_2}\right)^2 + \frac{1}{2}m_3\left(\frac{Q}{A_3}\right)^2\right] \tag{9}$$

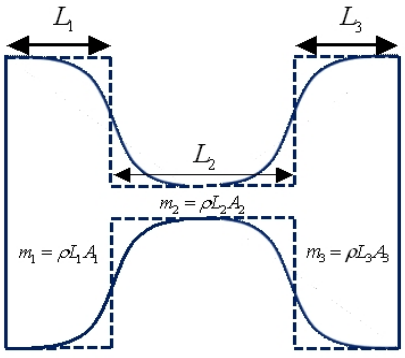

Figure 4-4. Three sections of the high inertance liquid piston.

Substituting $m_i = \rho L_i A_i$ for the masses of liquid in each flow region, differentiating, substituting $\dot{L}_1 = -Q/A_1$, $\dot{L}_2 = 0$ and $\dot{L}_3 = Q/A_3$, and solving for pressure, we obtain Equation 10:

$$P = \left[\frac{\rho L_1}{A_1} + \frac{\rho L_2}{A_2} + \frac{\rho L_3}{A_3} \right] \dot{Q} + \frac{\rho}{2} \left[\frac{1}{A_3^2} - \frac{1}{A_1^2} \right] Q^2 \tag{10}$$

which consists of a dynamic term relating P and $\dot{Q}$ through the inertance of the fluid slug and a steady-state term due to the area changes between regions. For our model, A_1 and A_3 are equal, thereby eliminating the steady state term. We can now describe the inertance as:

$$I = \left[\frac{\rho L_1}{A_1} + \frac{\rho L_2}{A_2} + \frac{\rho L_3}{A_3} \right] \tag{11}$$

Viscous losses of the liquid are modeled by a resistive term relating pressure and volumetric flow, taken from the Darcy-Weisbach equation:

$$R = \frac{8\rho}{\pi^2 d_2^4} Q \cdot f \frac{L_2}{d_2} \tag{12}$$

where ρ is the density of the fluid (water), and d_2 is the diameter of the high inertance tube. The friction factor f was (conservatively) taken from the Moody Chart to be 0.025.

A stiffness term is also developed, relating pressure *P* to the change in volume of the outer sections of the liquid piston due to the expansion of the diaphragms. Willhite [8] describes the experimental technique used to measure this relationship for a sample diaphragm, which is almost linear. For our optimization model, we will assume a linear relationship, such that:

$$P = K\Delta V \text{ , noting that } \Delta V = \int Q \tag{13}$$

Combining the relationships in Equations (11) through (13), the total dynamics of the piston are given by:

$$\Delta P = I\dot{Q} + RQ + K_{tot} \tag{14}$$

Experimental Piston Dynamics Model Validation. An experimental setup of the liquid piston was used to validate the dynamic model of the high inertance liquid piston (shown in Figure 4-5). The liquid piston is housed by two hemispherical sections on each end, connected by the high inertance tube with a 7.9 mm inner diameter and a length of 1680 mm. The piston liquid is captured by two diaphragms with diameters of 25.4 mm. On the opposite side of each diaphragm is a sealed chamber of air. Testing consisted of supplying step-like driving pressures of varying amplitudes to one of the air chambers via a three-way valve. The response of the piston was measured by observing the pressure rise in the sealed chamber on the other end of the liquid piston (response chamber). Simulations of these experiments were then conducted, using the piston model in the same configuration as the test. Stiffness of the diaphragms was experimentally determined beforehand. The responses of the piston were plotted against model responses to the same pressure driving functions. One example of these responses to a maximum driving pressure of 750 kPa is shown in Figure 4-6. Note that two different modeled responses are present; one model assumes isothermal behavior of the response chamber and the other assumes an adiabatic process. Since the piston response in this test is on the same order of magnitude time scale as the pump stroke of the HI-FLPC, it is assumed that the piston model developed captures all significant dynamics of the liquid.

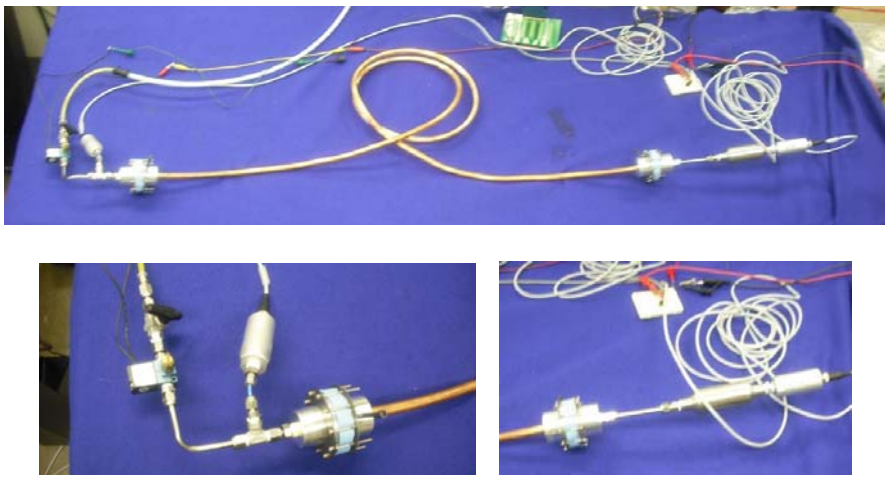

Figure 4-5. Experimental setup used to validate the liquid piston model. Shown on the left is a three-way valve used to provide a driving pressure, along with a pressure sensor. The tube shown on top contains the liquid piston trapped by two diaphragms. Shown on the right is a sealed air chamber and pressure sensor used to (indirectly) measure the piston response

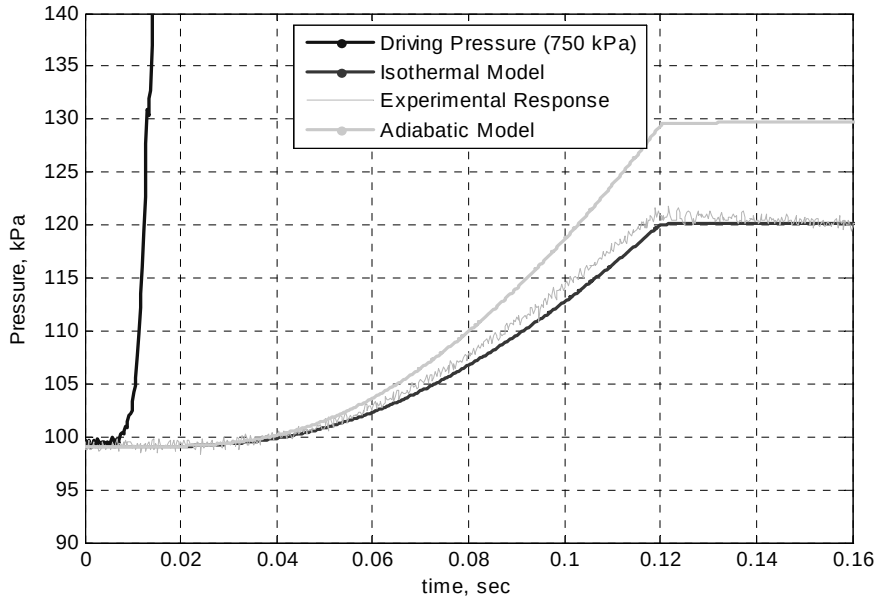

Figure 4-6. Experimental piston response compared to the liquid piston dynamic model (for adiabatic and isothermal models of the response chamber).

4.3 Model-based Optimization Studies

An experimental prototype of the HI-FLPC is currently being developed. Performance targets for the device are centered around the need for a compact, efficient untethered power source for small-scale pneumatic power applications. These targets include overall system mass of under 2kg and an output of 75W, and an overall system efficiency of at least 10% from chemical potential of the fuel to cool pneumatic potential in the reservoir.

To develop the HI-FLPC prototype, a complete model of the device was implemented in MATLAB, using the control volume dynamics of Equations (5) and (6), the liquid piston dynamics as modeled with equation (14), and the combustion process as modeled in [6]. All valve opening and closing dynamics affecting each valve orifice area a_j were modeled as second order and fitted to experimental data for the valves chosen for the HI-FLPC (see Willhite, et al, [8] for examples).

Simulation Results for Proposed Experimental Prototype

Simulations were performed to tune the liquid piston dynamics for optimum performance of an experimental prototype of the HI-FLPC. Device parameters that were not adjusted during the simulations were: all valve parameters, piston diaphragm radius (25.4 mm) and pump chamber volume (3.43×10^4 mm^3). A design point for the prototype was chosen from these simulations, with liquid piston parameters A_2 and L_2 set at 324 mm^2 and at 1778 mm. Figure 4-7 shows the pressure profiles of the control volumes at this design point for the pump stroke of the HI-FLPC model. The output power for the

simulation is 136.8W, at a cycle frequency of 18 Hz and a total projected system mass of 2.07 kg. Efficiency of the cycle is calculated to be 27.4%.

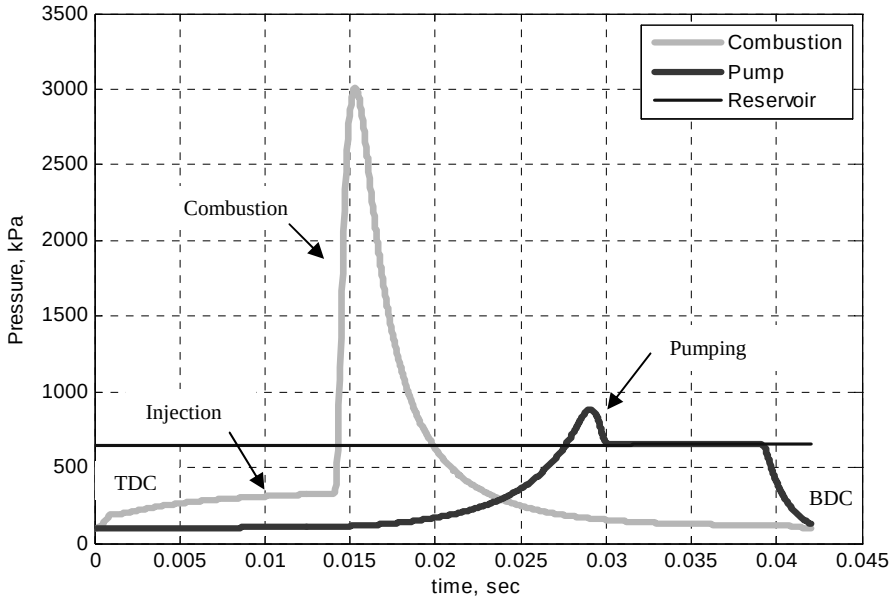

Figure 4-7. Control volume pressures for power stroke of HI-FLPC at the design point

Effects on Performance of Liquid Piston Characteristics

Simulation studies were performed to investigate how changes in the dynamic characteristics of the piston from the design point of Section 3.1 would affect overall performance of the HI-FLPC. These simulations separately varied the L_2 and A_2 geometry of the liquid piston, and the stiffness of the piston diaphragm in order to investigate their individual effects on efficiency and power density of the device. The following sections discuss the simulation results for the variation of these three parameters.

Varying Inertance Tube Cross-Sectional Area. Figure 4-8 shows simulation results for the maximum power density and system efficiency versus piston inertance, where the inertance is varied by adjusting the liquid piston cross-sectional area. Maximum power density is calculated from the amount of energy pumped into the reservoir per stroke, the stroke duration and the mass of the device. Each of these values vary for the different cross sectional areas simulated. A dry system mass of the HI-FLPC is assumed (fuel mass not included) that includes the mass of: the structure, all components, and the liquid piston. The frequency of operation assumes no pause between cycles of the engine. Efficiency is defined as the amount of pneumatic potential added to the reservoir divided by the chemical potential (lower heating value) of the hydrocarbon fuel. The performance of the device at the design point of Section 3.1 is shown for reference. To ensure a proper comparison, the air/fuel input was adjusted for each simulation to fully pump the air charge in the compressor chamber into the reservoir. This results in the same amount of output energy for each cycle.

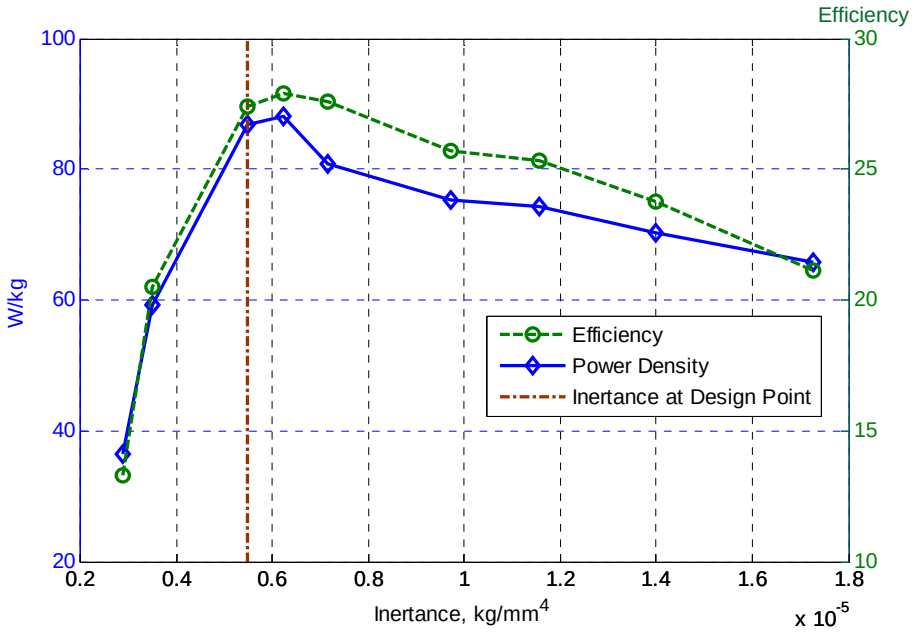

Figure 4-8. Power density and efficiency versus inertance by varying liquid piston cross-sectional area, A_2

While it is normally expected to see a trade-off between power and efficiency, certain characteristics of the HI-FLPC cause the coinciding power density and efficiency peaks. As inertance increases from the design point (5.46×10^{-6} kg/mm^4), the power density decline is due to a slower piston dynamics lengthening the pump stroke. The drop in efficiency is primarily a result of an increase in viscous losses of the piston due to the decrease of A_2. These dominant viscous losses for smaller cross-sectional piston areas (larger inertance) are the main reason for the chosen value of A_2.

For inertance below the design point, the steep drop-off in efficiency is predominantly caused by two factors. The first and most dominant factor is on the pump side: the piston dynamics are now too fast for the pump check valve to close in time, allowing for some backflow of reservoir air into the pump chamber. The second and

more minor factor is that the lower inertance provides less dynamic load on the air/fuel injection, resulting in a lower pressure of the air/fuel mass input just before combustion. This is similar to a smaller compression ratio in a traditional four stroke engine.

Varying Inertance Tube Length. Next, the inertance of the piston was varied by changing the length L_2 of the liquid piston while holding A_2 constant at the current design point. Once again, the dropoff in efficiency and power density for lower inertances is due to the inability of the pump check valve to react fast enough to the piston dynamics. As inertance gets higher, power density decreases due to longer pump stroke durations. Efficiency increases up to and beyond the design point due to better pump check valve performance and the higher pressure of the air/fuel mass input just before combustion. However, as inertance increases further this effect is dominated by viscous losses of the piston, and efficiency peaks.

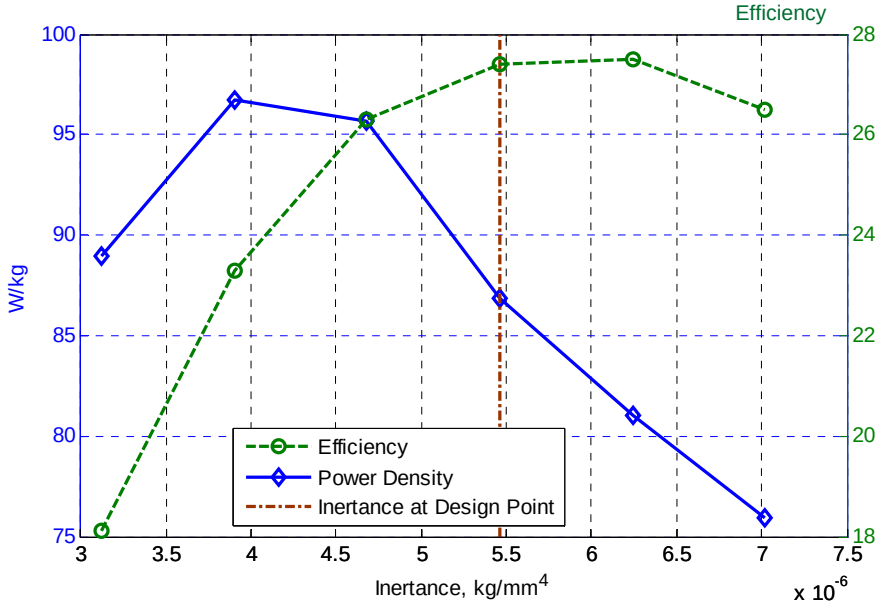

Figure 4-9. Maximum Power Density and Efficiency Versus Inertance by Varying Liquid Piston Inertance Tube Length

Varying Diaphragm Stiffness. Variations of diaphragm stiffness yields a fairly straight-forward trade-off between power and efficiency. Increasing the diaphragm stiffness stores more combustion energy during the pump stroke, thereby speeding up the return stroke which reduces the overall system cycle time. The extra energy needed from combustion to fully expand the diaphragms decreases overall efficiency, while the higher operating frequency increases output power. Note that for the current design point, some efficiency is being sacrificed for better power density. Less stiff diaphragms may be experimented with once the prototype is complete to maximize efficiency while still maintaining the output power targets.

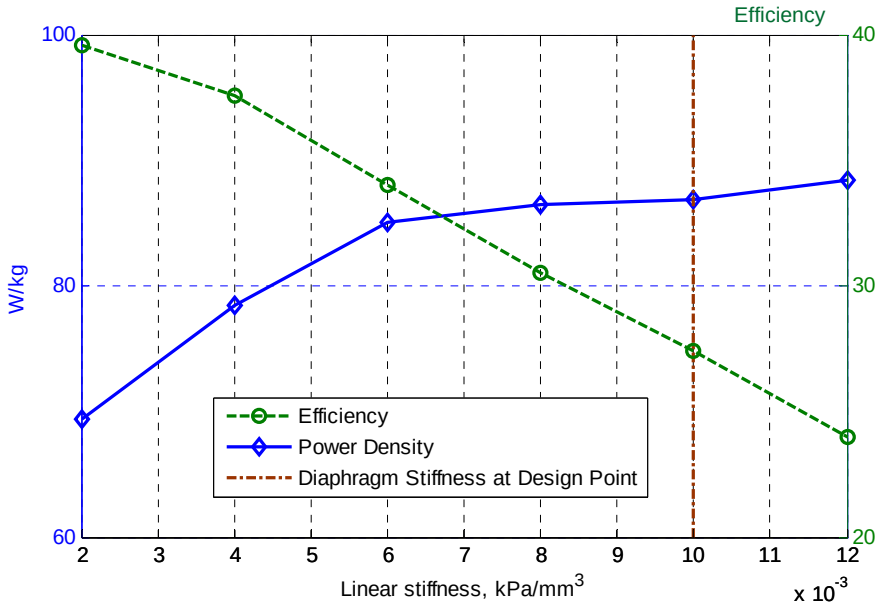

Figure 4-10. Maximum power density and efficiency versus diaphragm stiffness

4.4 Conclusions

This paper presented the operation of a high inertance free liquid piston compressor (HI-FLPC). A review of the development of a dynamic model for the HI-FLPC was

presented. Experimental validation of the liquid piston dynamics was performed. Simulation studies were performed to optimize the piston dynamics for best overall performance of the engine and pump subsystems of the HI-FLPC.

Now that all components of the proposed experimental prototype are specified, fabrication of the HI-FLPC device has begun. The engine section, complete with injection and exhaust valve, is shown in Figure 4-11. Testing of engine-side performance (only loaded by the liquid piston) has begun, and will be followed by compressor section fabrication and a complete experimental characterization of the performance of the complete HI-FLPC engine compressor.

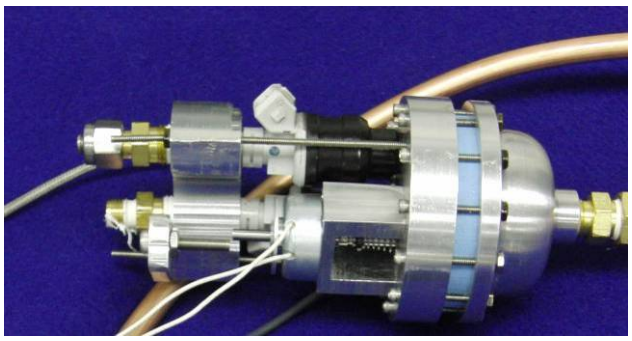

Figure 4-11. Experimental prototype combustion head mounted to liquid piston

4.5 References

[1] Pescara, R. P., "Motor Compressor Apparatus," U.S. Patent No. 1,657,641, Jan. 31, 1928.

[2] Johansen, T. A.; Egeland, O.; Johannessen, E. A.; Kvamsdal, R, "Free-Piston Diesel Engine Timing and Control – Toward Electronic Cam- and Crankshaft," *IEEE Transactions on Control Systems Technology*, vol. 10, no. 2, March 2002, pp. 177 – 190.

[3] Mikalsen, R. and Roskilly, A. P., "A Review of Free-Piston Engine History and Applications," *Applied Thermal Engineering*, vol. 27, 2007, pp. 2339 – 2352.

[4] Riofrio, J and Barth, E. J., "Design and Analysis of a Resonating Free Liquid-Piston Engine Compressor," *2007 ASME International Mechanical Engineering Congress and Exposition (IMECE)*, IMECE2007-42369, November 11-15, 2007, Seattle, WA.

[5] Willhite, J. A. and Barth, E. J., "Reducing Piston Mass in a Free Piston Engine Compressor by Exploiting the Inertance of a Liquid Piston". *2009 ASME Dynamic Systems and Control Conference & Bath/ASME Symposium on Fluid Power and Motion Control*. DSCC2009-2730, pp. 1-6, October 12-14, 2009, Hollywood, CA.

[6] C. Yong, C.; Riofrio J. A.; and Barth, E. J., "Modeling and Control of a Free-Liquid-Piston Engine Compressor," *Bath/ASME Symposium on Fluid Power and Motion Control (FPMC 2008)*, pp. 245-257, September 2008.

[7] Richer, E., and Hurmuzlu, Y., "A High Performance Pneumatic Force Actuator System: Part 1 – Nonlinear Mathematical Model". *ASME Journal of Dynamic Systems, Measurement and Control*, 122, September, 2000, pp. 416-425.

[8] Willhite, J. A. and Barth, E. J., "Experimental Characterization of Critical Dynamic Model Parameters for a Free Liquid Piston Engine Compressor," *6th FPNI Ph.D. Symposium*, Purdue University, June 2010, to appear.

CHAPTER V

MANUSCRIPT IV

THE HIGH INERTANCE FREE PISTON ENGINE COMPRESSOR PART 1: DYNAMIC MODELING

Joel A. Willhite

Chao Yong

Eric J. Barth

Department of Mechanical Engineering

Vanderbilt University

Nashville TN 37235

To be submitted as a full journal paper to the *ASME Journal of Dynamic Systems, Measurement, and Control*.

5.0 Abstract

Free piston engine compressors have recently been investigated for the purpose of providing a high pressure air supply for untethered, pneumatically actuated robotic systems. Given that free piston engine performance is highly dependent on the dynamic characteristics of the piston, this paper presents the idea of incorporating a liquid piston whose geometry can be manipulated to achieve the desired piston dynamics while maintaining the compactness and light weight necessary for applications in the power output range of 100W. An inertance-based dynamic model of the liquid piston is developed and validated experimentally. The piston model is incorporated into a complete system dynamic model of a proposed high inertance free liquid piston compressor (HIFLPC.) Critical model parameters for individual components and subsystems of a proposed HIFLPC prototype are experimentally characterized. Simulation results for the proposed prototype are shown and discussed.

5.1 Introduction

One of the largest obstacles impeding the advancement of untethered robotic systems with power needs in the neighborhood of 100 Watts is the inability of current power supply and actuation methods to perform human-scale mechanical work for significant durations of time [1]. The vast majority of systems are actuated by DC servo motors powered by NIMH or Li-ion batteries, due to the relative ease of servo control. With such systems, the energy density of the batteries limits the useful work of the system between re-fueling, while the bulkiness of the electromagnetic actuators limits power

density. For example, the Honda P3 humanoid robot carries a 30-kg battery pack that provides only 15-25 minutes of low-power work [2].

Apart from a large leap in battery technology, other energetic domains offer opportunities to address these power density and energy density issues. One alternative to improve power density is the use of linear pneumatic actuators, which possess an order of magnitude better volumetric power density and five times better mass specific power density than state of the art electric motors [3]. In addition, pneumatic actuation offers a number of dynamic properties that are arguably a better match to systems like walking robots. Such properties include variable stiffness, energy storage, and regeneration. Thus, the use of pneumatics has recently been investigated for small scale robotics to exploit these advantages, with efforts focused on addressing two main obstacles for the realization of such systems: first, developing adequate position, force, and impedance control (true stiffness control and imposed impedance control) for pneumatic actuators, and second, the development of on-board pneumatic power supplies that can provide useful amounts of supply air in a compact and efficient manner. Recent work by Zhu, et al [4], and Guihard [5] are examples of work addressing the first issue, showing that the control of pneumatic actuators can be precise enough to compete with DC servomotors in this application. The work described here is a continuation of efforts in addressing the latter obstacle.

Since storing enough compressed air for a useful duty cycle is size and weight prohibitive, effective on-board production of pressurized gas has been investigated. Goldfarb, et al [6] used catalytic decomposition of hydrogen peroxide to successfully

drive pneumatic actuators directly, i.e., no storage of pneumatic potential, with measured system energy density competitive with that of batteries/motors [7].

Recently, the work of Riofrio, et al, [8,9,10] has addressed the need for an efficient, compact conversion of fuel to pneumatic potential by utilizing the unique dynamic characteristics of a free piston engine compressor. The term “free piston engine” is used to describe a class of positive displacement machines that lack any kinematic constraints on the piston motion. This characteristic leads to a mechanically simpler design, which is promising for small-scale applications. For example, the friction losses and extra mass associated with the slider-crank mechanism of conventional engines scale down poorly with output power of the device, yielding poor efficiency and power density. A free piston device would have no such losses. Riofrio’s Free Liquid Piston Compressor (FLPC) demonstrated the viability of such a design. This paper uses the FLPC as the starting point, with the goal of addressing the limitations of that design and thus creating a lighter weight, more efficient, more operationally robust power source. To this end, the author recommends a review of [8,9,10].

Along with utilizing the free piston idea, Riofrio, et al, incorporated several unique features into the FLPC design that were well-suited for the function of compact and efficient air compression. On the engine side, high-pressure air from the reservoir mixed with propane was used for combustion, eliminating the need for an intake or compression stroke. A separated combustion chamber with a magnetically–latched combustion valve was incorporated to hold the high-pressure of the air/fuel mix until ignition, similar to maintaining a high compression ratio. After combustion, the valve “breaks” open and high-pressure combustion products enter the expansion chamber to drive the piston. This

"inject and fire" method allows for start-on-demand operation with no need for engine idling.

Another feature unique to the FLPC was the replacement of a solid piston and sliding seals with a liquid slug trapped between two elastomeric diaphragms. This liquid piston was incorporated into the FLPC to eliminate friction and blowby loss trade-offs associated with traditional solid pistons. The energy stored in the diaphragms during the pump stroke could drive the return stroke of the piston, eliminating the need for a bounce chamber or mechanical spring on the compressor side of the piston. Figure 1 shows a solid model representation of the FLPC with key features labelled.

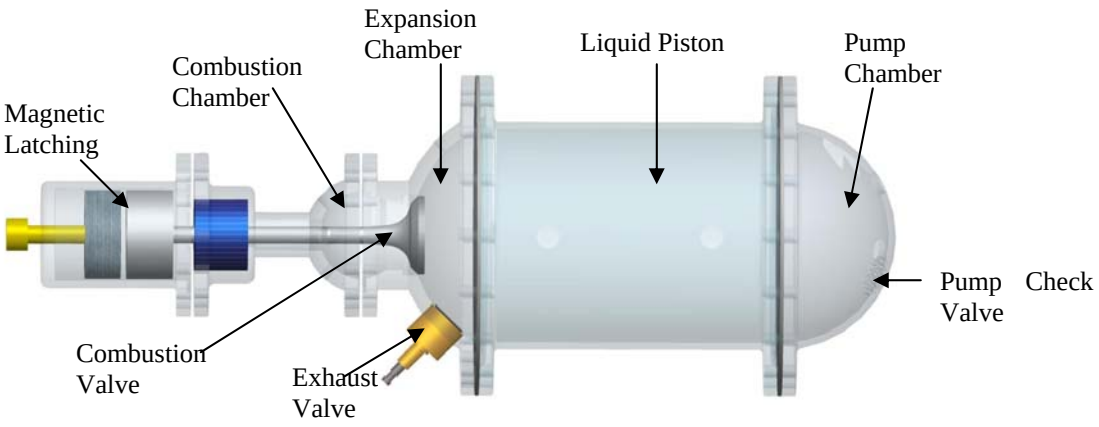

Figure 5-1. FLPC major features.

Part 1 of this work begins in Section 5.2 with an analysis of the FLPC with the goal of mitigating the major loss mechanisms of the device, leading to the idea of the High Inertance Free Piston Engine Compressor (HIFLPC). Section 5.3 develops an inertance-based dynamic model of the liquid piston, which is then incorporated into the system

model of the HIFLPC (that incorporates all dynamic elements of the device) in Section 5.4. In Section 5.5, critical model parameters for individual components and subsystems of a proposed HIFLPC prototype will be experimentally validated to be incorporated into the fully coupled system model. Simulation results for the proposed HIFLPC prototype are shown and discussed in Section 5.6.

5.2 Analysis of FLPC Performance

Performance of the FLPC was characterized in [10], with a measured efficiency of 2.01%, corresponding to 931 kJ of cool gas pneumatic potential per kilogram of fuel. While these results showed the viability of using a free piston device as a small-scale pneumatic power supply, there were some limitations that led to sub-optimal performance. The following is a list of loss mechanisms associated with the FLPC design that limit the performance of the device:

- Scavenging problems due to the fixed volume of the separated combustion chamber, leading to intermittent firing.
- Flow losses around the combustion valve.
- Incomplete combustion due to unspent fuel passing through the combustion valve and into the expansion chamber.
- Added mass and complexity of the combustion valve and magnet.
- Extra dead volume associated with magnet/combustion valve sealing.
- “Backflow” from the reservoir into the pump chamber through the pump check valve at the end of the pump stroke.

All of these characteristics were associated with either the separated combustion chamber apparatus on the engine side or the pump check valve on the compressor side. It became clear the pump stroke of the FLPC was too “fast”—leading to the necessity of the separated combustion chamber in the engine section and the high capacity (and therefore slow-closing) pump check valve in the compressor section. An increase in piston inertia by adding fluid volume would allow for slower dynamics and more efficient operation, but the added size and mass of such a piston would be unacceptable.

Since the FLPC utilized a liquid piston, the property of liquid inertance could increase the system’s effective inertia by exploiting the liquid piston’s geometry. The dynamics of the system could be made slower without necessarily adding mass to the system. With a high enough inertance, the dynamic load of the piston could be sufficient to eliminate the need of the FLPC’s separated combustion chamber altogether by dynamically holding the air/fuel pressure high enough during injection to maintain a high pre-combustion pressure. Also, slower flow rate of air during the pump stroke allows for a smaller, faster, check valve that can mitigate backflow while not causing unacceptable flow losses. A design which exploits these high-inertance effects, the High Inertance Free Liquid Piston Compressor (HIFLPC), is the focus of this paper and is shown schematically in Fig. 2.

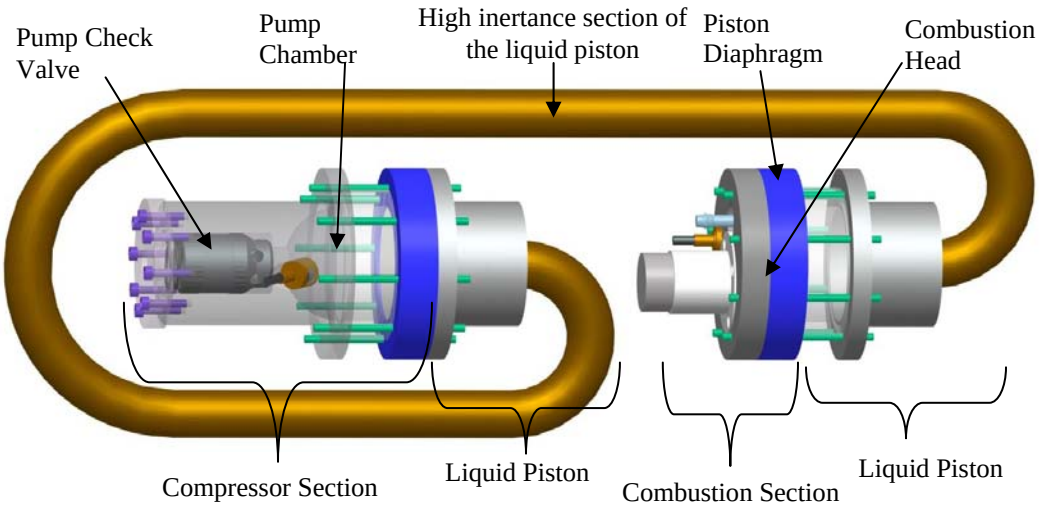

Figure 5-2. Schematic of the High Inertance Free Liquid Piston Compressor (HIFLPC)

5.3 Inertance-based Liquid Piston Model

This section develops the dynamic model for the HIFLPC's liquid piston. The components of this model include the piston inertance, viscous losses of the fluid flowing through the tube, and the energy storage, or stiffness, of the elastomeric diaphragms that capture the piston fluid.

Liquid Piston Inertance

Consider a fluid filled pipe approximated with three regions of effective lengths L_1, L_2, and L_3, with distinct cross sectional areas and liquid masses as shown in Fig. 3. This configuration represents a liquid piston trapped between two moving seals, such as solid pistons or, in the case of the HIFLPC, elastomeric diaphragms. Thus, the left and right boundaries of the liquid piston can be varied (L_1 and L_3 are not fixed) with a pressure difference acting on the moving seals, causing fluid flow through the chambers.

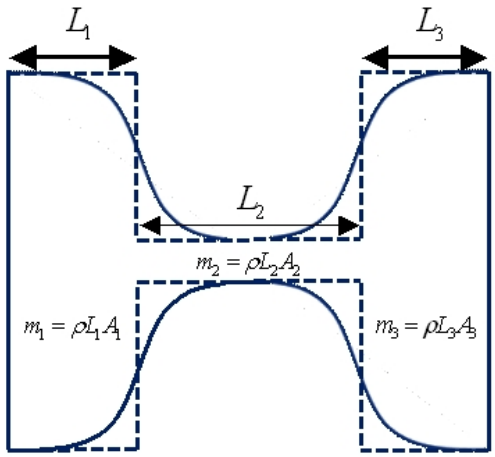

Figure 5-3. Three regions of a generic liquid piston contained by diaphragms or sliding pistons on both ends

A power balance based on fluid flow due to movement of the piston boundaries is given by the time derivative of the kinetic energies of the fluid in each of the flow regions:

$$PQ = \frac{d}{dt}\left[\frac{1}{2}m_1\left(\frac{Q}{A_1}\right)^2 + \frac{1}{2}m_2\left(\frac{Q}{A_2}\right)^2 + \frac{1}{2}m_3\left(\frac{Q}{A_3}\right)^2\right] \tag{1}$$

where P is the pressure difference across the left and right moving boundaries, and Q is the volumetric flow rate of the piston fluid. After substituting $m_i = \rho L_i A_i$ for the masses of liquid in each flow region and differentiating, then substituting $\dot{L}_1 = -Q/A_1$, $\dot{L}_2 = 0$ and $\dot{L}_3 = Q/A_3$ (since L_1 and L_3 vary due to movement of the boundaries), the pressure can be solved for to obtain Eq. 2:

$$P = \left[\frac{\rho L_1}{A_1} + \frac{\rho L_2}{A_2} + \frac{\rho L_3}{A_3}\right]\dot{Q} + \frac{\rho}{2}\left[\frac{1}{A_3^2} - \frac{1}{A_1^2}\right]Q^2 \tag{2}$$

This relationship between pressure and flow rate of Eq. 2 consists of a dynamic term relating P and $\dot{Q}$ through the inertance of the fluid and a steady-state term due to the area changes between regions. The inertance, I, of the liquid piston is therefore:

$$I = \left[\frac{\rho L_1}{A_1} + \frac{\rho L_2}{A_2} + \frac{\rho L_3}{A_3} \right] \tag{3}$$

The steady flow term, when $\dot{Q} = 0$, relating P and Q^2 is

$$\frac{\rho}{2}\left[\frac{1}{A_3^{\,2}} - \frac{1}{A_1^{\,2}} \right] \tag{4}$$

It is interesting to note that, assuming $A_1 >> A_3$ for Eq. (4) and solving for *Q*, the standard hydraulic flow equation is obtained:

$$Q = A_3 \sqrt{\frac{2}{\rho}} \sqrt{\Delta P} \tag{5}$$

It can be seen that the second region of this configuration, termed the high inertance (HI) section, can be given a large length-to-area ratio L_2 / A_2 to dominate the inertance in Eq. 3. The fluid piston as a dynamic load can then be made larger primarily through the geometry of the high-inertance section, rather than adding fluid mass to the piston.

Viscous Losses

While the goal of a "high inertance" liquid piston would be to slow the dynamics of the engine, viscous losses between the fluid and the tube wall need to be accounted for and balanced against the advantages of increasing piston inertance while decreasing piston mass (i.e., decreasing A_2 and lengthening L_2.) Therefore, the model of the piston

would need to include not only the inertance, but also viscous effects between the fluid and the wall. This viscous loss is modeled by a resistive term relating pressure and volumetric flow, taken from the Darcy-Weisbach equation:

$$R = \frac{8\rho}{\pi^2 d_2^{\,4}} Q \cdot f \frac{L_2}{d_2} \tag{6}$$

where ρ is the density of the fluid (water), d_2 is the diameter of the high inertance tube, and f is a friction factor that can be empirically calculated or taken from the Moody Chart.

Piston Diaphragm Stiffness

For the HIFLPC design, each end of the liquid piston is sealed and mated to the combustion and compression chambers, respectively, by elastomeric diaphragms similar to those used in the FLPC. The final component of the piston model is a stiffness term accounting for the energy storage of these diaphragms; mass of the diaphragms along with any damping effects were considered negligible compared to that of the liquid piston. Since the other terms of the model relate pressure and volumetric flow rate, the spring stiffness used relates pressure differential across the piston to volume displaced by the combustion chamber due to diaphragm expansion, shown in Eq. 7:

$$\Delta P = K_{tot} \Delta V, \quad \text{where } K_{tot} = f(\Delta V), \quad \text{noting that } \Delta V = \int Q \tag{7}$$

Minimizing the stiffness of the diaphragms would allow for a more efficient pump stroke since the diaphragms would store less energy as they expand (energy stored in the diaphragms is unavailable to do pumping work). However, since there is no "bounce chamber" effect of the gas when full pumping is achieved, the energy stored in the

diaphragms is the only driver of the return stroke of the HIFLPC. Therefore, the shape of K_{tot} is a critical parameter when optimizing overall power output versus efficiency of the compressor, essentially dividing combustion energy between pump stroke and return stroke. A higher stiffness K_{tot} raises output power by increasing operational frequency due to a faster return stroke. A less stiff K_{tot} increases efficiency by storing less energy in the diaphragms, but lowers output power potential by slowing the return stroke.

Complete piston dynamic model

Combining the relationships in Equations (2), (6), and (7), the total dynamics of the piston are given by Eq. (8), where A_c is the steady state term from Eq. (4).

$$\Delta P = I\dot{Q} + A_c Q^2 + RQ + K_{tot}\Delta V \tag{8}$$

5.4 System Dynamic Model of the HIFLPC

Unlike conventional IC engines, the behavior of free piston engines (including the HIFLPC) are more heavily influenced by the dynamic responses and dynamic interactions of their components. For example, the stroke length of a conventional IC engine is kinematically defined by a mechanical linkage to a crankshaft; a free piston engine's stroke length and velocity profile are determined by the dynamic response of the piston and the dynamics of the loads on each side of the piston, which include combustion, compression/pumping and valve response rates. For this reason, a dynamic model is necessary for determination of performance and design optimization of the HIFLPC. More subtly, the fully coupled dynamics determine how energy is distributed

in each domain at each moment in time, which heavily influences the losses in the system (this will be discussed in more detail in section 6.)

The model developed in this section consists of three control volumes representing the combustion chamber, the pump chamber, and the reservoir, as seen in Fig. 4. The following section is an overview of the derivation of the pressure and temperature dynamics of the gas for each of the modeled control volumes. For a more detailed treatment of this derivation, see [8] and [11].

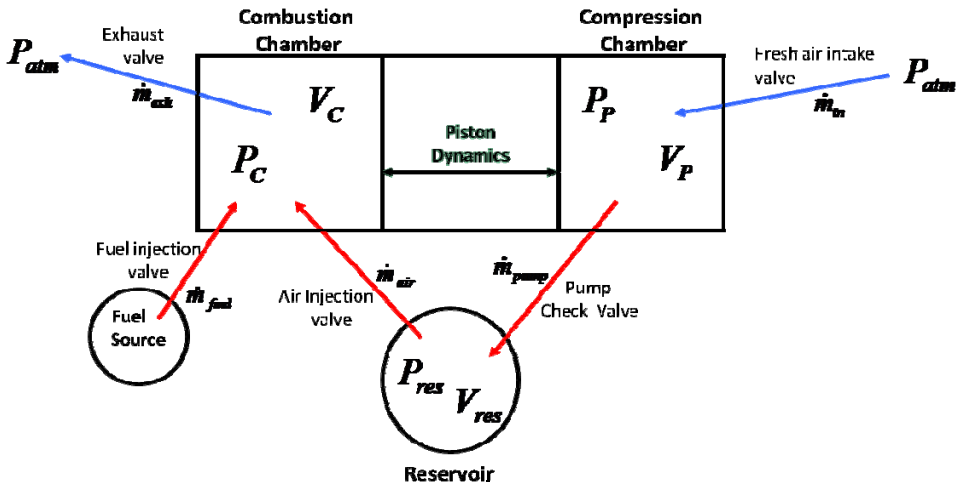

Figure 5-4. Diagram of the HIFLPC control volumes and mass flows

Control volume pressure dynamics

Equation (9) represents the power balance for each j^{th} control volume (specifically, the combustion chamber, the pump chamber, and the reservoir):

$$\dot{U}_j = \dot{H}_j + \dot{Q}_j - \dot{W}_j \tag{9}$$

where $\dot{U}$ is the rate of change of internal energy, $\dot{H}$ is the net enthalpy flowing into the control volume, $\dot{Q}$ is the rate of heat transfer into the control volume and $\dot{W}$ is the work

rate done by the gas. Assuming ideal gas, each term in Eq. (9) can be expanded for each modeled control volume as follows:

$$\dot{H} = \sum_k \dot{m}_k \left(c_{p_{in/out}}\right)_k \left(T_{in/out}\right)_k \tag{10}$$

$$\dot{W} = P\dot{V} \tag{11}$$

$$\dot{U} = \dot{m}(c_v)T + m(c_v)\dot{T} = \frac{1}{\gamma - 1}\left(\dot{P}V + P\dot{V}\right) \tag{12}$$

where $\dot{m}$ is the net sum of the k mass flow rates entering or leaving the control volume, with constant-pressure specific heat $c_{p_{in/out}}$ and temperature $T_{in/out}$. P and V are the pressure and volume in the control volume, c_v is the constant volume specific heat and γ is the ratio of specific heats of the gas in the control volume. Equations (10-12) can be used to form the differential equation (13), which describes the pressure and temperature dynamics of the gas in each control volume.

$$\dot{P} = \frac{(\gamma - 1)\sum_k \dot{m}_k (c_{p_k})(T_k) + (\gamma - 1)\dot{Q} - \gamma P\dot{V}}{V} \tag{13}$$

Given the sign convention for mass flows entering and leaving the control volumes as established in Fig. 4, Eq. (13) can then be expanded for the combustion chamber, compression chamber, and reservoir control volumes, respectively, by Eqs. (14) through (16), where R is the gas constant. Section 4.3 describes the dynamic model used to determine each of the mass flows entering and leaving the control volumes through either active or passive valves.

$$\dot{P}_{comb} = \frac{(\gamma - 1)[\dot{m}_{fuel}(c_{p_{fuel}})(T_{fuel}) + \dot{m}_{air}(c_{p_{res}})(T_{res}) - \dot{m}_{exh}(c_{p_{comb}})(T_{comb})] + (\gamma - 1)\dot{Q}_{comb} - \gamma P_{comb}\dot{V}_{comb}}{V_{comb}} \tag{14}$$

$$\dot{P}_{comp} = \frac{(\gamma-1)[\dot{m}_{in}(c_{p_{atm}})(T_{atm}) - \dot{m}_{pump}(c_{p_{comp}})(T_{comp})] + (\gamma-1)\dot{Q}_{comp} - \gamma P_{comp}\dot{V}_{comp}}{V_{comp}} \quad (15)$$

$$\dot{P}_{res} = \frac{(\gamma-1)[\dot{m}_{pump}(c_{p_{comp}})(T_{comp}) - \dot{m}_{air}(c_{p_{res}})(T_{res})] + (\gamma-1)\dot{Q}_{res}}{V_{res}} \quad (16)$$

The next section in this work formulates a dynamic combustion model that integrates into the combustion chamber CV of Eq. 14 through the heat rate input term, $\dot{Q}_{comb}$. The $\dot{Q}$ terms in Eqs. (15-16) represent heat dissipation of the reservoir and pump chamber CV's.

With the $-\gamma P\dot{V}$ term in Eqs. (14) and (15), the volumes and pressures of the combustion chamber and compression chamber can be coupled to the liquid piston dynamics of Eq. (8). Since expansion of the combustion chamber results in piston flow due to the expansion of the mated piston diaphragm, the piston dynamic model of Eq. (8) can be restated with flow rate in terms of $\dot{V}$ of the combustion chamber.

$$\left(P_{comb} - P_{comp}\right) = I\ddot{V}_{comb} + A_c\dot{V}_{comb}^{\ 2} + R\dot{V}_{comb} + K_{tot}\Delta V_{comb} \quad (17)$$

The change in volume of the compressor side is also due to piston flow expanding the diaphragm, such that:

$$\dot{V}_{comb} = -\dot{V}_{comp} \quad (18)$$

The temperatures in each control volume at any instant in time are determined by Eq's. (19-21), using the ideal gas law:

$$T_{comb} = \frac{P_{comb}V_{comb}}{m_{comb}R} \quad (19)$$

$$T_{comp} = \frac{P_{comp}V_{comp}}{m_{comp}R} \quad (20)$$

$$T_{res} = \frac{P_{res} V_{res}}{m_{res} R} \tag{21}$$

Combustion Model

Given that the time-scale of the combustion process is not orders of magnitude faster than the pump stroke of the device, a dynamic model of the heat release rate during combustion should be included. The following is a summary of the combustion model for the FLPC prototype developed by Yong, et al [11].

The total energy stored in the combustion chamber's air/fuel mixture at the time of the spark can be computed by $E_c = \Delta H_r m_c \Big|_{t_{spark}}$, where m_c is the total mass of air and fuel in the combustion chamber, and ΔH_r is computed from the lower heating value for the stoichiometric combustion of propane,

$$\begin{aligned} \Delta H_r &= \frac{46350\,\text{kJ}}{\text{kg fuel}} \times \frac{1\,\text{kg fuel}}{16.63\,\text{kg air/fuel mixture}} \\ &= 2787\,\frac{\text{kJ}}{\text{kg air/fuel mixture}} \end{aligned} \tag{22}$$

The rate at which heat is released by combustion in the combustion chamber is given by,

$$\dot{Q}_{comb} = \Delta H_r \dot{m}_{cc} \tag{23}$$

where m_{cc} is the mass of the combustion products.

Using the Arrehnius law, which is a standard model in combustion research [12], to compute the reaction rate, the following temperature-dependent equation is obtained:

$$\dot{m}_{cc} = K e^{-E_a / R_c T_c} m_{uc} \tag{24}$$

where $\dot{m}_{cc}$ is the rate of emergence of combustion products, E_a is the activation energy, and K is the pre-exponential factor. The mass of un-combusted material m_{uc} in the combustion chamber is given by

$$m_{uc} = m_c - \int_{t_{spark}}^{t} \dot{m}_{cc} dt \tag{25}$$

In the Laplace domain, Equations (23), (24) and (25) can be represented as a first order impulse response function (with a slight abuse of notation given the functional dependency of τ on temperature):

$$Q_{comb} = \frac{E_c}{\tau s + 1} \frac{1}{s} \delta(s) \tag{26}$$

where

$$\tau = \frac{1}{Ke^{-E_a / R_c T_c}} \tag{27}$$

and $\delta(t)$ represents the spark event.

The Arrehnius law assumes that the fuel is homogeneously combusted and the temperature is same within all regions of the combustion chamber. However, since the combustion is in our case spark-ignited, the first order model will not adequately capture the spatial propagation dynamics of the combustion process. Therefore, a second-order model is applied to account for the additional complexities associated with combustion flame propagation and temperature distribution within the chamber. The overall heat release is then given as,

$$Q_{comb} = \frac{E_c \omega_c^2}{s^2 + 2\xi\omega_c s + \omega_c^2} \frac{1}{s} \delta(s) \tag{28}$$

The temperature-dependent rate is still given by the Arrehnius law: $\omega_c = Ke^{-E_a/R_cT_c}$. Given that the reaction is assumed irreversible, the damping ratio must satisfy $\xi \geq 1$. $\dot{Q}_{comb}$ then represents the effective heat release rate which "contributes" to pressure dynamics of Eq. (14). ω_c can be further simplified as,

$$\omega_c = Ke^{-A/T_c} \tag{29}$$

where K and A are empirically obtained constants. These constants will be determined from experimental data from the HIFLPC prototype in Part 2 of this work.

Mass Flows

The mass flows in and out of each control volume (as seen in Fig. 4) are modeled by Equations (30) and (31), which describe isentropic flow through an orifice (Richer and Hurmuzlu [13]):

$$\begin{aligned} \dot{m}_j &= a_j \psi_j \left(P_u, P_d\right) \\ &= \begin{cases} C_d C_1 \dfrac{P_u}{\sqrt{T_u}} & \text{if} \quad \dfrac{P_d}{P_u} \leq P_{cr} \\ C_d C_2 \dfrac{P_u}{\sqrt{T_u}} \left(\dfrac{P_d}{P_u}\right)^{1/\gamma_u} \sqrt{1-\left(\dfrac{P_d}{P_u}\right)^{\gamma_u - 1/\gamma_u}} & \text{if} \quad \dfrac{P_d}{P_u} > P_{cr} \end{cases} \end{aligned} \tag{30}$$

where C_d is a non-dimensional discharge coefficient of the valve, a_j is the area of the valve orifice, P_u and P_d are the upstream and downstream pressures, T_u is the upstream temperature, γ_u is the ratio of specific heats of the upstream gas. The constants C_1, C_2, and the critical pressure for choked flow, P_{cr}, are determined by:

$$C_1 = \sqrt{\frac{\gamma_u}{R_u}\left(\frac{2}{\gamma_u+1}\right)^{\gamma_u+1/\gamma_u-1}} \quad , \quad C_2 = \sqrt{\frac{2\gamma_u}{R_u(\gamma_u-1)}} \quad , \text{ and}$$

$$P_{cr} = \left(\frac{2}{\gamma_u+1}\right)^{\gamma_u/\gamma_u-1} \tag{31}$$

where R_u is the gas constant of the upstream substance.

The dynamic responses of valves can then be modeled as varying the effective orifice area, a_j. In the case of electronically actuated valves, the lift of the valve and the subsequent revealing of the orifice can be modeled as a second order response to a current. In the case of a check valve, the variable orifice area is due to the dynamic response of a differential driving pressure lifting the valve off the seat. The change in effective cross-sectional area a_j for all valves in the model is represented with the second order dynamic:

$$\frac{a_j(s)}{u(s)} = \frac{\omega_n^{\,2}}{s^2 + 2\xi\omega_n + \omega_n^{\,2}} \tag{32}$$

where ξ is assumed to be 1.

5.5 Experimental Characterization of Model Components

In order to evaluate whether the design changes of the HIFLPC are advantageous versus the FLPC design, components for the experimental prototype were chosen that would allow the HIFLPC to be comparable in output power, size, and weight to the FLPC. The most critical of the components chosen and designed were experimentally characterized individually to tune critical model parameters for the system model. Section 5.1 is a validation of the liquid piston model developed in section 3.

Experimental determination of the piston diaphragm stiffness curve is presented in section 5.2. Model parameters are determined for the air and fuel injector models in section 5.3, and for the pump check valve model in section 5.4.

Liquid Piston Dynamic Model Validation

The experimental setup for independently validating the dynamic model of the high inertance liquid piston, separate from the influences of combustion, compression, and other aspects of the complete HIFLPC device, is shown in the top view of Fig. 5. The liquid piston is configured with two hemispherical sections with diameters of 50.8 mm on each end, connected by a tube with a 7.9 mm inner diameter and a length of 1680 mm. Water, used as the piston fluid, is captured by two diaphragms that mate the hemispherical ends of the piston to sealed chambers of air; one to provide a driving pressure to the piston, the other to act as a response chamber used to (indirectly) measure the piston response. Shown on the left of Fig. 5 is the driving chamber, which uses a three-way valve to provide a driving air pressure to the piston, along with a pressure sensor. Shown in the right view is the response air chamber and pressure sensor. Testing consisted of supplying step-like pressure increases of varying amplitudes to the driving chamber. The travel of the piston was (indirectly) measured by observing the pressure rise in the response chamber.

Simulations of these experiments were then conducted, with the piston and chamber control volumes modeled in the same configuration as the experiment. The stiffness of the diaphragms, K_{tot} was experimentally determined beforehand by a method described in detail in Willhite [14], yielding $K_{tot} = -2\times10^{-8}\Delta V + 2.7\times10^{-3}$ (note that for

the experimental prototype a different diaphragm, characterized in section 5.2, was used). The friction factor for the piston's viscous losses was set at $f = 0.02$ according to the Moody chart. Figure 6 shows an example of simulated responses of the piston plotted against model responses to the same pressure driving function (roughly a 750kPa step.) Note that two different modeled responses are present; one model assumes isothermal behavior of the air in the response chamber and the other assumes an adiabatic process. Noting that the modeled and experimental responses display a piston travel time of about 120 ms, it can be assumed that the piston model developed captures all significant dynamics of the liquid at our time scale of interest.

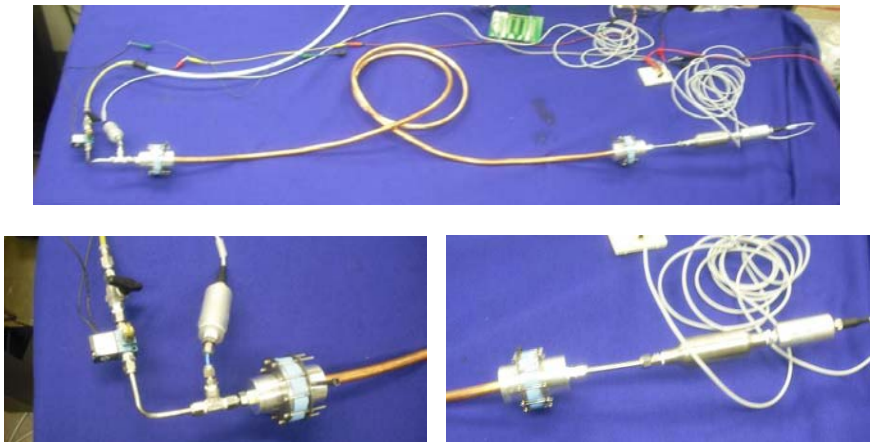

Figure 5-5. Experimental setup used to validate the liquid piston model.

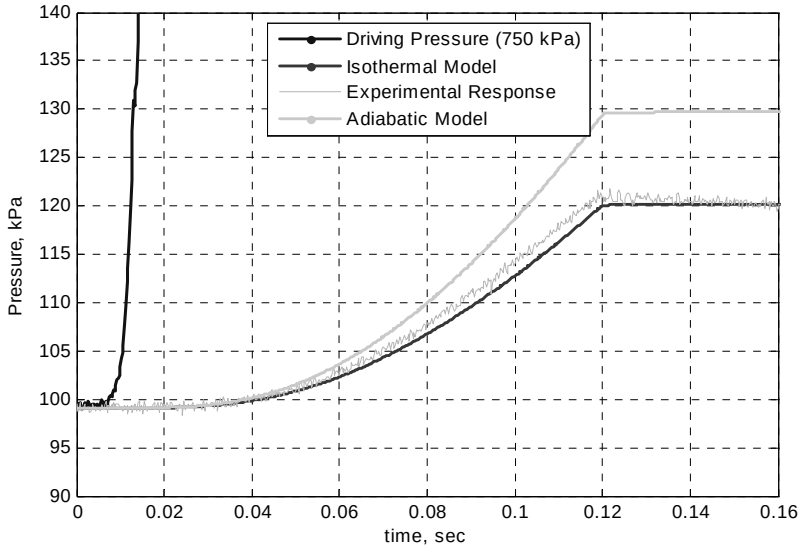

Figure 5-6. Experimental piston response compared to the liquid piston dynamic model (for adiabatic and isothermal models of the response chamber).

Diaphragm Stiffness Characterization

A test measuring volume displaced by the diaphragm for different pressure differentials was conducted to determine the stiffness curve, K_{tot}, of Eq. (7). In the test set-up shown in Fig 7, a sample diaphragm is clamped between two sealed volumes: a driving chamber connected to a high-pressure air source, and a fluid-filled response chamber. The response chamber includes a graduated cylinder that is open to atmosphere, providing a column of fluid with which to measure volume displaced by the diaphragm in response to pressure in the driving chamber.

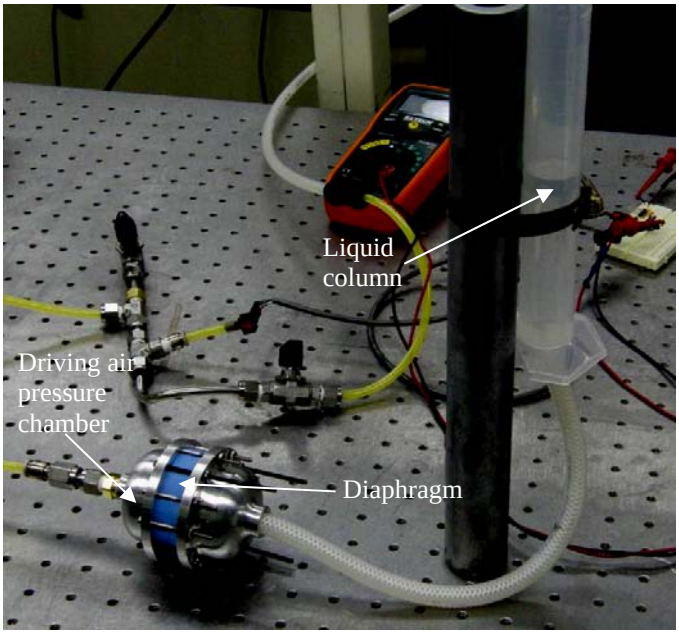

Fig. 5-7. Diaphragm Stiffness Test Setup

Figure 8 shows test results for a 2.38 mm thick, 40A durometer, 50.8 mm diameter silicone diaphragm. Measured volume displacements are plotted against different driving pressures, with the least squares fit of Eq. (33) shown to determine $K_{tot}/2$, noting that K_{tot} accounts for both pistons of the diaphragm. No measurable hysteresis was observed during the test.

$$K_{tot}/2 = -4.3\times10^{-18}\Delta V^3 + 3.2\times10^{-12}\Delta V^2 - 2.4\times10^{-7}\Delta V + 0.0074 \qquad (33)$$

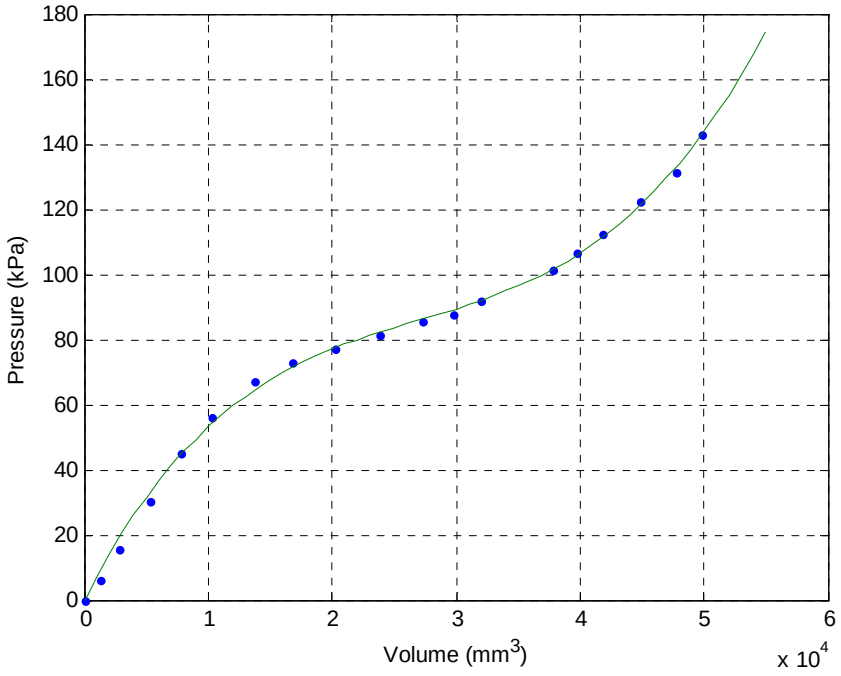

Fig. 5-8. Volume displaced by the diaphragm for given pressure differentials, and the least squares fit of Eq. (33)

Air/Fuel Injection Valve

The air and fuel injector dynamic flow characteristics are crucial in determining the effectiveness of piston inertance with regard to maintaining a high combustion chamber pressure during injection up to the moment of the spark. The injectors need to open fast enough, and also have a large enough "full-open" flow rate, to inject the needed amount of fuel and air for the compression stroke while also maintaining the highest possible pre-combustion pressure (maximizing combustion efficiency by minimizing the amount of combustion chamber volume expansion during injection due to piston motion). Characterization of the injectors' behavior will therefore allow us to make a model-based determination of the design architecture's ability to dynamically maintain a high air/fuel

pre-combustion pressure using a high inertance, versus a separated fixed-volume combustion chamber design.

For the HIFLPC air/fuel injection valve, the *Bosch 0 280 150 846 CNG* fuel injector (see Figure 9) was chosen due to its fast response time, adequate full-open flow rate, and specific design for gaseous fuel (as opposed to standard automobile liquid fuel injectors). One drawback of the valve, however, is that it was designed for a relatively low-pressure downstream environment; the pressure of combustion on the valve would force it open, causing backflow of exhaust products into the air and fuel lines. To prevent this, two 0.38 *mm* thick metal check valve flaps covering both injector ports on the combustion head were added, as seen in Fig. 10(b). The model for the air and fuel injectors (as developed in section 4.3) was augmented to include effects of these check valves by empirically curve fitting to include the cracking pressure, and an effective flow orifice revealed by the bending of the flap until saturated by the maximum orifice area as dictated by the injector's geometric orifice area, as shown in Eq.'s (34-35):

$$a_{A/F,tot} = c_{ck\_flap} a_{A/F} \tag{34}$$

$$c_{ck\_flap} = \begin{cases} 0 & \Delta P < P_{crack} \\ f(P) & P_{crack} \le \Delta P < P_{full} \\ 1 & \Delta P \ge P_{full} \end{cases} \tag{35}$$

where c_{ck_flap} is a fractional factor to augment the injector orifice area, $a_{A/F}$, to include check valve effects.

The experimental setup for the characterization of the valve is similar to the method described in Willhite, et al, [14], and is shown Fig. 11. The injectors (and check flaps) were mounted and sealed to the combustion head that will be used for the HIFLPC.

The combustion head is mounted to a 3.8 cc fixed-volume chamber to measure the pressure rise due to injection.

Fig. 5-9. Bosch 0 280 150 846 CNG fuel injector

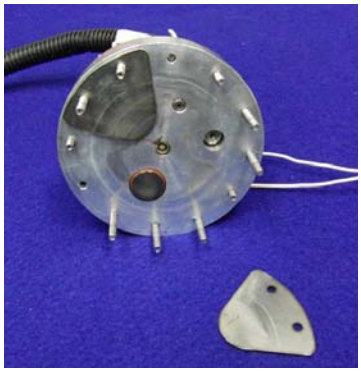

Fig. 5-10. (a) Injectors mounted to combustion head. (b) Injector check valve flaps

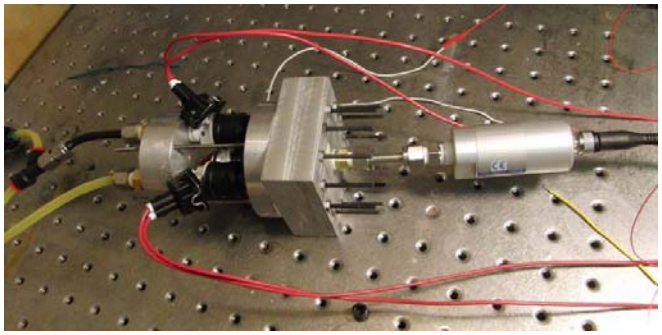

Fig. 5-11. Air/Fuel Injection Test Setup

One of the injectors was opened for 250 milliseconds and the pressure rise in the test chamber was recorded. This is longer than the expected injection time of the compressor prototype, which is around 20 ms, due to the fact that the downstream volume in the test is much larger than the combustion chamber volume of the HIFLPC. This larger volume allowed for a higher precision test. Simulation of the injection test was performed to tune the ξ, ω_n, and c_{ck_flap} model parameters.

Figure 12 shows the modeled versus measured pressure response with an upstream driving pressure of 647kPa. Figure 13 shows the results for a smaller driving pressure of 431 kPa. This is a representative range for the reservoir air pressure during HIFLPC operation.

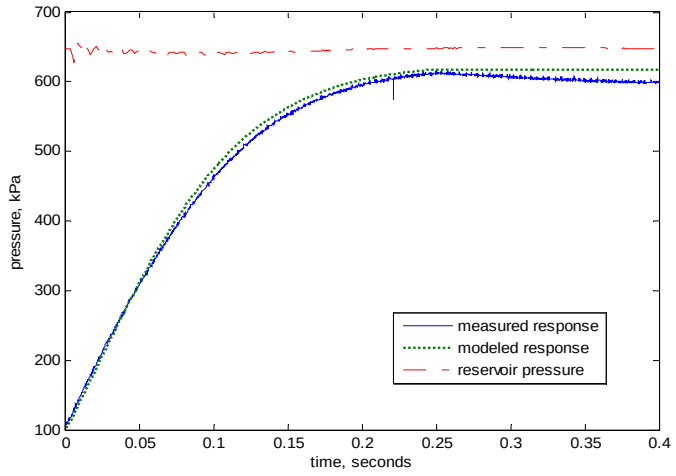

Figure 5-12. Measured vs. modeled response of the air and fuel injectors for a driving pressure of 647 kPa (79.2 psig)

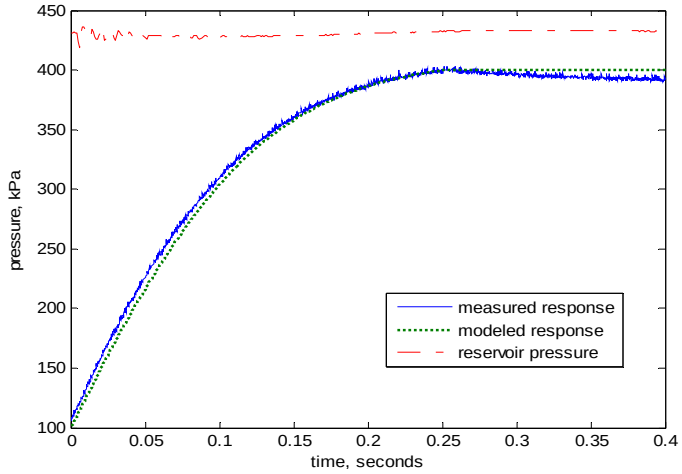

Figure 5-13. Measured vs. modeled response of the air and fuel injectors for a driving pressure of 431 kPa (47.9 psig)

From this model study, the effective cross-sectional area of the air and fuel injector is taken to be $a_{A/F}$ = 1.82 mm^2 and the response natural frequency is determined to be ω_n=785 rad/sec with $\xi = 1$. The check valve function, c_{ck_flap}, was empirically determined (Eq 36) and is plotted in Fig. 14.

$$c_{ck\_flap} = \begin{cases} 0 & \Delta P < P_{crack} \\ \sqrt{\dfrac{\Delta P - P_{crack}}{P_{full} - P_{crack}}} & P_{crack} \le \Delta P < P_{full} \\ 1 & \Delta P \ge P_{full} \end{cases} \qquad (36)$$

where P_{crack} is 27.58 kPa and P_{full} is 393.0 kPa.

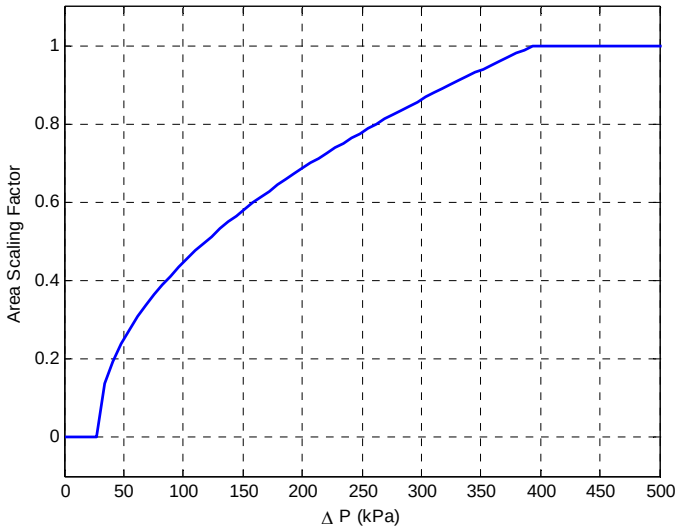

Fig. 5-14. Empirical determination of metal-flap check valve influence on air and fuel injectors

Compressor Section Pump Check Valve

As discussed in section 2, the dynamic characteristics of the pump check valve chosen for the new device will be crucial in optimizing pumping performance. Like the other valves in the model, flow through the pump check valve is modeled by Equations (30) and (31). However, the a_j term determining the piston's open/close dynamics are represented as the lumped parameter second-order model as shown in Equation (37) and (38).

$$M_{ck}\ddot{x}_{ck} + b_{ck}\dot{x}_{ck} + k_{ck}(x_{ck} - x_o) = \Delta P A_{ck} \tag{37}$$

where

$$a_j = 2\pi r_{ck} x_{ck} \quad \text{and} \quad a_{j,\max} = A_v \tag{38}$$

M_{ck}, k_{ck}, and A_{ck} are directly measured from the check valve, while b_{ck} is calculated using an assumed damping ratio ξ_{ck}. When installed, the spring has an initial

compression x_o. Table 1 lists values and descriptions of the parameters used in the pump check valve model.

(a)  (b) 

Fig. 5-15: (a) Pump check valve piston and spring. (b) Check valve location in compression chamber.

Table 5-1. Measured pump check valve dimensions

Parameter	Value	Description
M_{ck}	0.0184 kg	Mass of check valve piston
k_{ck}	583.2973 N/mm	Spring constant for pump check valve spring
ξ_{ck}	0.05	Damping ratio for pump check valve (estimate)
r_{ck}	5.56 mm	Radius of check valve face area
A_{ck}	97.0 mm^2	Piston face area of check valve
A_v	110.84 mm^2	Maximum flow-through area of check valve piston
x_o	6.5 mm	Initial (minimum) spring compression

5.6 HIFLPC System Model simulation

A complete system model of the HIFLPC device was implemented in MATLAB/Simulink comprising all component and subsystem models developed in

sections 3 through 5, namely: the control volume dynamics of Equations (14), (15), and (16), the liquid piston dynamics as modeled with equation (8), the heat rate input of combustion modeled with Eq. (28), and all mass flow and valve dynamic models as described in Eq.'s (30), (31), and (32). The HIFLPC model incorporates the experimentally determined model dynamic parameters of section 5, summarized in Table 2.

Table 5-2. Summary of component model parameters

Parameter	Value	Description
$K_{tot,piston}$	(see Eq. 33)	Stiffness curve for liquid piston diaphragms
f_{piston}	0.15	Friction factor used for liquid piston viscous loss term, R
$a_{A/F,tot}$	1.82 mm^2	Air and fuel valve maximum cross-sectional area
$\omega_{n,A/F}$	785 rad/sec	Air and fuel valve response natural frequency
c_{ck_flap}	(see Eq. 36)	Metal-flap check valve adjustment to air and fuel valve response
a_{in}	28.01 mm^2	Compression chamber intake valve cross-sectional area
$\omega_{n,IN}$	785 rad/sec	Compression chamber intake valve response natural frequency
a_{exh}	78.54 mm^2	Exhaust valve maximum cross-sectional area
$\omega_{n,exh}$	785 rad/sec	Exhaust valve response natural frequency
ξ_{valve}	1	Damping ratio assumed for all valves
M_{ck}	0.0184 kg	Mass of pump check valve piston
k_{ck}	583.2 N/mm	Spring constant for pump check valve spring
ξ_{ck}	0.05	Damping ratio for pump check valve (estimate)
r_{ck}	5.56 mm	Radius of pump check valve face area
a_{ck}	97.0 mm^2	Piston face area of pump check valve
$a_{v,ck}$	110.84 mm^2	Maximum flow-through area of pump check valve piston
$x_{o,ck}$	6.5 mm	Initial (minimum) pump check valve spring compression

The model used to generate the simulation results shown in this section was given the piston dimensions and control volume sizes listed in Table 3 (corresponding to the HIFLPC experimental prototype developed in [15].)

Table 5-3: Physical Parameters overview of HIFLPC model:

Parameter	Value	Description
A_1	2026.8	Cross-sectional area of hemispherical liquid piston region that mates to combustion chamber with diaphragm.
A_3	2026.8	Cross-sectional area of hemispherical liquid piston that mates to combustion chamber with diaphragm.
A_2	285.02	Cross-sectional area of high-inertance tube of liquid piston
L_2	1828.8	Length of high-inertance tube of liquid piston
I	$6.404\times10^6\, kg/mm^4$	Calculated inertance of liquid piston
$D_{diaphragm}$	50.8 mm	Diaphragm diameter
D_{comb}	50.8 mm	Combustion chamber inner diameter?
D_{comp}	50.8 mm	Compressor chamber diameter
V_{res}	517000 mm^3	Volume of reservoir

Simulation results

Figure 16(a) shows simulated pressures for the combustion, compression, and reservoir control volumes of the HIFLPC model for an individual cycle. Dynamic volumes of the combustion and compression chamber are shown in Fig. 16(b). The cycle begins with injection of air and fuel into the combustion chamber, which begins to expand slightly. When injection is complete ignition occurs, and the ensuing combustion pressure spike accelerates the liquid piston. The piston motion decreases the compressor chamber volume, raising the pressure up to and over that of the reservoir, allowing for

pumping through the pump check valve. The air and fuel injection duration of 20.5 *msec* was set to fully pump the compressor air charge into the reservoir.

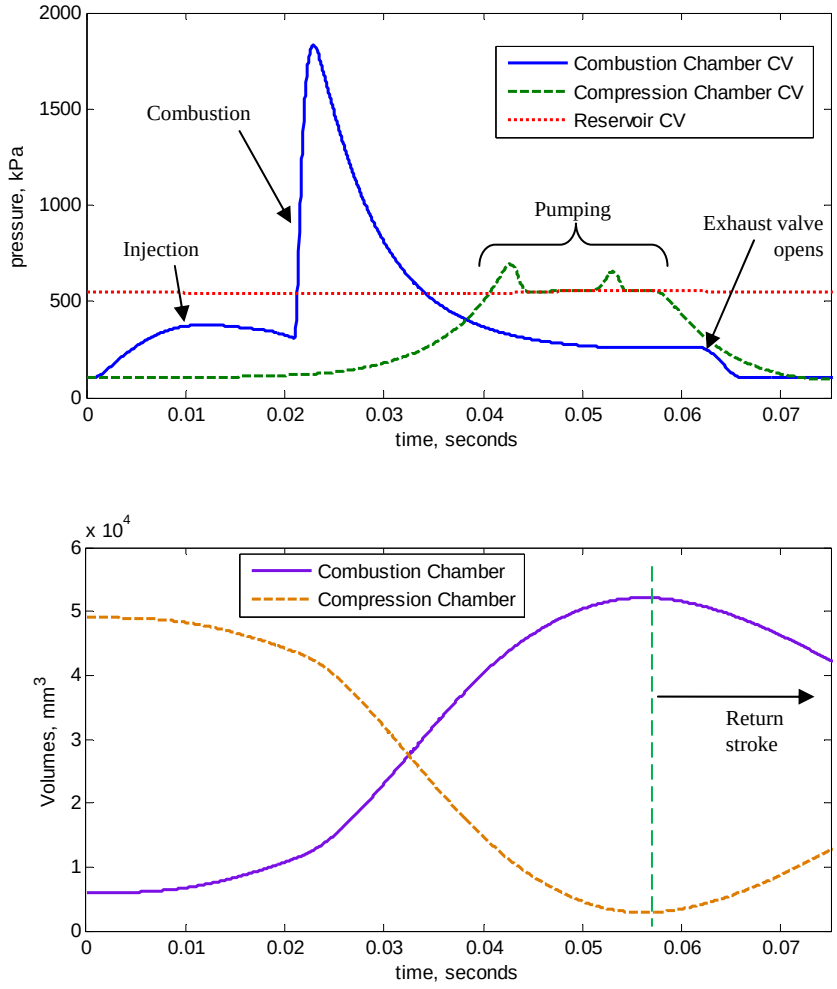

Figure 5-16. (a) Control volume pressures for simulated HIFLPC cycle.
(b)Volumes of the combustion and compression chamber during cycle

On the engine side of the device, the expansion of the combustion chamber volume during the injection cycle is dynamically held by piston inertance to maintain an air/fuel pressure at the point of ignition of around 350 kPa, demonstrating that the piston

dynamics can be used to achieve an effective pressure "compression ratio" of around 3.5, which corresponds to an effective volumetric compression ratio of 2.4 for an engine with 100% volumetric efficiency.

For the compressor section of the device, the inertance of the piston dictates the speed of the pump stroke, and thus the mass flow rate of air from the compression chamber to the reservoir through the pump check valve. Simulated results of this mass flow rate, shown in Fig. 17, indicate that the piston stroke is slow enough to effectively eliminate any backflow into the compressor chamber due to check valve dynamics.

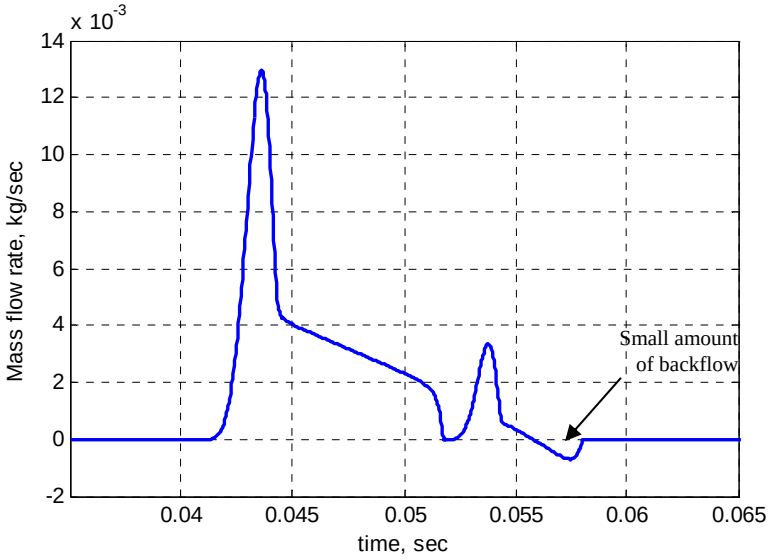

Figure 5-17. Mass flow from reservoir to compression chamber

Another important function of the piston's dynamic behavior can be seen by observing where energy is stored in the system during the cycle. Fig. 18 shows the potential energy in each of the HIFLPC control volumes, along with the piston kinetic energy and the energy stored in the piston diaphragms as a function of time. It can be

seen that the load against combustion is primarily the piston inertia. Also, the dominant driver of the compression chamber pressure increase (particularly up to when pumping occurs) is the piston kinetic energy. These characteristics highlight the importance of the piston dynamics, which allow for an optimization of load matching between the engine side and compressor side of the device.

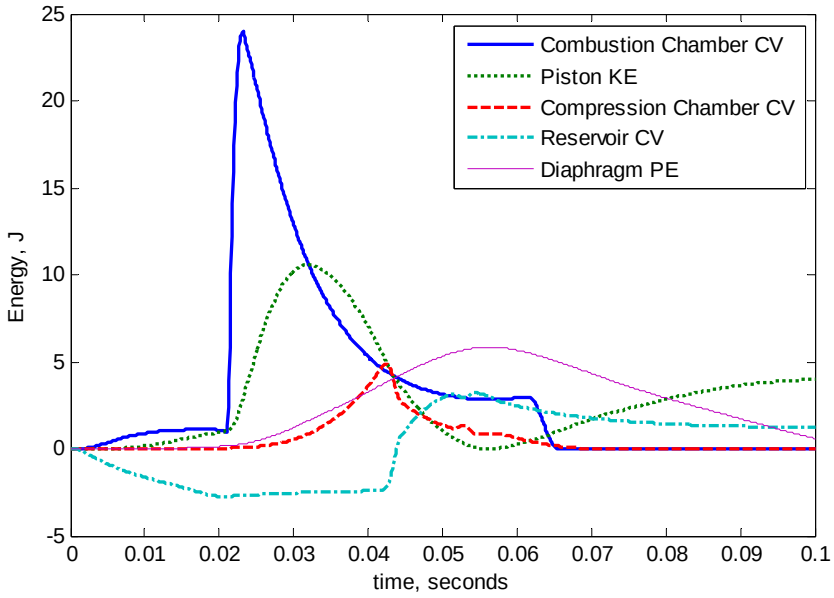

Figure 5-18. Energy storage in HIFLPC cycle

To demonstrate the system size and weight advantages of achieving the desired piston dynamics using a high inertance, consider that the simulated pump stroke duration of around 40 *msec* was achieved with a piston fluid mass of 0.61 kg. For a piston model with a cylindrical geometry, i.e., no inertance tube with small cross-sectional area, the piston would need to be 13 m long with a fluid mass of 26 kg to exhibit the same dynamic behavior.

5.7 Conclusions

The idea of using liquid inertance to dynamically tune the performance of a free piston engine was the impetus for the HIFLPC design. An inertance-based dynamic model for the liquid piston was developed, validated, and incorporated into a system model of the device. Critical model parameters for components and subsystems of the model were experimentally characterized independently for use in the system model. Simulations were performed that support the effectiveness of the liquid piston dynamics on overall performance of the HIFLPC. Specifically, the piston provides a desirable load against combustion, and its kinetic energy is well-matched to drive the compressor load.

Using the simulation results as a guide, Part 2 of this work (the companion paper [15]) describes the fabrication of an HIFLPC experimental prototype, which is evaluated experimentally and used to validate the dynamic system model.

5.8 References

[1] Dunn-Rankin, D., Leal, E. M., and Walther, D. C., (2005) "Personal Power Systems". *Progress in Energy and Combusion Scence*, vol. 31, pp. 422–465.

[2] Hirai, K., Hirose, M., Haikawa, Y., and Takenaka, T., (1998) "The Development of Honda Humanoid Robot," *Proceedings of the 1998 IEEE International Conference on Robotics & Automation (ICRA)*, Leuven, Belgium, pp. 1321-1326.

[3] Kuribayashi, K., (1993) "Criteria for the evaluation of new actuators as energy converters," *Advanced Robotics*, vol. 7, no. 4, pp. 289-37.

[4] Zhu, Y., Barth, E. J., (2008) “An energetic control methodology for exploiting the passive dynamics of pneumatically actuated hopping,”. *ASME Journal of Dynamic Systems, Measurement and Control*, vol. 130, issue 4, pp.041004-1 – 041004-11.

[5] Guihard, M. and Gorce, P., (2004) “Dynamic Control of a Large Scale of Pneumatic Multichain Systems,” Journal of Robotic Systems, vol. 21, no. 4, pp. 183-192.

[6] Goldfarb, M., Barth, E. J., Gogola, M. A., and Wehrmeyer, J. A., (2003) “Design and Energetic Characterization of a Liquid-Propellant-Powered Actuator for Self-Powered Robots,” *IEEE/ASME Transactions on Mechatronics*, vol. 8, no. 2, pp. 254-262.

[7] Fite, K. B., and Goldfarb, M., (2006) "Design and Energetic Characterization of a Proportional-Injector Monopropellant-Powered Actuator," *IEEE/ASME Transactions on Mechatronics*, vol. 11, no.2, pp. 196-204.

[8] Riofrio, J.A.; Barth, E.J. (2007) “Design and analysis of a resonating free liquid-piston compressor,” *ASME International Mechanical Engineering Congress and Exposition (IMECE).* IMECE2007-42369, Nov. 11-15, Seattle,Wa.

[9] Riofrio, J.A.; Barth, E.J. (2008) “Design and analysis of a resonating free liquid-piston compressor,” *ASME International Mechanical Engineering Congress and Exposition (IMECE).* IMECE2007-42369, Nov. 11-15, Seattle,Wa.

[10] Riofrio, J.A. (2007) “Design, modeling, and experimental characterization of a free liquid-piston engine compressor with separated combustion chamber,” Ph.D. Dissertation. Vanderbilt University. Print.

[11] Yong, C.; Barth, E.J.**,** (2009) “Modeling and control of a high pressure combined air/fuel injection system,” *ASME Dynamic Systems and Control Conference & Bath/ASME Symposium on Fluid Power and Motion Control*. DSCC2009-2769, pp. 1-8, October 12-14, Hollywood, CA.

[12] Annamalai, K., Puri, I. K., (2006) “Combustion Science and Engineering,” *CRC*, pp. 195-196.

[13] Richer, E., and Hurmuzlu, Y., “A High Performance Pneumatic Force Actuator System: Part 1 – Nonlinear Mathematical Model”. *ASME Journal of Dynamic Systems, Measurement and Control*, 122, September, 2000, pp. 416-425.

[14] Willhite, J. A. and Barth, E. J., “Experimental Characterization of Critical Dynamic Model Parameters for a Free Liquid Piston Engine Compressor,” *6th FPNI Ph.D. Symposium*, Purdue University, June 2010, to appear.

[15] Willhite, J. A. and Barth, E. J., (2011) “The high inertance free piston engine compressor
part 2: design and experimental evaluation,” *ASME Journal of Dynamic Systems, Measurement and Control*, to be submitted.

CHAPTER VI

MANUSCRIPT V

THE HIGH INERTANCE FREE PISTON ENGINE COMPRESSOR PART 2: DESIGN AND EXPERIMENTAL EVALUATION

Joel A. Willhite

Chao Yong

Eric J. Barth

Department of Mechanical Engineering

Vanderbilt University

Nashville TN 37235

To be submitted as a full journal paper to the *ASME Journal of Dynamic Systems, Measurement, and Control*.

6.0 Abstract

Pneumatically actuated robotic systems are attractive alternatives to traditional electromechanical systems due to the power density advantage of pneumatic actuators. This assumes that a power source is available to provide the pneumatic supply at a sufficient energy density to compete with batteries. To this end, a high inertance free liquid piston compressor (HIFLPC) was developed as a portable, efficient, compact power supply for pneumatically actuated systems. This paper presents the model-based design and operation of the HIFLPC, as well as the fabrication and evaluation of an experimental prototype of the device. Efficiency, power output, and other operational characteristics of the prototype are experimentally assessed. A validation of the dynamic model developed for the HIFLPC is conducted, and model-based studies are performed to investigate the influence on system performance by varying liquid piston dynamics.

6.1 Introduction

The use of free piston engines for compressors is not a new idea. In fact, the first free piston machine designed by Pescara [1] in 1928 was used as an air compressor. Free piston engine compressors were used through the mid-twentieth century, such as the Junkers-designed compressor used in German submarines [2]. Other applications for the technology were investigated, such as gas generators for use in automobiles [3,4] and small power plants. However, the lack of adequate sensing and control technology led to the free piston engine being largely abandoned after 1960 [5]. Modern electronic controls available today have led to a second generation of free piston engine research. Most of this research, however, uses free piston engine technology for hydraulic pumps

[6,7] and small-scale electrical power generators [8,9,10], not as air compressors. An extensive review of both early free-piston engine compressor and gas generator applications as well as the recent resurgence in research in free piston hydraulic pumps and linear alternators has been conducted by Mikalsen et al [11].

Interest in free piston air compressors has also recently resumed for the purpose of providing a compact, energy-dense, untethered power source for pneumatically actuated autonomous human-scale robotic systems. A free piston engine that uses a hydrocarbon fuel to produce a pneumatic supply is an attractive method to achieve this goal due to the high specific energy density of the fuel. For example, propane has an energy density of 46,350 kJ/kg, which is nearly two orders of magnitude greater than the storage potential of state-of-the-art batteries (Li-ion batteries have an energy density approaching 700 kJ/kg [12]). However, the conversion process from petrochemical potential to cool compressed gas is relatively complex; conventional commercially available engines and compressors at the size scale of interest have efficiencies that are prohibitively low. Figure 1 shows the energetic transductions from stored potential to mechanical output power for both battery/servomotor and propane/pneumatic actuator scenarios. Assuming an actuator efficiency of 50% (see Goldfarb, et al [13],) the pneumatic system will outperform the traditional electromechanical system by more than a factor of 2 if the engine compressor could attain a 5.4% conversion efficiency. Even if the pneumatic system only matches the energy density of batteries, the significantly lower weight of pneumatic actuators over DC servomotors for equivalent actuation power (i.e., significantly higher power density) makes such a system desirable.

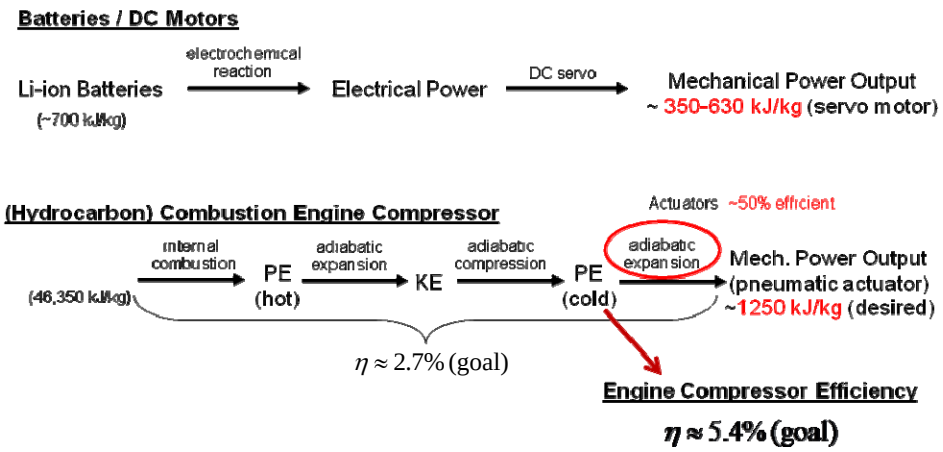

Figure 6-1. Comparison of energy transductions from storage to mechanical output power for batteries/DC motors and for a free piston compressor.

With this goal in mind, a dynamic model of a High Inertance Free Liquid Piston Compressor (HIFLPC) was developed and presented in the companion paper, Part 1 [14]. This work (Part 2) continues by investigating the HIFLPC idea experimentally. Section 2 of this work is an overview of the design and basic operation of the HIFLPC system. Section 3 describes in detail the fabrication and experimental setup of the HIFLPC prototype, whose performance is assessed in section 4. Validation of the dynamic model from Part 1 using experimental data is discussed in section 5, and section 6 is a model-based simulation study of device performance over a range of liquid piston dynamic behaviors.

6.2 Basic Operation of the HIFLPC

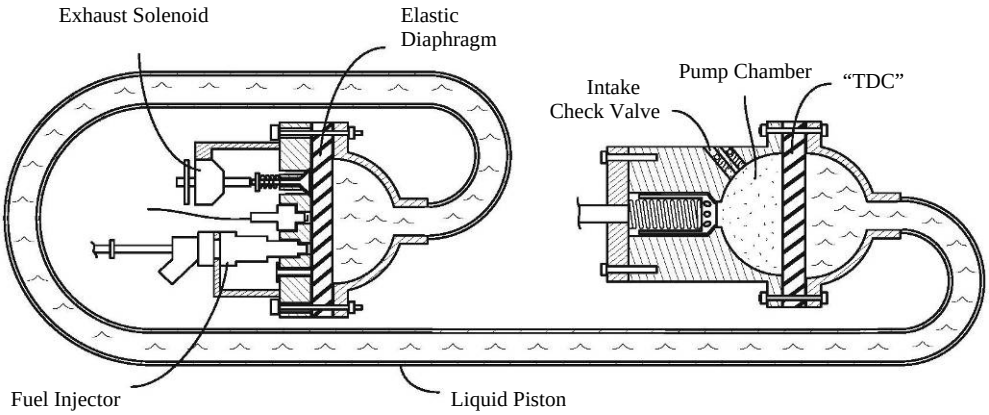

Figure 6-2(a). Schematic of HIFLPC at effective TDC

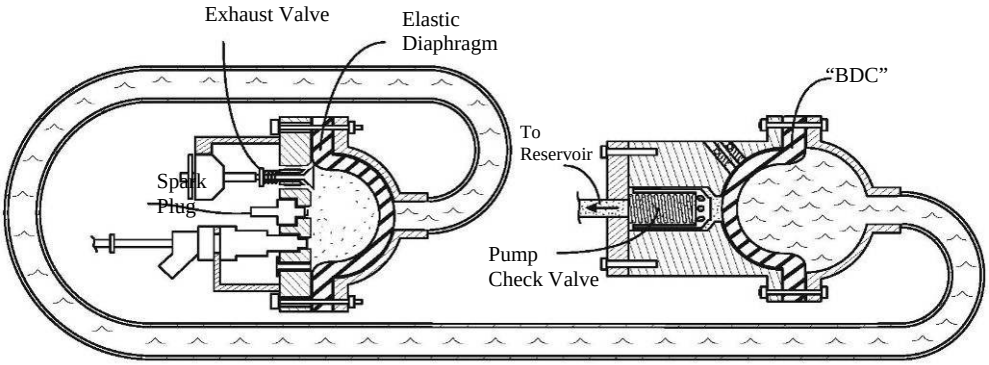

Figure 6-2(b). Schematic of HIFLPC at effective BDC

Figure 2 shows two schematic representations of the HIFLPC design, with key features labeled. Figure 2(a) shows device orientation just before the power stroke of the engine, when the liquid piston diaphragms are relaxed. This is analogous to Top Dead Center (TDC) in conventional engines. The power stroke begins with injection of

pressurized air from the system reservoir and pressurized gaseous fuel, causing the elastic diaphragm to begin to stretch and the combustion chamber volume to increase. The dynamic inertial load of the liquid piston limits the expansion so that injection and ignition can occur without an appreciable drop in air/fuel pre-combustion pressure. This dynamic process eliminates the need for a compression stroke. The mixture then combusts, rapidly increasing the pump chamber volume and converting the heat released during combustion into kinetic energy of the liquid piston. On the compressor side of the piston, this kinetic energy is used to compress and pump the air from the pump chamber. Once the pump chamber air pressure exceeds the reservoir pressure, the pump check valve opens and mass flow into the reservoir occurs. Figure 2(b) illustrates the configuration of the device at the moment pumping is completed, similar to conventional Bottom Dead Center (BDC). At this point, the combustion exhaust valve is opened and the piston diaphragms begin to relax, reversing the flow direction of the liquid piston. During this return stroke, exhaust is expelled from the combustion chamber and fresh air enters the pump chamber through a check valve. Note that diaphragm stiffness is the only driver of the return stroke. Once the piston has returned to its original TDC position, the cycle can be repeated.

The lack of a compression stroke allows the engine compressor to “fire on demand”- that is, there is no need to have a starting routing or maintain an idle cycle. This allows the HI-FLPC to operate at varying frequencies by controlling the delay between TDC and the command for air/fuel injection.

6.3 Prototype Fabrication and Experimental Setup of the HIFLPC

An experimental prototype of the HIFLPC device, shown in Fig. 3, was fabricated for performance evaluation and dynamic model validation. The device as configured for testing has an approximate weight of 2.6 kg, with a footprint of around 18" by 18" with the liquid piston configuration shown. Note that the overall shape of the system can be customized for particular applications by the orientation and shape of the liquid piston.

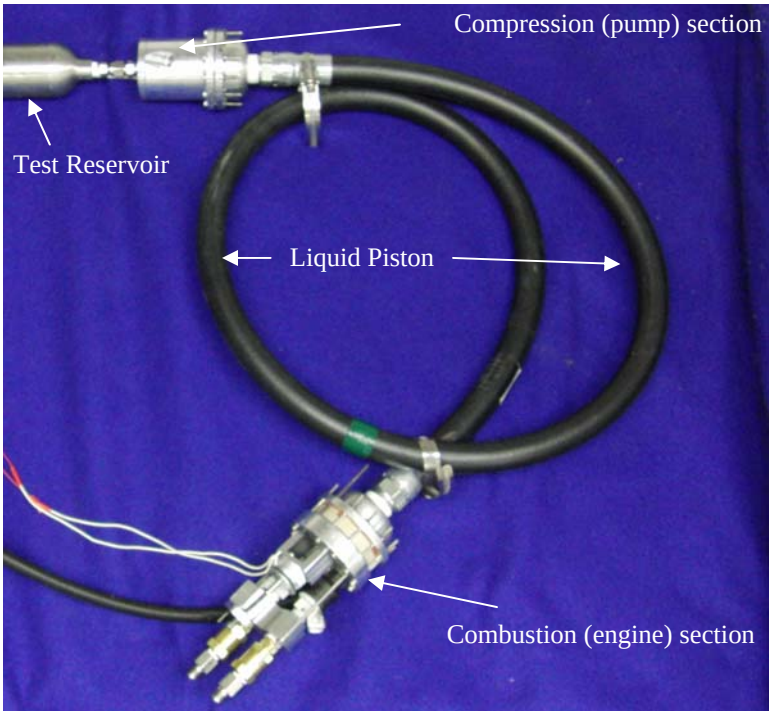

Figure 6-3. Assembled HIFLPC Prototype

Combustion section

Figure 4(a) shows the exterior side of the combustion head assembly. Visible in this view are the two *Bosch 0 280 150 846 CNG* air and fuel injectors, the *Ledex 124911-028* solenoid that opens the exhaust valve, and the *NGK ME8* spark plug. Figure 4(b)

shows the interior side of the combustion head that mounts directly to the piston diaphragms. The commercially available model airplane engine exhaust valve is manually open. Figure 4(c) is also an interior view of the combustion head, showing the position of the pressure sensor and the metal-plate check valve flaps used to prevent backflow through the air and fuel injectors.

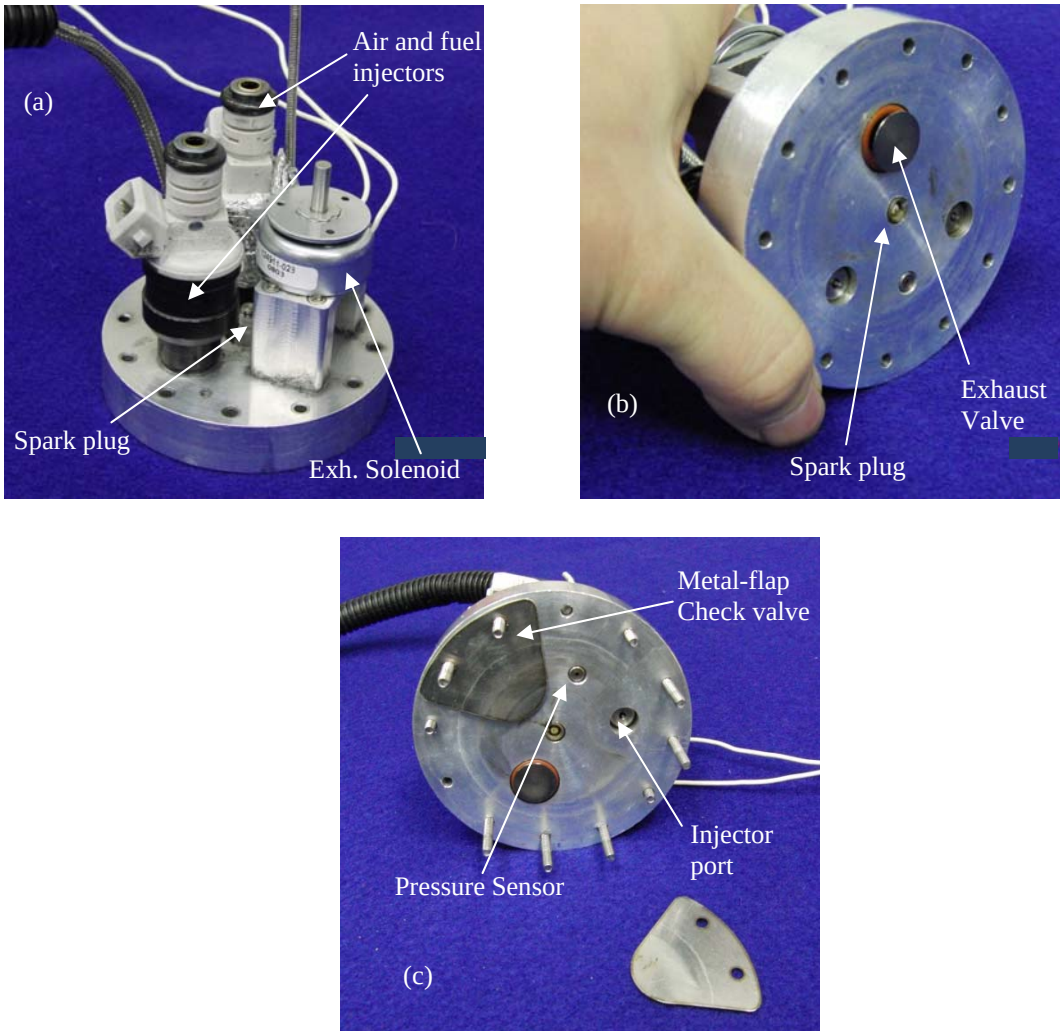

Figure 6-4. (a) Top view of combustion head. (b)interior view of combustion head with exhaust valve open. (c) interior view showing check valves for injectors

Compressor Assembly

The compressor section of the prototype is shown in Fig 5(a) and (b). View (a) shows the ports for sending pumped air to the reservoir and for fresh air intake during the return stroke of the piston. The interior view of the compression chamber is shown in 5(b), with the pump check valve, intake check valve, and pressure sensor labeled. Note that the pump check valve port is protected by a wire mesh that prevents the diaphragm from protruding into the check valve port.

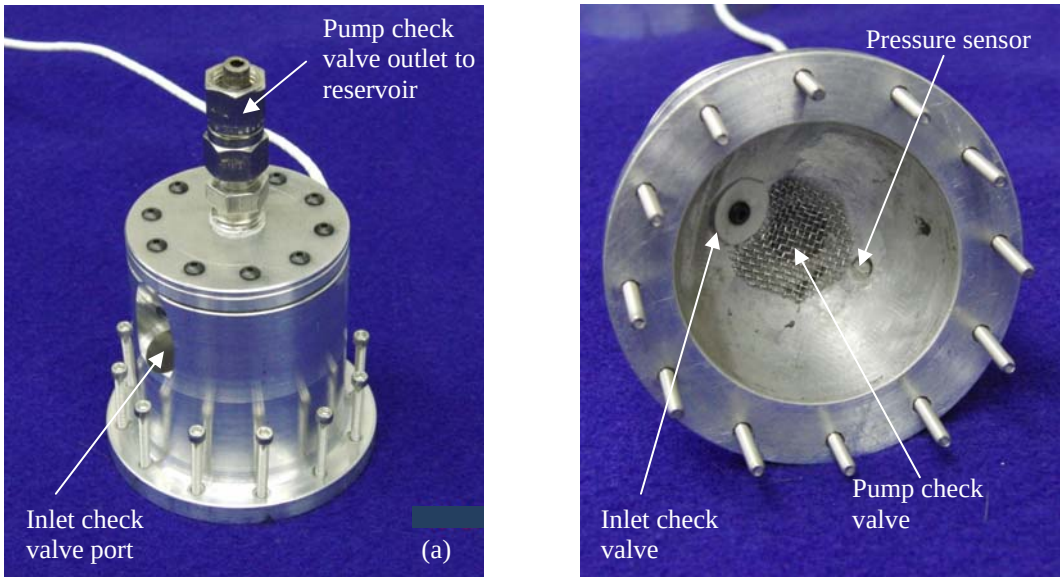

Figure 6-5. a) Compressor section. b)Interior view of compressor section.

3.3 Liquid piston assembly

The liquid piston as described in Part 1 of this work [14] is shown in Fig. 6. The hemispherical regions on each end of the piston mate to the compressor section and combustion section, respectively, through the piston diaphragm, serving to transition the fluid's cross-sectional area from that of the diaphragms to that of the inertance section. A

Parker Parflex model *540N-12* hydraulic hose is used for the high inertance region of the piston.

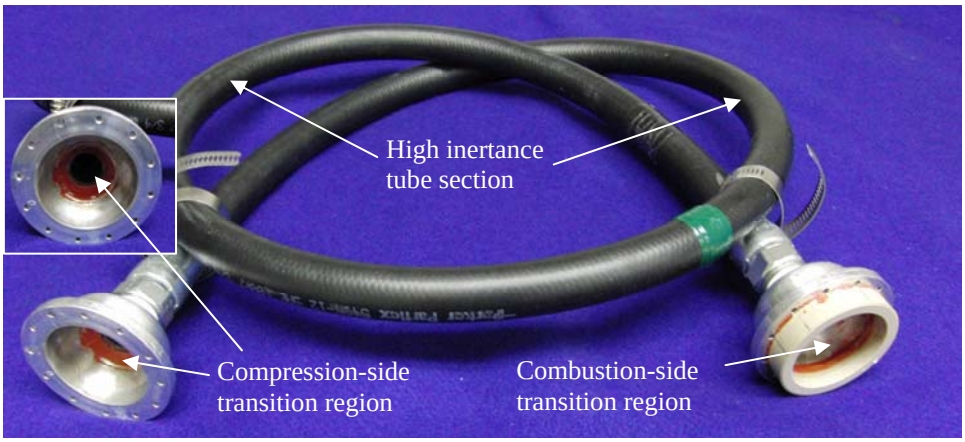

Figure 6-6. Liquid piston housing

Critical physical parameters of prototype

Table 1 lists critical physical parameters of prototype components. The liquid piston dimensions were sized based on an optimization discussed in Willhite [15].

Table 6-1: Physical Parameter overview of HIFLPC prototype:

Parameter	Value	Description
A_1, A_3	2026.8	Cross-sectional area of hemispherical liquid piston region that mates to combustion chamber with diaphragm.
A_2	285.02	Cross-sectional area of high-inertance tube of liquid piston
L_2	1828.8	Length of high-inertance tube of liquid piston
I	$6.40\times10^{6}\,kg/mm^{4}$	Calculated inertance of liquid piston
$D_{diaphragm}$	50.8 mm	Diaphragm working diameter
D_{comb}	50.8 mm	Combustion chamber inner diameter
D_{comp}	50.8 mm	Compressor chamber diameter

V_{comp}	$5.40\times10^{4}\,mm^{3}$	Compressor chamber initial volume
V_{res}	$5.17\times10^{5}\,mm^{3}$	Volume of reservoir

Experimental Test set-up

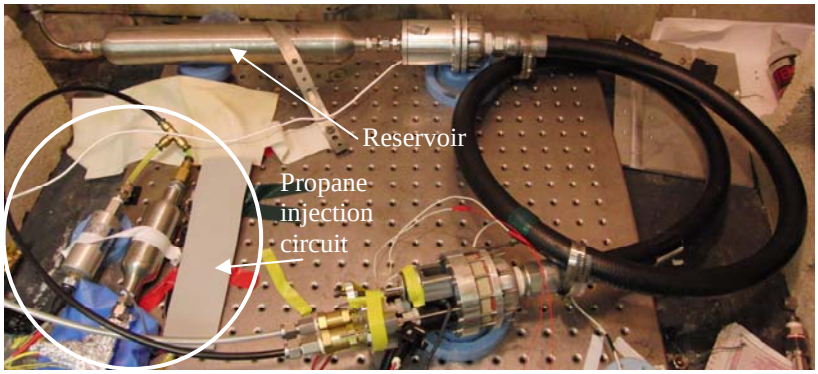

Figure 6-7. HIFLPC test configuration.

The test configuration of the HIFLPC system is shown if Fig. 7, with reservoir and fuel injection circuit. Recall that the reservoir tank not only receives pressurized air from the compressor, it also routs a portion of that air back to the air injector on the engine to be mixed with fuel. Propane is supplied to the fuel injector via the injection circuit, a schematic of which is shown in Figure 8. The propane source is a standard 16.4 oz. propane tank for small outdoor stoves (*Coleman model #5103B164T*.) Since injecting propane at its vapor pressure would result in injection durations too short for the injector valve to achieve, an intermediate "buffer tank" is used for the propane supply upstream of the injector. A 2-way solenoid vale (*Parker Series 9*), driven by a simple on/off controller, regulates the buffer tank propane pressure (measured by a *Festo SDE-16-10V* sensor.)

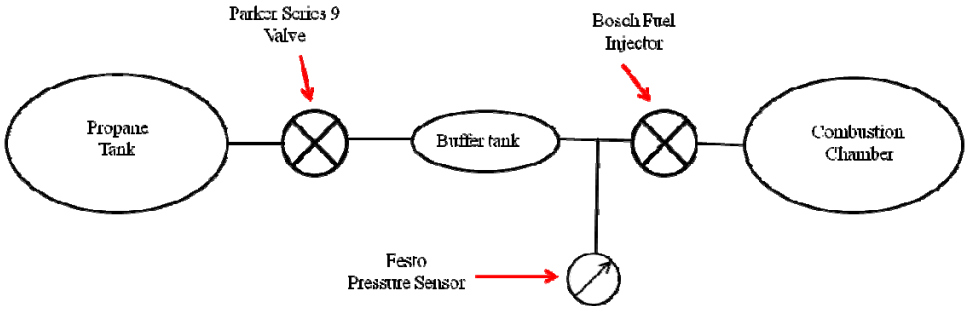

Fig. 6-8. Fuel injection circuit

MATLAB/Simulink's Real-Time Workshop was used to send (open-loop) control signals to the drivers of the active valves and spark ignition, as well as to acquire the pressure data (sampled at 10kHz) from the combustion chamber, compression chamber, and reservoir. The pressure data was acquired with an *Optrand AutoPSI* pressure sensor (model *C22294-Q*) installed in the combustion chamber, a *Kulite XTL190-300A* pressure sensor installed in the compression chamber, and a *Festo SDE-16-10V* sensor measuring reservoir pressure.

6.4 Performance Assessment

Performance tests of the device were conducted at an operating frequency of 4 Hz, as dictated by the (open-loop) controlled timing of the valves and spark. Figure 9 is a representation of the signal timing used for data collection, tuned for consistent cycle-to-cycle operation of the HIFLPC at the tested reservoir loads. The vertical axis only indicates on/off with slight offsets to distinguish the signals.

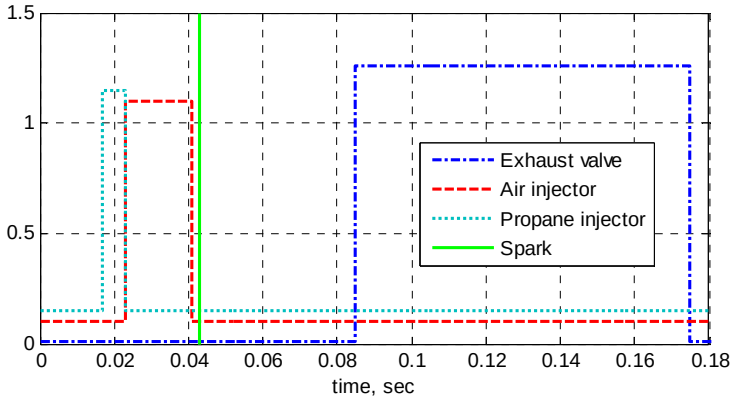

Figure 6-9. Signal timing for prototype operation

Fig. 10 shows measured pressures versus time for (a) the combustion chamber, (b) compression chamber, and (c) reservoir during device operation. The data reflects consistent cycle-to-cycle combustion events, resulting in a reservoir pressure increase from 542 to 589 *kPa* (about 64 to 71 *psig*) over a period of 3.5 seconds. This performance data will be used for the efficiency and power assessments of the device conducted in section 4.2, as well as the dynamic model comparison in section 5.

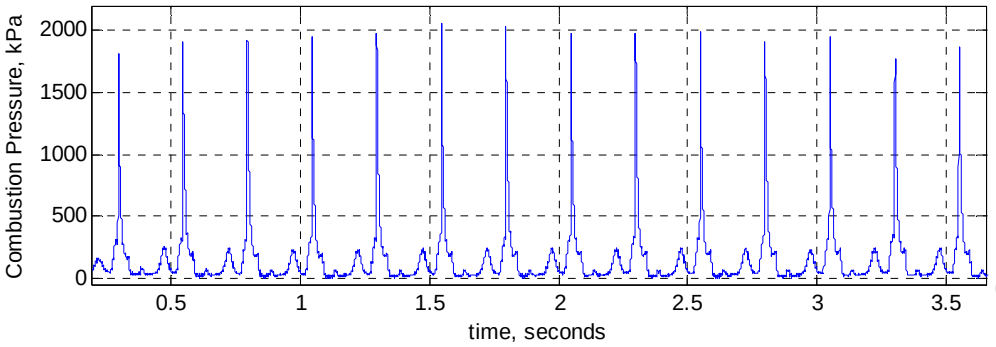

(a)

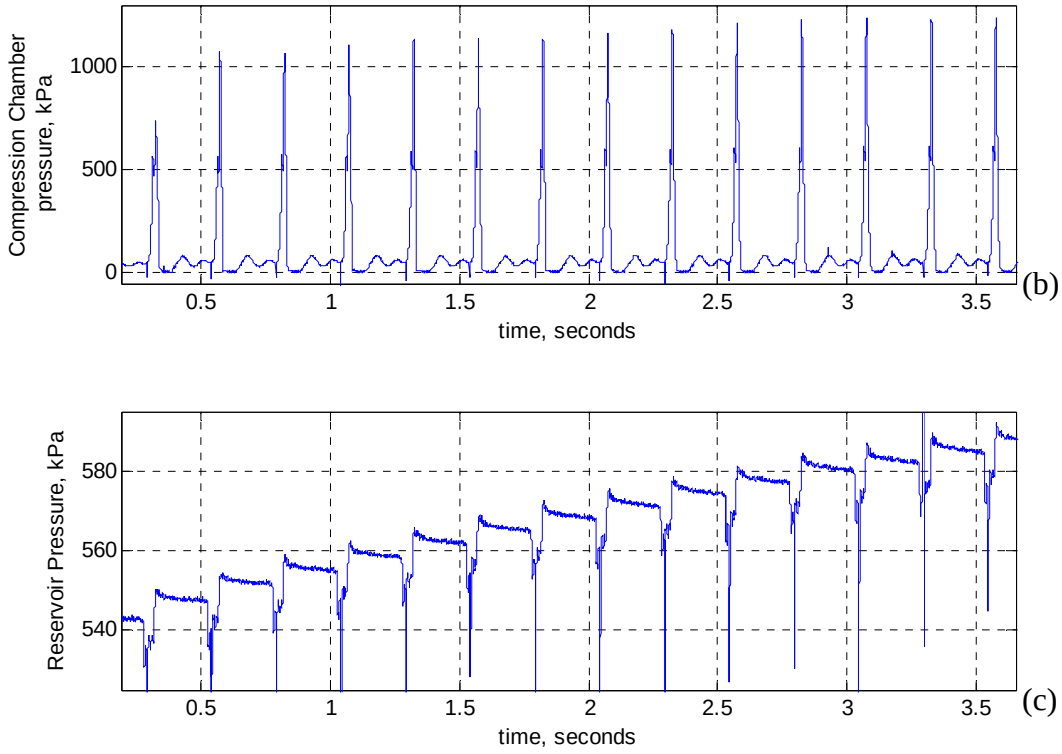

Fig. 6-10 Measured pressures for HIFLPC operation at 4 Hz for the (a) Combustion chamber, (b) Compression chamber, and (c) reservoir

Efficiency and power calculations

The efficiency of the HIFLPC can be calculated on a per cycle basis by Eq (1):

$$\eta_{cycle} = \frac{E_{out}}{E_{in}} = \frac{(E_{res,f} - E_{res,i})}{E_{propane}} \tag{1}$$

where $E_{res,i}$ and $E_{res,f}$ are the reservoir pneumatic potential energies before and after the cycle, respectively, $E_{propane}$ is the amount of petrochemical potential of the mass of propane injected for combustion (the lower heating value). The pneumatic potential of the reservoir is considered to be the amount of work that can be done by fully expanding a pressurized ideal gas:

$$E_{res} = W_{\exp} = \int_{V_{res}}^{V_{atm}} P dV \tag{2}$$

Whether the expansion of reservoir air should be considered adiabatic or thermal (or somewhere between) depends on the characteristics of the pneumatic actuators that would be the end users of the pneumatic supply delivered by the HIFLPC. Therefore, two efficiencies will be calculated for the device, one based on adiabatic reservoir potential, $E_{res,adb}$, and one based on isothermal potential, $E_{res,iso}$.

Assuming adiabatic behavior,

$$PV^{\gamma} = \text{constant} \tag{3}$$

Eq (2) can be written as:

$$E_{res,adb} = \frac{P_{res} V_{res}}{1-\gamma_{air}} \left[\left(\frac{P_{res}}{P_{atm}} \right)^{\frac{1-\gamma_{air}}{\gamma_{air}}} - 1 \right] \tag{4}$$

Given that, for isothermal expansions,

$$PV = \text{constant} \tag{5}$$

the reservoir potential can be written as:

$$E_{res,iso} = P_{res} V_{res} \ln\left(\frac{P_{res}}{P_{atm}} \right) \tag{6}$$

Figure 11 shows reservoir pressure data for one cycle of the device operation as seen in Fig 10. This cycle will be used in the following example for calculating the adiabatic and isothermal HIFLPC efficiencies.

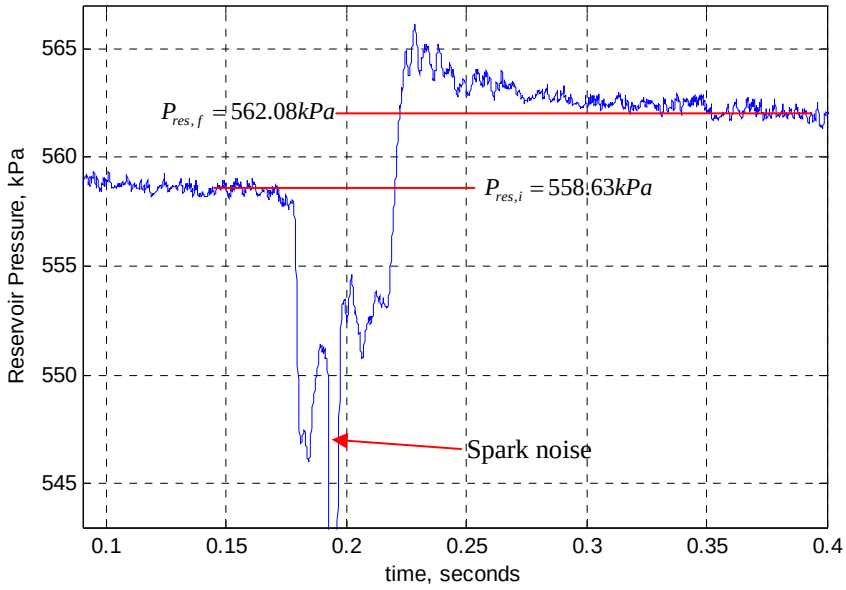

Fig. 6-11. Single cycle reservoir pressure gain

Using the initial and final pressures noted in Fig. 11, the adiabatically determined net energy gain in the reservoir for the pump cycle shown is calculated as follows in Eq.'s (7), (8), and (9):

$$E_{res,adb,i} = \frac{(558.63kPa)(5.17\times10^{6}\,mm^{3})}{1-\gamma_{air}}\left[\left(\frac{(558.63kPa)}{(P_{atm})}\right)^{\frac{1-\gamma_{air}}{\gamma_{air}}} - 1\right] = 279.2 \text{ Joules} \quad (7)$$

$$E_{res,adb,f} = \frac{(562.08kPa)(5.17\times10^{6}\,mm^{3})}{1-\gamma_{air}}\left[\left(\frac{(562.08kPa)}{(P_{atm})}\right)^{\frac{1-\gamma_{air}}{\gamma_{air}}} - 1\right] = 281.7 \text{ Joules} \quad (8)$$

$$\boxed{E_{out,adb} = E_{res,adb,f} - E_{res,adb,i} \approx 2.5 \text{ J}} \quad (9)$$

Equations (10), (11), and (12) show calculation of the reservoir isothermal potential gain for this cycle:

$$E_{res,iso,i} = (558.63kPa)(5.17\times10^{6}\,mm^{3})\ln\left(\frac{(558.63kPa)}{P_{atm}}\right) = 493.0 \text{ Joules} \quad (10)$$

$$E_{res,iso,f} = (562.08kPa)(5.17\times10^{6}\,mm^{3})\ln\left(\frac{(562.08kPa)}{P_{atm}}\right) = 497.8 \text{ Joules} \quad (11)$$

$$\boxed{E_{out,iso} = E_{res,iso,f} - E_{res,iso,i} \approx 4.8 \text{ J}} \quad (12)$$

Determining the energy investment of the fuel, $E_{propane}$, is not trivial, due to the small amount of propane injected per cycle. However, during cycles in which the propane injection circuit's regulating valve (see Fig. 8) does not open to allow flow from the propane source, the mass of propane injected can be determined by measuring the pressure drop in the fixed-volume propane buffer tank (once again assuming ideal gas):

$$m_{propane} = \frac{(P_{propane,i} - P_{propane,f})V_{buffer}}{R_{propane}T_{propane}} \quad (13)$$

For this cycle, the regulating valve was not opened, and the propane buffer tank pressures before and after injection are presented in Fig. 12. From this data, the mass of propane for this cycle is calculated to be:

$$m_{propane} = 1.562\times10^{-6} \text{ kg} \quad (14)$$

Therefore, the potential of the fuel can then be calculated as:

$$E_{propane} = m_{propane}e = 72.4 \text{ J} \quad (15)$$

where e is the specific energy density of propane (46,350,000 J/kg), calculated from the lower heating value of the fuel.

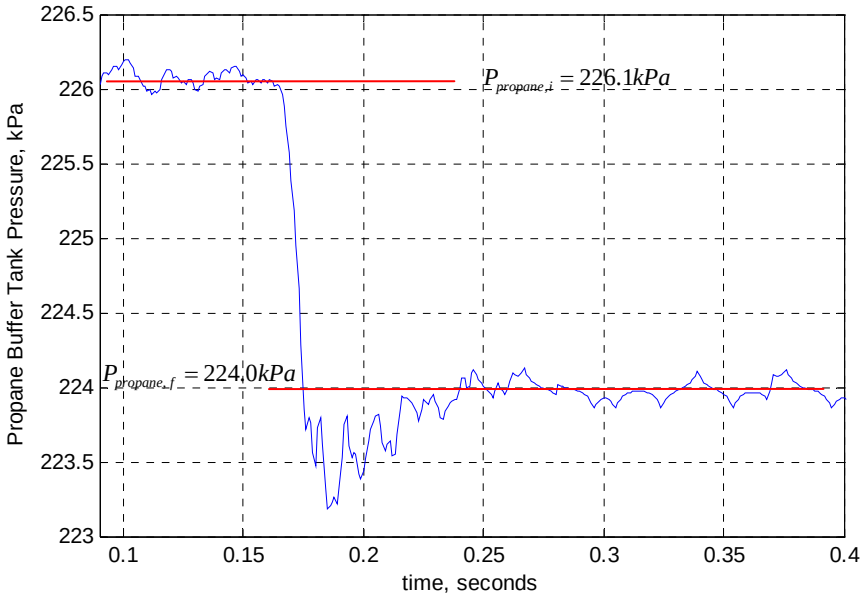

Fig. 6-12. Fuel circuit buffer tank pressure for one cycle

Using Eq. (1), the isothermal and adiabatic efficiencies for this cycle are determined:

$$\eta_{cycle,adb} \approx \frac{2.4J}{72.4J} = 3.45\% \tag{16}$$

$$\eta_{cycle,iso} \approx \frac{4.8J}{72.4J} = 6.63\% \tag{17}$$

For the performance data shown in Fig. 10, the first ten cycles shown (from 0 to 2.5 sec) occurred without the propane regulating valve opening, so the efficiency calculation method used in the above example was valid for for all ten cycles. The efficiency over these ten cycles were calculated:

$$\eta_{avg,adb} = 3.35\%, \text{ and } \eta_{avg,iso} = 6.26\% \tag{18}$$

Average power output was also calculated for the same ten cycles, given 4 Hz operating frequency:

$$P_{avg,adb} = 9.6\,\text{W}, \text{ and } P_{avg,iso} = 17.9\,\text{W} \tag{19}$$

6.5 Dynamic Model Validation

This section compares the experimentally measured data of section 4 to simulation results of the HIFLPC dynamic model. The model used for this comparison is described in of Part 1 of this work [14], with the addition of the parameter tuning discussed in section 5.1.

Model parameter tuning with system performance data:

Due to their dependence on complicated system interactions, some model parameters could not be characterized on a sub-systems level as discussed in Part 1 [14]. Observed pressure data of HIFLPC prototype operation was necessary to determine these parameters, which are described below and whose values are summarized in Table 2.

The *K* and *A* empirical parameters of the combustion model (see section 4.2 of Part 1 [14]) were tuned to match combustion pressure test data. This is typically done in combustion modeling since the pre-combustion factor and the activation energy each have a fairly broad range for a given fuel. An additional parameter, C_{H_r}, was introduced to scale ΔH_r, the energy potential of the injection air and fuel mass, to account for a non-ideal (i.e., not stoichiometric) mass ratio or incomplete mixing in the chamber.

To match the observed drops in measured reservoir pressure, and thus reservoir pneumatic potential, due to heat loss from the higher temperature of the pumped gas, the following simple heat loss model for the reservoir control volume was implemented:

$$\dot{Q}_{res} = H_{res} A_{res} \left(T_{res} - T_{atm} \right) \tag{20}$$

where A_{res} is the surface area of the reservoir, and H_{res} is the heat transfer coefficient.

The final parameter estimated using system performance data was initial volume of the combustion chamber when injection begins, $V_{comb,i}$. Physically, this parameter adjusts for both plastic deformation of the piston diaphragms (observed in testing, but not severe), and displacement of the piston from its resting state due to oscillatory piston motion left over from the previous cycle. In other words, $V_{comb,i}$ sets an initial condition on the displacement of the liquid piston. This parameter is crucial for properly modeling the mass investment of injection, as well as the total initial volume of fresh intake air in the compression chamber at the beginning of the pump stroke.

Table 6-2. Model parameter values determined from HIFLPC test data

Parameter	Value	Description
K	2600	Pre-combustion factor for combustion model
A	$27.5\,K$	Combustion model constant (activation energy divided by univeral gas constant)
C_{H_r}	0.62	Scaling factor for ΔH_r
A_{res}	$5.03\times10^{3}\,mm^2$	Surface area of reservoir
H_{res}	$3976\ \ kW/(mm^2K)$	Heat transfer coefficient for reservoir heat loss model
$V_{comp,i}$	$5.398\times10^{4}\,mm^3$	Compressor chamber initial volume

Model comparison and implications

Fig. 13 presents simulated pressures in each modeled control volume alongside the measured pressures of the device for two single cycles at different reservoir pressures. The following behaviors of the modeled pressures agree well with measured data: 1) overall stroke duration, 2) the combustion pressure peaks, 3) combustion chamber expansion (indicated by pressure profile, 4) the pressure rise in the compression chamber,

5) time at which the pump check valve opens, 6) the duration of pumping into the reservoir, 7) initial pressure drop in the reservoir due to expansion, and 8) the overall rise in reservoir pressure from pumping.

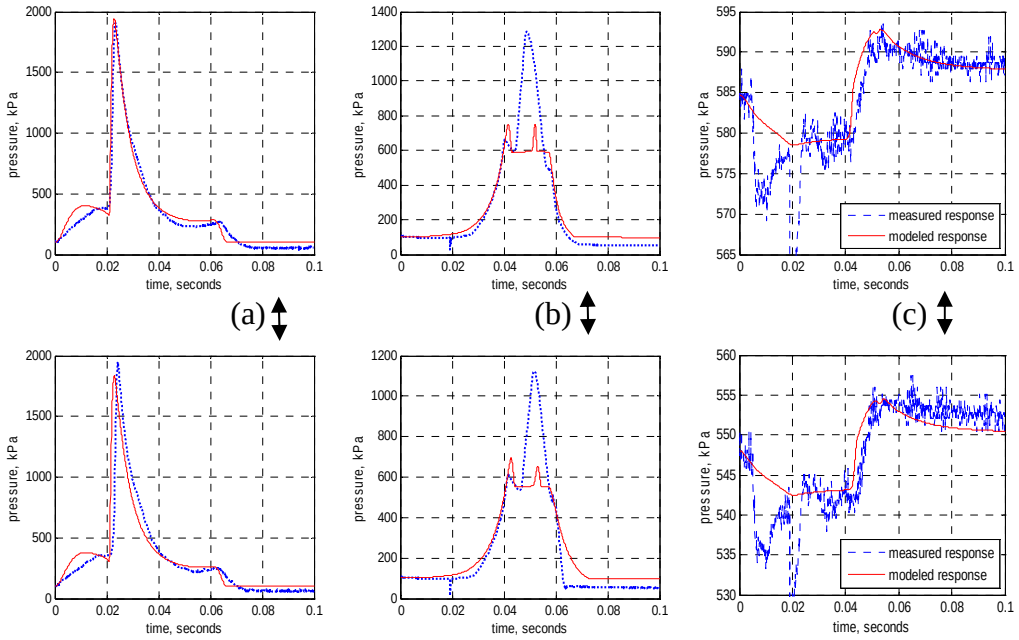

Figure 6-13. Modelled and experimentally measured pressure data for two reservoir loads: (a) combustion chamber pressure. (b) compression chamber pressure. (c) reservoir pressure

During the injection phase, the measured combustion section pressure profile indicates unmodeled effects. A possible explanation for this result is that the initial dead volume at injection may be changing due to piston motion. As discussed in section 5.1, the model allows for an initial condition on piston position, but not initial piston velocity. However, since the combustion, expansion, and compression dynamics agree well with measured data, it is assumed that the modeled mass of air and fuel injected is consistent with injection in the physical prototype.

The large spike in compressor chamber pressure measured in testing can be attributed to the pressure sensor location. It is assumed that the small dead volume where the sensor is recessed becomes sealed and compressed by the piston diaphragm late in the pump stroke.

An accurate model allows for investigation of otherwise unmeasurable states, such as transient mass flows. For example, modeled pump check valve mass flow can suggest backflow from the reservoir (or lack thereof) at the end of the pump stroke.

6.6 Model-based Study of Liquid Piston Dynamics

Simulation studies similar to those described in [14] were performed to determine the relative sensitivity of the dynamic characteristics of the piston on performance of the HIFLPC. These simulations separately varied the liquid piston's length, L_2, and its cross-sectional area, A_2, in order to investigate their individual effects on efficiency and power density of the device. Figure 14 shows simulation results for the maximum power density and (adiabatic) system efficiency by varying liquid piston cross-sectional area A_2, with the prototype design point shown for reference. Maximum power density is calculated from the potential energy gain of the reservoir per stroke, the max operating frequency based on pump and return stroke duration, and the total mass of the prototype (adjusting for the varying mass of piston liquid for each simulation due to the area change.) The only other model parameter adjusted was the air and fuel injection duration, which was set for each simulation to fully pump the air charge in the compressor chamber into the reservoir.

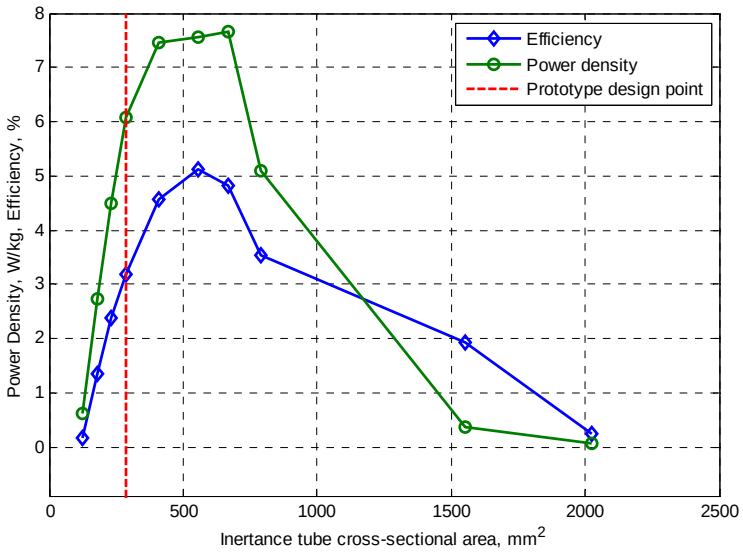

Figure 6-14. Maximum power density and efficiency versus inertance by varying liquid piston cross-sectional area, A_2

Contrary to expected trade-offs between power and efficiency, the HIFLPC's performance characteristics cause coinciding power density and efficiency peaks, which are desirable and quite uncommon for engines. The decline from the peak value in power density as A_2 decreases from about 559 mm^2 (inertance increasing) is a result of the lengthening of the pump stroke duration. The drop in efficiency with decreasing A_2 is primarily a result of an increase in piston viscous losses necessitating more fuel investment to fully pump the charge of air in the compression chamber. For increasing values of A_2, the downward trend from peak efficiency and power density is the result of two main factors. The first and most dominant factor is on the pump side: the piston dynamics become too fast for the pump check valve to close in time, allowing for some backflow of reservoir air into the pump chamber. The second factor is that the decreasing inertance provides less dynamic load on air/fuel injection, resulting in a lower pressure of

the air/fuel mass input just before combustion. This is similar to a smaller compression ratio in a traditional four stroke engine. Fig. 14 implies that lowering the inertance of the piston by increasing cross-sectional area A_2 by around a factor of two (from 285 to $559\,mm^2$) would yield efficiency and power density gains as compared to the tested device, all other parameters being equal.

Fig. (15) shows the simulation results of varying piston tube length, L_2 while holding A_2 at the dimension of the experimental prototype. Once again, the dropoff in efficiency and power density for lower inertances (smaller L_2 values) is due to the inability of the pump check valve to react fast enough to the piston dynamics. Power density decreases from the peak value as L_2 increases due to longer pump stroke durations, and efficiency drops again due to added viscous losses. One implication of Fig. 15 is that decreasing inertance by increasing tube length will not help power density or efficiency, as it did with adding cross-sectional area.

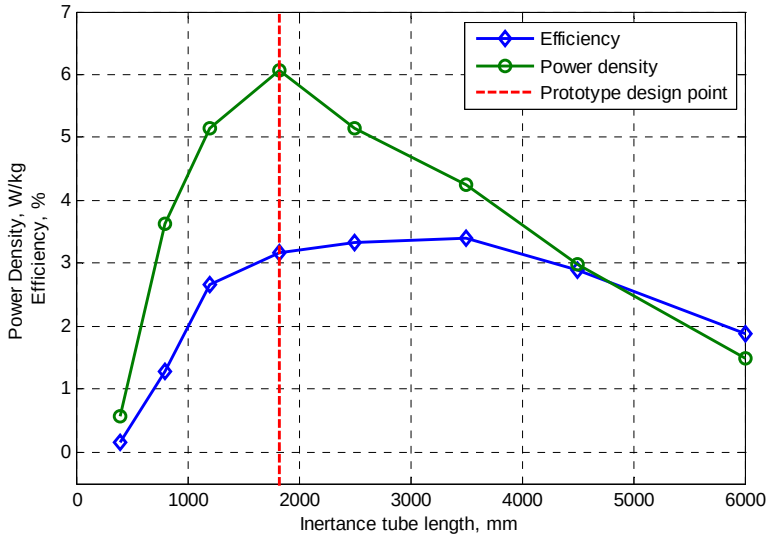

Figure 6-15. Maximum power density and efficiency versus inertance by varying liquid piston inertance tube length

Variations of diaphragm stiffness were also simulated to investigate the effects on performance (Fig. 16.). As expected, efficiency decreases as stiffness increases due to the extra input energy needed from combustion to fully expand the diaphragms during the pump stroke. Also as expected, power density increases as stiffness increases up to the prototype diaphragm stiffness due to the faster return stroke. The drop in power density for stiffnesses higher than the design point are due to the fact that full pumping can no longer occur. This phenomenon arises from the fact that the increased mass of air and fuel required due the high stiffness cannot be injected fast enough to maintain a pre-combustion pressure and compressure chamber volume necessary for effective combustion.

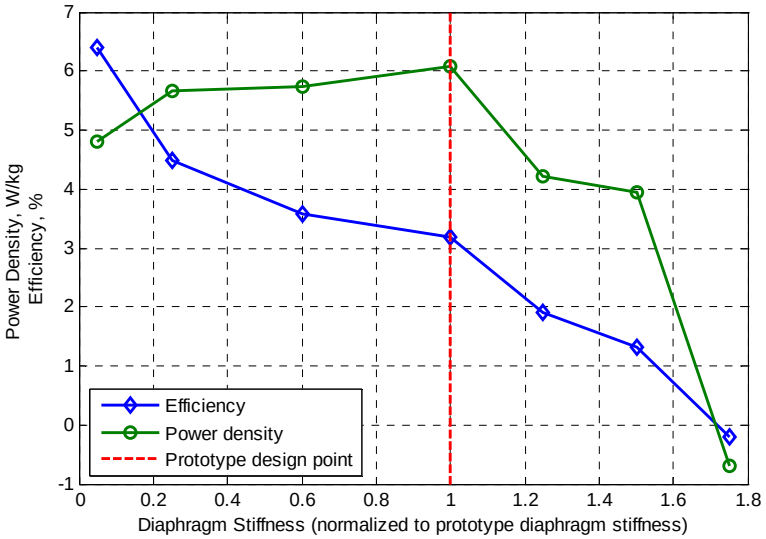

Figure 6-16. Maximum power density and efficiency versus diaphragm stiffness

6.7 Conclusions

A model-based design for a high inertance liquid free piston engine compressor was developed in this work. An experimental prototype of the device was fabricated and experimentally evaluated. Consistent operation of the device was achieved, and efficiency and power output of the device as tested were assessed. Test data was used to validate the dynamic model developed for the device. Model-based studies investigated the effect of varying liquid piston dynamics on overall system performance. Future work for the HIFLPC will include the development of a closed-loop controller capable of achieving consistent and efficient operation of the device over a full range of reservoir loads.

The measured efficiency range of 3.45-6.63% suggests that pneumatic systems using the HIFLPC as a power source would exhibit system energy densities comparable to, if not better than, the best electromechanical systems. Combined with the inherent advantages of pneumatic actuators over DC servomotors, devices like the HIFLPC position pneumatically actuated systems as an attractive option for human-scale, untethered robotic systems.

6.8 References

[1] Pescara, R. P., (1928) “Motor Compressor Apparatus,” *U.S. Patent No. 1,657,641*.

[2] Nakahara, M., (2001) "Free Piston Kikai-Kouzou to Rekisi". Shinko-Techno Gihou, Vol.13, No. 25 & 26.

[3] Klotsch, P., (1959) “Ford Free-Piston Engine Development,” *SAE Technical Paper Series*, 590045, vol. 67, pp. 373-378.

[4] Underwood, A. F., (1957) “The GMR 4-4 ‘Hyprex’ Engine: A Concept of the Free-Piston Engine for Automotive Use,” *SAE Technical Paper Series*, 570032, vol. 65, pp. 377-391.

[5] Johansen, T. A.; Egeland, O.; Johannessen, E. A.; Kvamsdal, R, (2002) “Free-Piston Diesel Engine Timing and Control – Toward Electronic Cam- and Crankshaft,” *IEEE Transactions on Control Systems Technology*, vol. 10, no. 2, March, pp. 177 – 190.

[6] Beachley, N. H. and Fronczak, F. J., (1992) “Design of a Free-Piston Engine-Pump,” *SAE Technical Paper Series*, 921740, pp. 1-8.

[7] Achten, P. A., Van Den Oeven, J. P. J., Potma, J., and Vael, G. E. M. (2000) ‘Horsepower with Brains: the design of the CHIRON free piston engine,” *SAE Technical Paper* 012545.

[8] Aichlmayr, H. T., Kittelson, D. B., and Zachariah, M. R., (2002a) “Miniature free-piston homogenous charge compression ignition engine-compressor concept – Part I: performance estimation and design considerations unique to small dimensions,” *Chemical Engineering Science*, 57, pp. 4161-4171.

[9] Aichlmayr, H. T., Kittelson, D. B., and Zachariah, M. R., (2002b) “Miniature free-piston homogenous charge compression ignition engine-compressor concept – Part II: modeling HCCI combustion in small scales with detailed homogeneous gas phase chemical kinetics,” *Chemical Engineering Science*, 57, pp. 4173-4186.

[10] Aichlmayr, H. T., Kittelson, D. B., and Zachariah, M. R., (2003) “Micro-HCCI combustion: experimental characterization and development of a detailed chemical kinetic model with coupled piston motion,” *Combustion and Flame*, 135, pp. 227-248.

[11] Mikalsen, R., and Roskilly, A. P., (2007) "A Review of Free-Piston Engine History and Applications," *Applied Thermal Engineering*, vol. 27, pp. 2339-2352.

[12] (2007) “Overview of lithium ion batteries,” Panasonic. Website. http://www.panasonic.com/industrial/includes/pdf/Panasonic_LiIon_Overview.pdf

[13] Fite, K. B., and Goldfarb, M., (2006) "Design and Energetic Characterization of a Proportional-Injector Monopropellant-Powered Actuator," *IEEE/ASME Transactions on Mechatronics*, vol. 11, no.2, pp. 196-204.

[14] Willhite, J. A. and Barth, E. J., (2011) “The high inertance free piston engine compressor
part 1: dynamic modeling,” *ASME Journal of Dynamic Systems, Measurement and Control*, to be submitted.

[15] Willhite, J. A. and Barth, E. J., (2010) “Optimization of liquid piston dynamics for efficiency and power density in a free liquid piston engine compressor.” *Bath/ASME Symposium on Fluid Power & Motion Control* (FPMC 2010), Bath, UK

CHAPTER VII

RECOMMENDATIONS

7.1 Testing Recommendations

Operation of the prototype of the HIFLPC design developed in this work was demonstrated and evaluated in Chapter 6. Much work went into the test setup used for data acquisition and control of the device's active elements. The following is a list of suggestions to aid future testing for HIFLPC devices based on problems that were encountered and addressed during the testing process.

Achieving steady operation

One aspect of operation not predicted in the model was residual oscillation of the piston between cycles, leading to non-ideal initial compression chamber volumes at the time of injection which adversely affect combustion. For the testing in this work, this piston action was controlled by careful adjustment of exhaust timing, specifically exhaust duration and when the exhaust valve closes in relation to the next injection of fuel and air. Other suggestions that might mitigate this problem are: careful adjustment of the frequency of operation to coincide with injecting air and fuel when the combustion chamber approaches a minimum; incorporating a hemispherical inner surface of the combustion head to maintain diaphragm stiffness at the initial piston position, helping to hold the combustion chamber volume small at the beginning of the cycle.

Minimizing sensor noise by isolating high-current components

Noise problems (leading to large DC offset jumps) were a big issue with the Optrand pressure sensor used in the compression chamber. This was due to a confluence of the inductive behaviour of the spark plug and injector coils located near the sensor on the engine head. The following are recommendations for mitigating such sensor noise problems: if automotive-type injectors are used, use "peak and hold" driving circuit using a chip such as the *LM-1949* will help isolate the "peak" current used to force open the valve; isolate the high currents produced in the ignition and valve circuits from their control signal paths with opto-isolators, such as the *MCT-62*; take care in providing direct ground paths for active components, especially the spark plug.

Sizing maximum compression volume larger than pump volume

The transition section of the piston from the combustion head diaphragm to the high inertance tube should have an available volume for diaphragm expansion (i.e., combustion chamber volume expansion) that is larger than the initial volume of the compression chamber. This will ensure the ability to fully pump compressor air, even when the diaphragm expansion might not be of a regular shape (see next paragraph.)

Close examination of piston diaphragm motion

A transparent piston transition section on the combustion side, along with a transparent compressor section, would allow for visual examination of piston motion. Piston position at the initiation of operating cycles could be verified, and diaphragm mode shape behavior during the pump and return stroke could be analyzed.

APPENDIX A

MATLAB SIMULINK DIAGRAMS

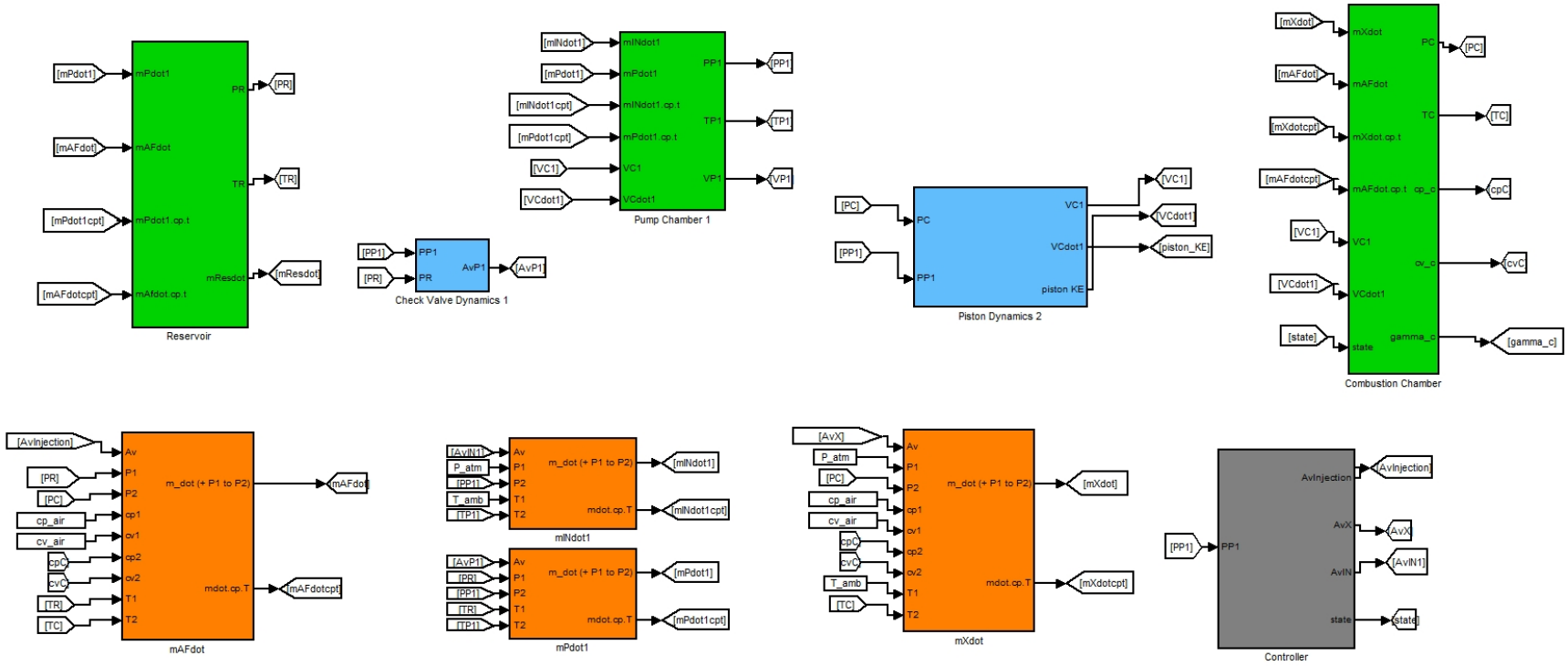

Figure A-1: MATLAB Simulink system block diagram of HIFLPC

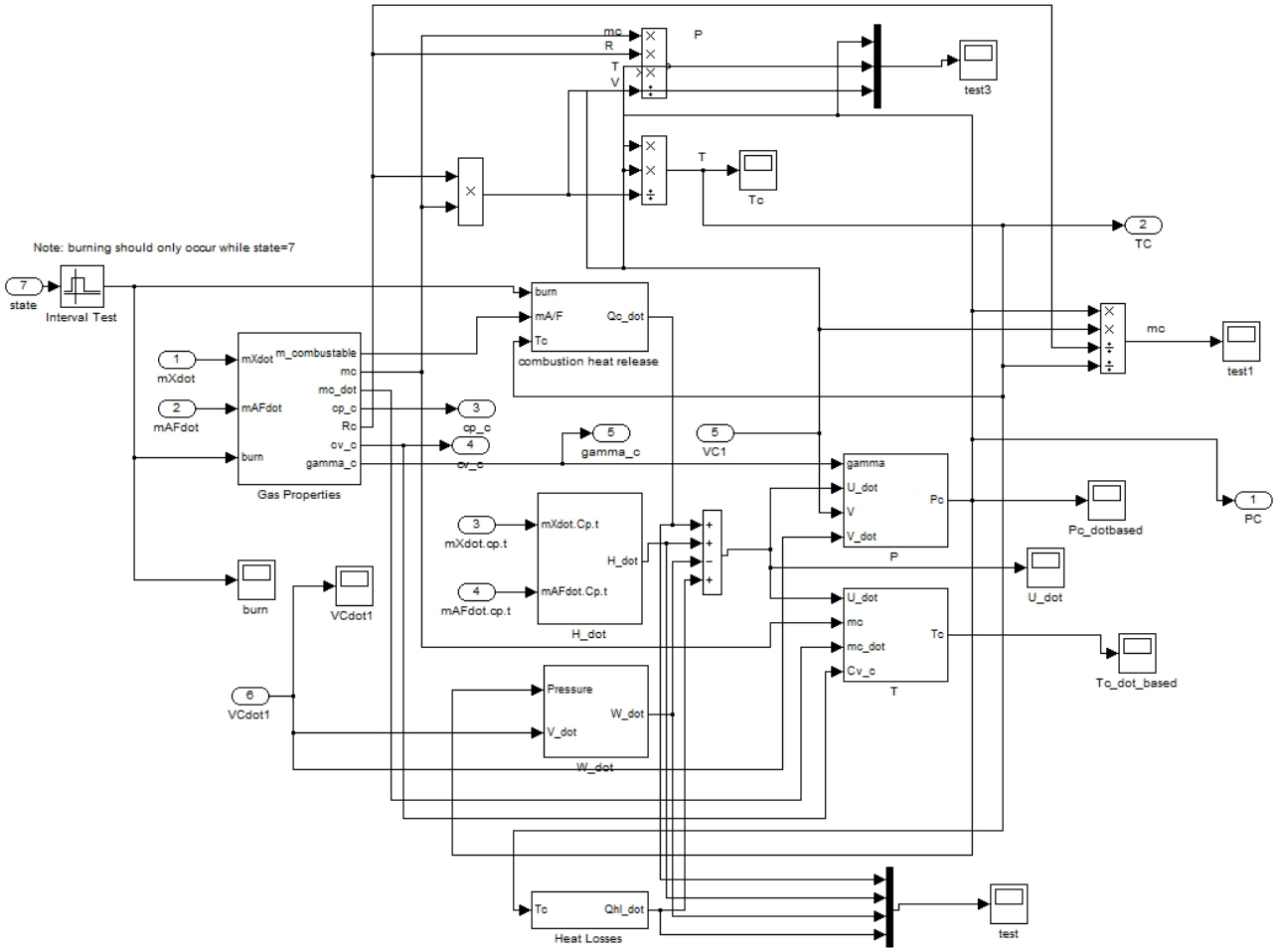

Figure A-1-1: Combustion Chamber Block

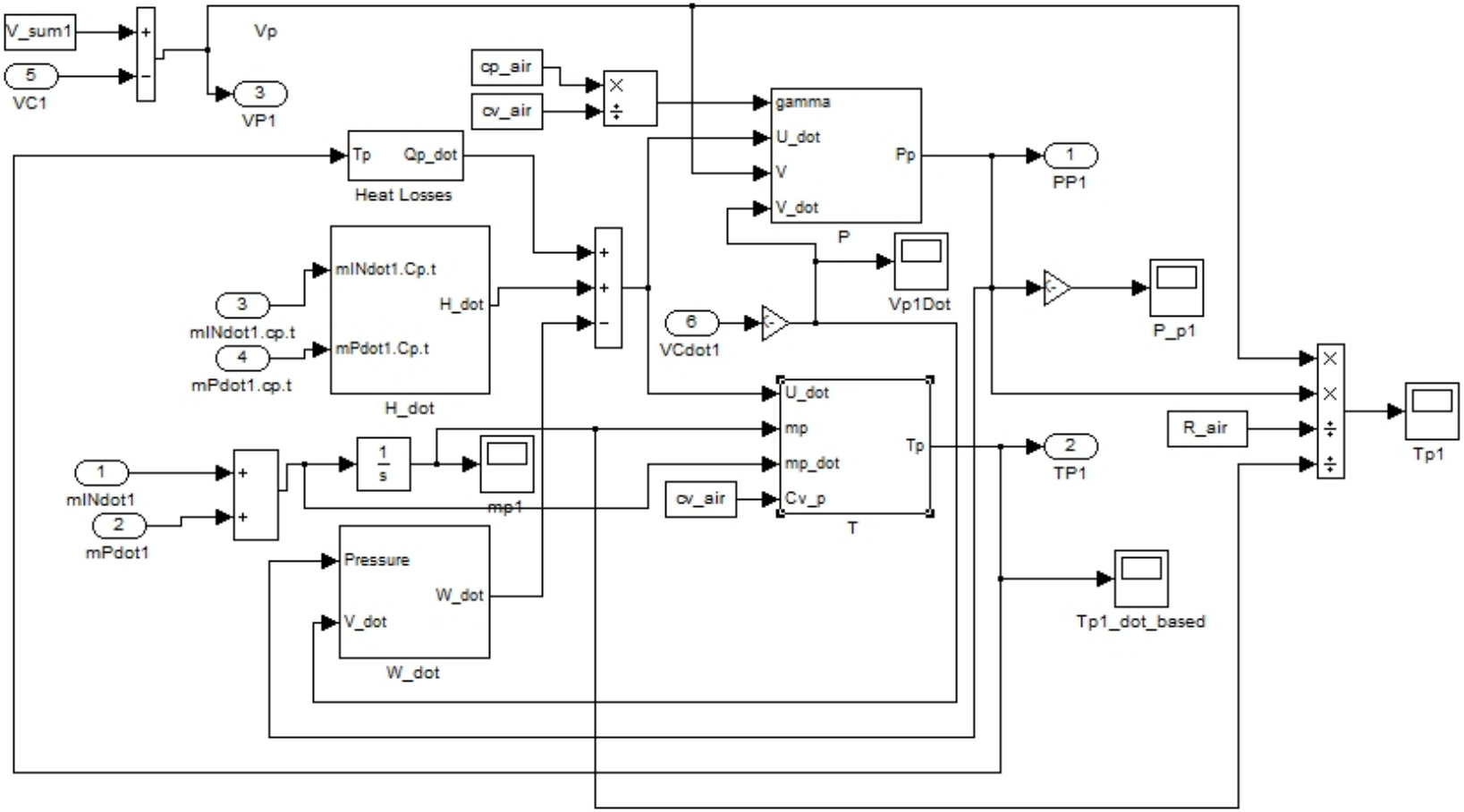

Figure A-1-2: Pump Chamber Block

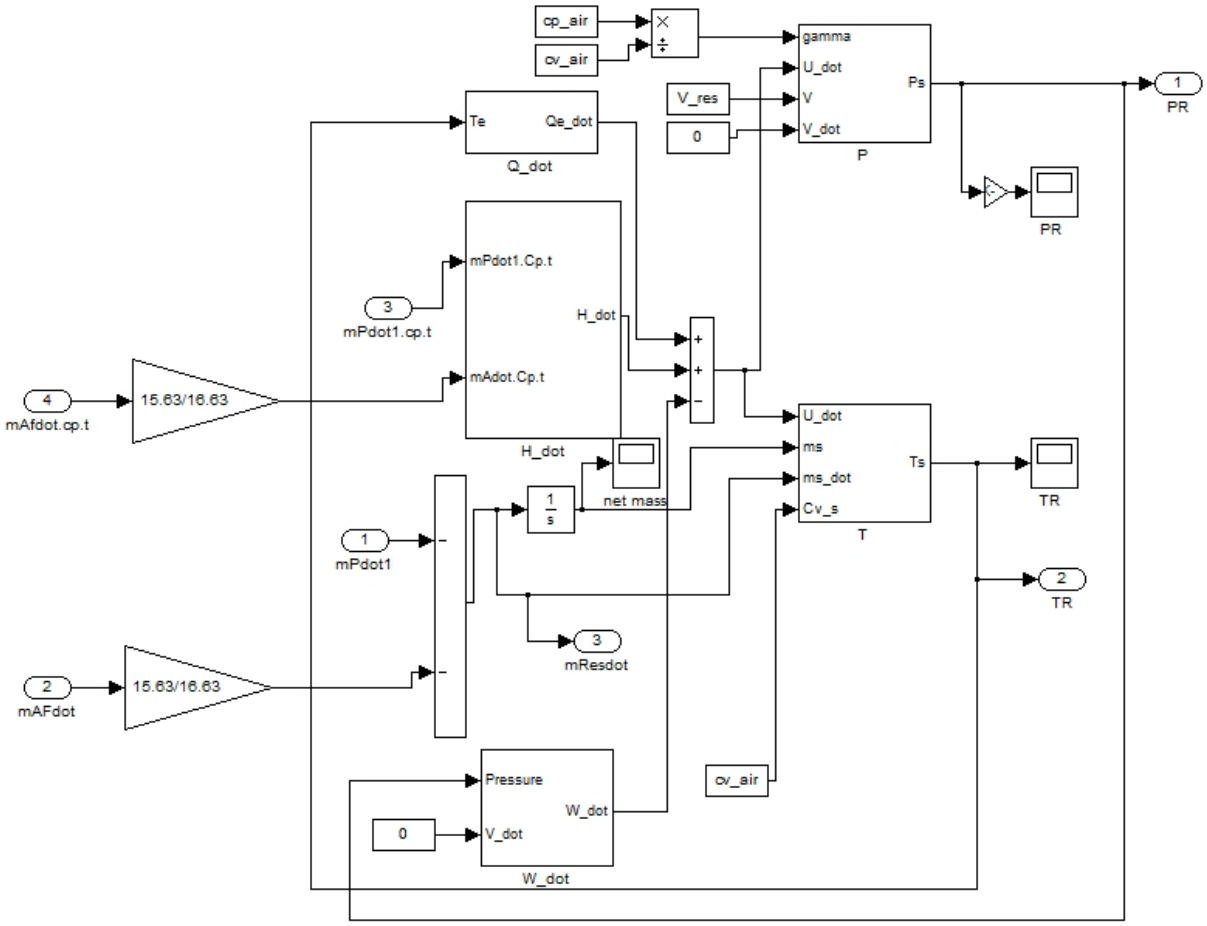

Figure A-1-3: Reservoir Chamber Block

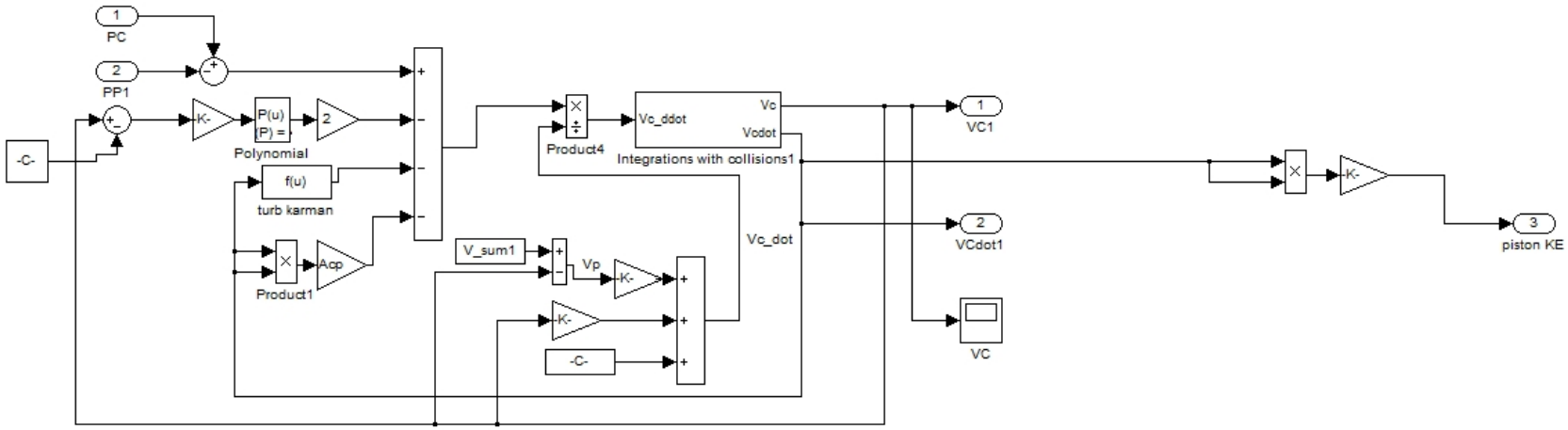

Figure A-1-4: Piston Dynamics Block

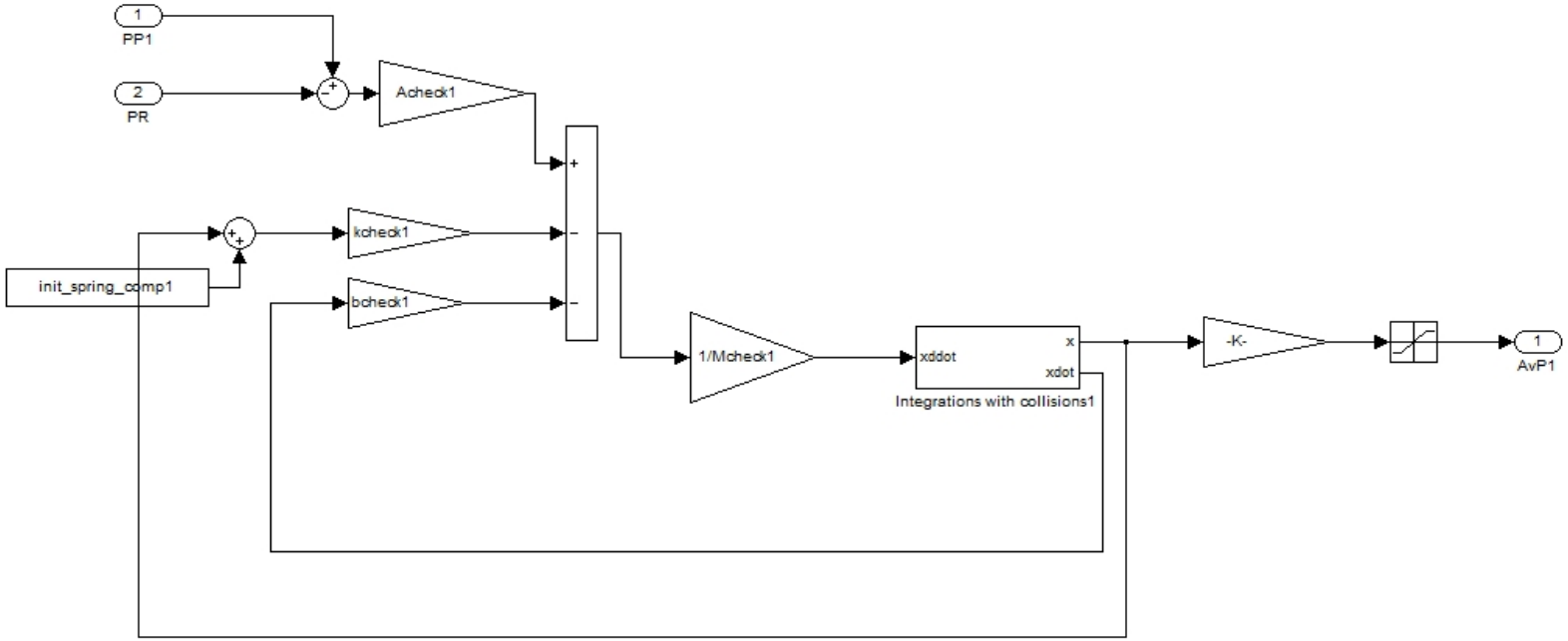

Figure A-1-5: Check Valve Dynamics Block

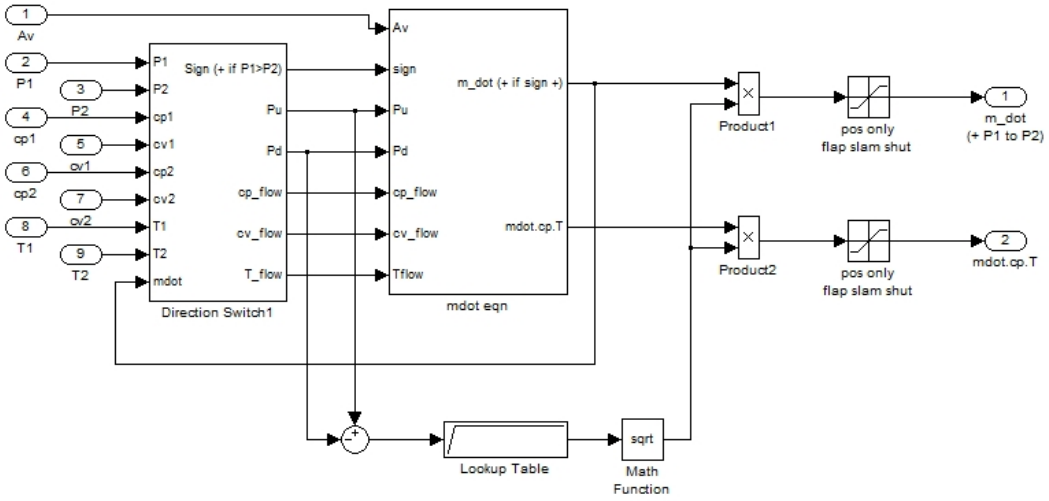

Figure A-1-6: mAFdot Block

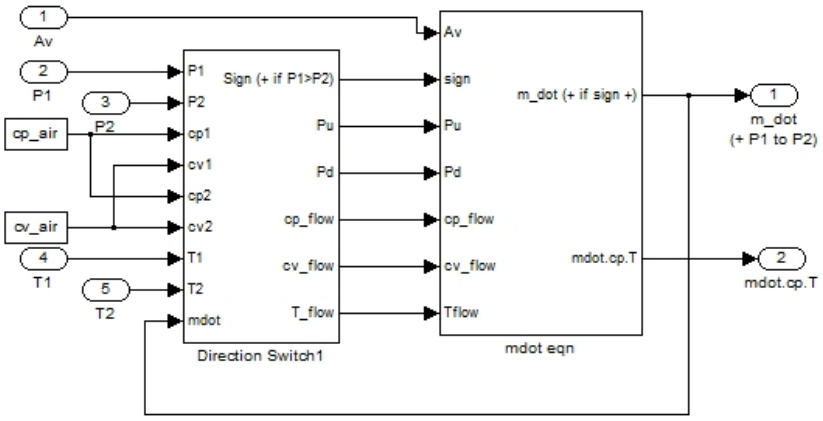

Figure A-1-7: mINdot Block

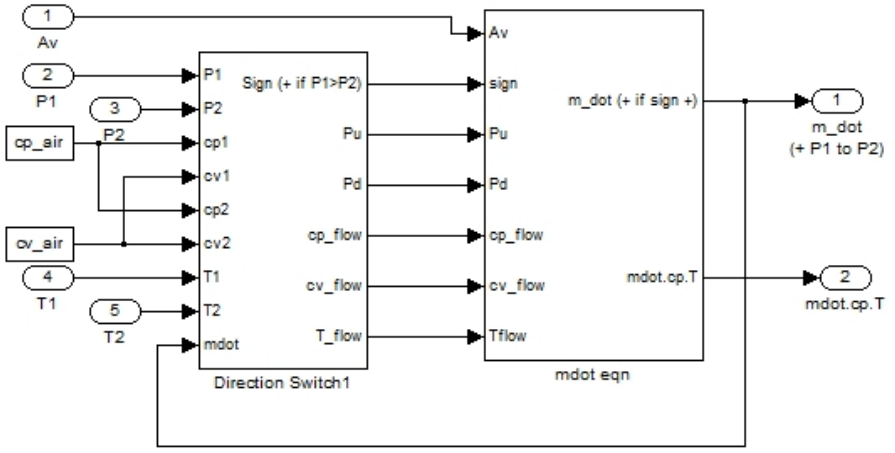

Figure A-1-8: mPdot Block

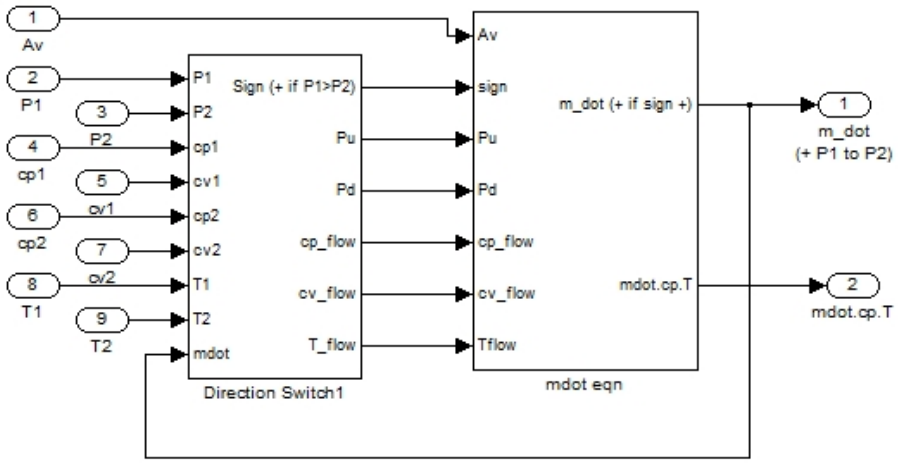

Figure A-1-9: mXdot Block

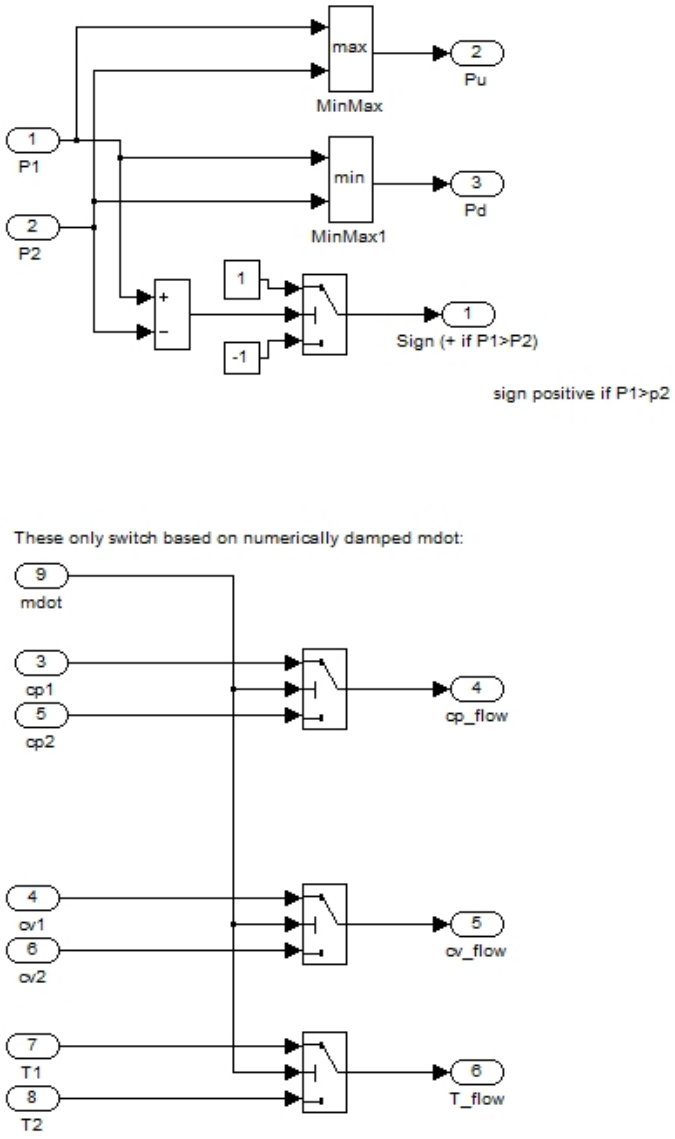

Figure A-1-9-1: Example of direction Switch Block

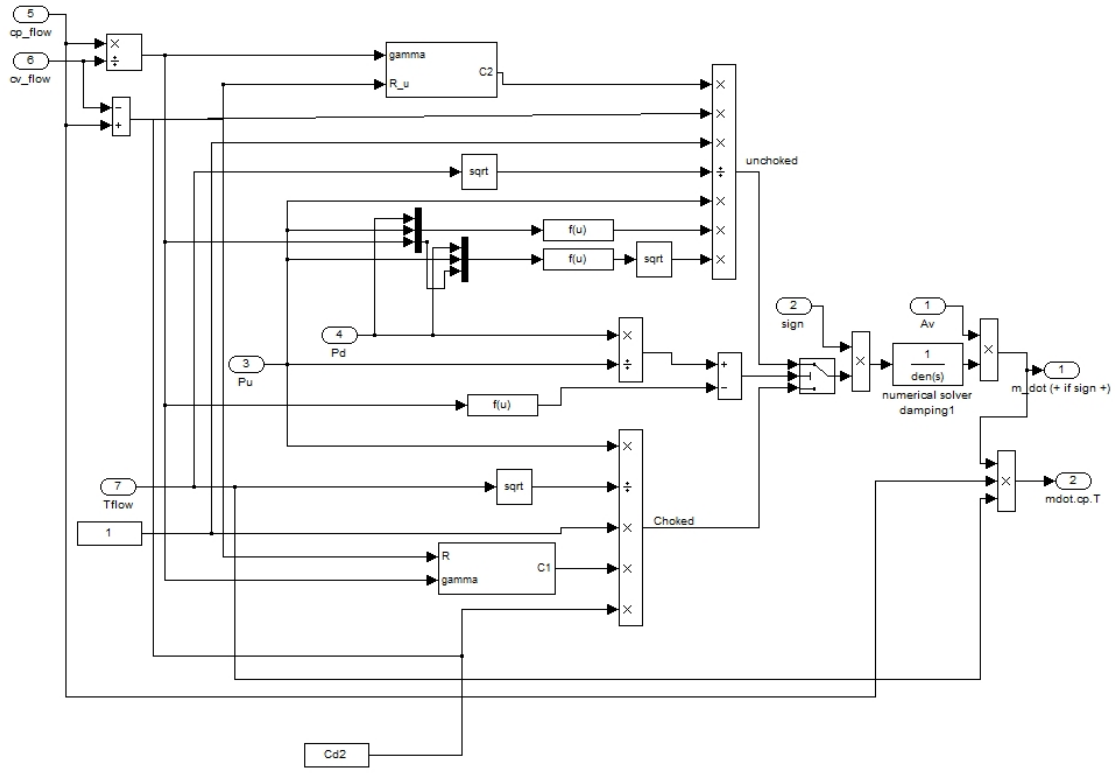

Figure A-1-9-2: Example of mdot eqn Block

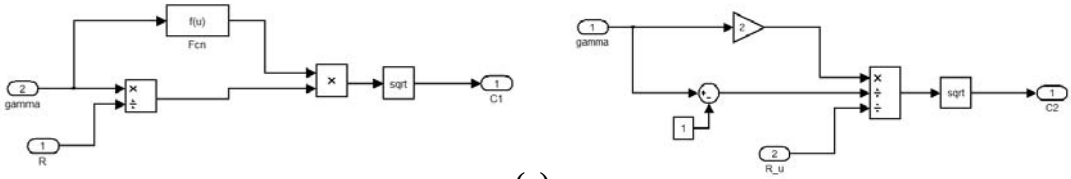

(a) (b)

Figure A-1-9-2-1: Examples of (a) C1 block and (b) C2 block

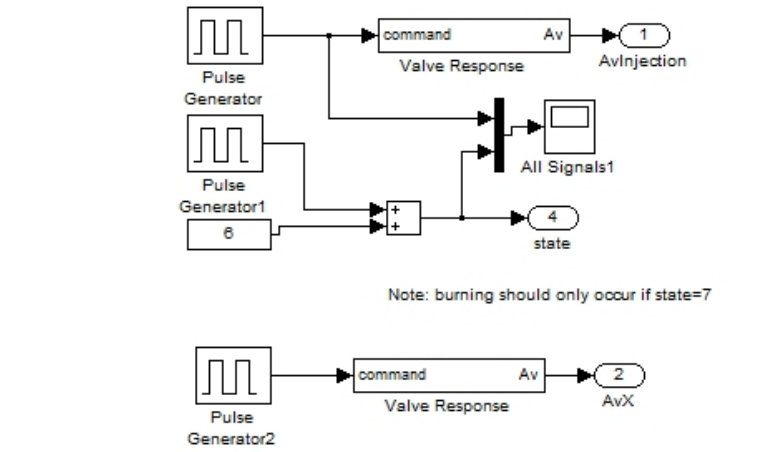

Figure A-1-10: Controller Block

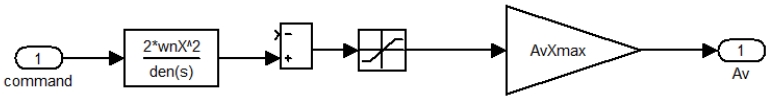

Figure A-1-10-1: Example of Valve Response Block

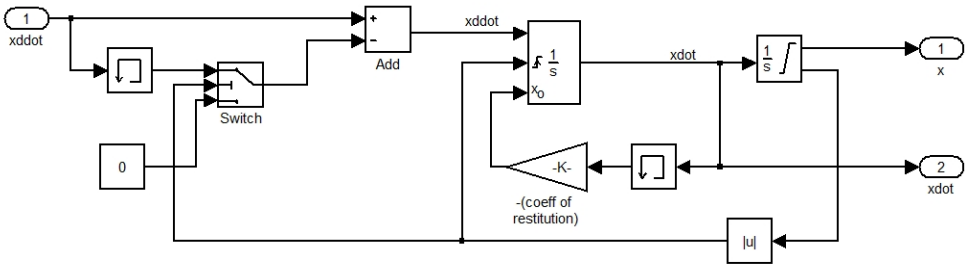

Figure A-1-5-1: Example of Integrations with collisions Block

APPENDIX B

MATLAB CODE

B-1. Matlab Code For HIFLPC Dynamic Model Simulation

```
%% Base Units:
%mm, kg, s, mN, kPa, microJ (uJ), microW (uW), K


%% General Thermodynamic Constants

P_atm=101.353; %Atmospheric pressure (in kPa)
T_amb=297; %Ambient temperature (in K)
T_aft=2250; %Adiabatic Flame Temperature (in K)
R_univ=8.3145*1e6; %Average gas constant (in uJ/mol/K)
cp_air=1012*1e6; %constant pressure specific heat (in uJ/kg/K)
cv_air=723.7*1e6; %constant volume specific heat (in uJ/kg/K)
R_air=cp_air-cv_air; %gas constant (in uJ/kg/K)
gamma_air=cp_air/cv_air; %ratio of specific heats (no dim)
Cr_air=(2/(gamma_air+1))^(gamma_air/(gamma_air-1)); % Condition for choked
                                                    % or unchoked flow

%% Piston parameters

%%properties of H2O @30deg Celsius
rho_h2o=996/1000^3;  %%density, kg/mm^3
mu_h2o=.799e-3*1000/1000^2;  %%viscosity, (mN*s)/m^2
nu_h2o=.802e-6*1000^2;  %%kinematic viscosity, m^2/s


d1=2*2.54*10;  %%diameter of comb chambers mm
A1=pi*d1^2/4;     %%area of comb chambers mm^2
d2=.75*2.54*10;  %% diameter of high inertance piston mm (0.8 is optimum for 70" length)
A2=pi*d2^2/4;     %%area of high inertance piston mm^2
L=72*2.54*10;    %%length of high inertance piston mm
d3=d1;  %%diameter of pump chamber mm
A3=pi*d3^2/4;     %%area of pump chamber mm^2
bumps=0.0015*1000;  %height of irregularities in pipe in mm
f=.15;
Acp=rho_h2o/2*((1/A3^2)-(1/A1^2));
stiffness_coeff=1;


coeff_restitution1=0.0001; % coefficient of restitution for piston collisions
coeff_restitution2=0.0001; % coefficient of restitution for piston collisions

%% Gas Properties of Combustion Products


cp_prod=cp_air; %constant pressure specific heat (in uJ/kg/K)
cv_prod=cv_air; %constant volume specific heat (in uJ/kg/K)
R_prod=R_air; %gas constant (in uJ/kg/K)
gamma_prod=gamma_air; %ratio of specific heats (no dim)


%% Combustion Chamber

e=.62*46350000/16.63*1e6; %mass energy constant of propane/air mixture (in uJ/kg)
VC1_min=6*1000; %mm^3 TUNED
VC01=6*1000; %mm^3 TUNED
com_K = 2600; %constant for Arrehnius Law
com_Ea = 2.75; %Ea for Arrehnius Law (kJ to uJ)
zeta_comb = 1; % because dynamics are nonlinear, this may need to be >1 to get no
oscillation. Compare "Q to release" with Total heat release inside combustion heat
release block
wn_comb=2*pi/0.0006; % speed of combustion

PC0=P_atm; %initial combustion Pressure (in kPa)
TC0=T_amb; %initial combustion temperature (in K)
```

```
HT_coeff_C=0*1e5;
RC0=R_prod; %initial gas constant(in uJ/kg/K)
mC0=PC0*VC01/(RC0*TC0); %initial mass of gases(in kg)


%% Initial Conditions in Pump Chamber

PP01=P_atm; %initial pressure (in kPa)
TP01=T_amb; %initial temperature (in K)
VP1_min=20; %much smaller than VC1_min, allows for chk valve and senseor dead vol
VP01=4/6*pi*(25.4)^3+(pi*25.4^2*9.7)-.8*VC01; %initial volume LARGER CHAMBER(in mm^3)
mP01=PP01*VP01/(R_air*TP01); %initial mass of air (in kg)


V_sum1=5.5e4; % 0.5*VC+VP1 (in mm^3)


%% Initial Conditions in reservior

PR0=(70+14.7)*6.895; %Pressure in reservoir (in kPa) (from psia)
V_res = 517000; %Volume of the reservoir (in mm^3)
TR0=T_amb; %initial temperature (in K)
mR0=PR0*V_res/(R_air*TR0); %initial mass of air (in kg)
HT_coeff_Res = 200*1e6; % heat transfer coeff in reservior Proportional to temperature
difference(matched to data);

%% Check Valve dynamics
Acheck1= pi*(0.4375*25.4/2)^2; % check valve piston area (mm^2)
AvPmax1= 6*pi*(4.85/2)^2; % max flow orifice area of check valve (mm^2)
Mcheck1= 18.4/1000; %kg
kcheck1= 4*165/1000*9.81/(11.1/1000); %mN/mm = N/m
zetacheck1=0.05;
bcheck1=sqrt(4*zetacheck1^2*kcheck1*Mcheck1); %effective viscous friction (in mN*s/mm);
init_spring_comp1= 6.5; % mm
max_travel_check1= 5.9; % mm
check1_restitution=0.0001 ;

%% Clippard Valve parameters

AvXmax=1*pi*((14-4)/2)^2; % mushroom valve minus stem in mm^2
AvINmax=24*pi*(0.048*25.4/2)^2; % in mm^2
AvBFmax=10*pi*(0.025*25.4/2)^2; % in mm^2
AvAFmax=2*pi*(0.06*25.4/2)^2; % in mm^2
Cd2=0.5; %discharge coefficient (no dim)
mdot_tao = 1e-5; % 1/(tao*s+1) for mdot damping (numerical solver issues);


%% Controller parameters

wnX=(1/0.015)*2*pi; % exhaust valve dynamic response
wnIN=(1/0.015)*2*pi; % inlet valve dynamic response
wnBF=(1/0.015)*2*pi; % backfill valve dynamic response
wnAF=(1/0.008)*2*pi; % A/F valve dynamic response

T_inj=0.0195; % A/F injection command duration TUNED
T_delay=0.002; % delay time to wait for A/F valve to close
T_X=0.2; % quench/exhuast command duration
T_X_delay=0.031; % delay time to wait for exhaust valve
inj_delay=0.000;
```

APPENDIX C

REAL-TIME WORKSHOP DIAGRAMS

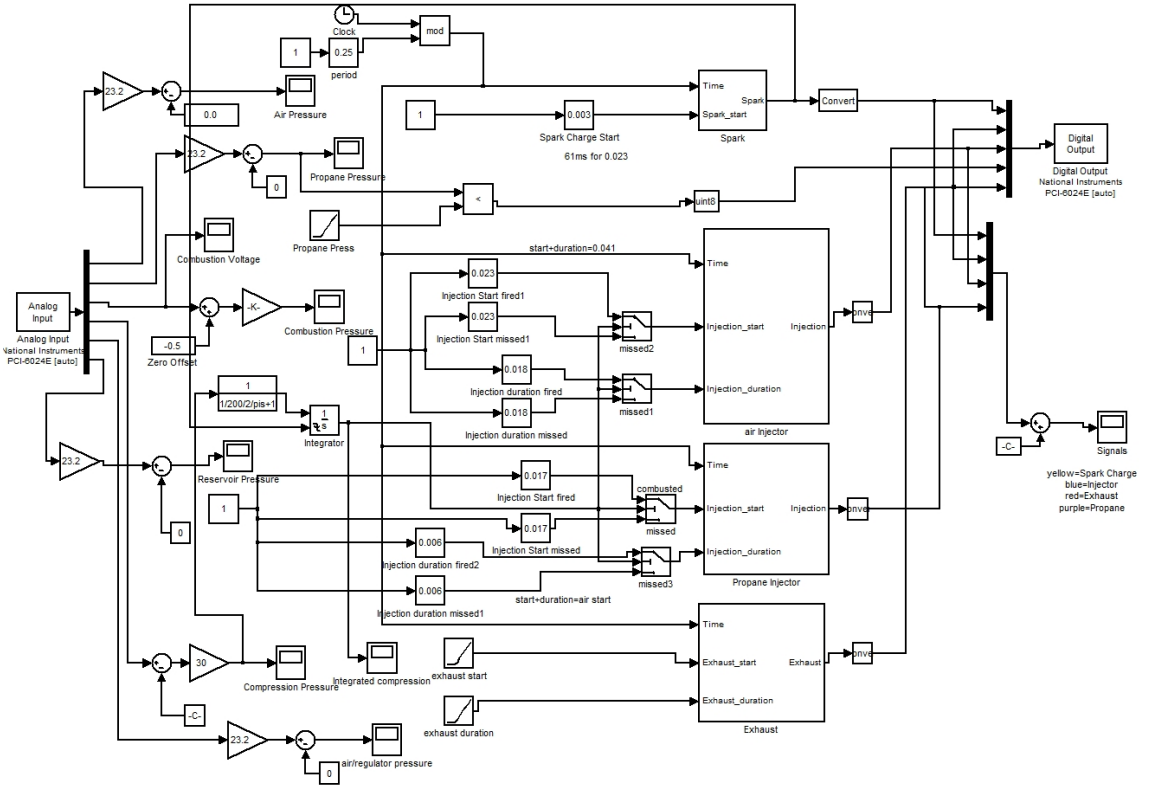

Figure C-1: Real Time Workshop Control Block

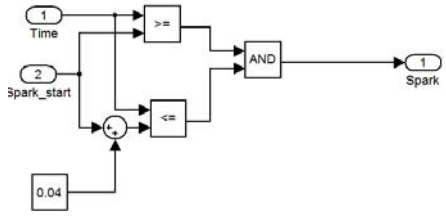

Figure C-1-1: Spark Block

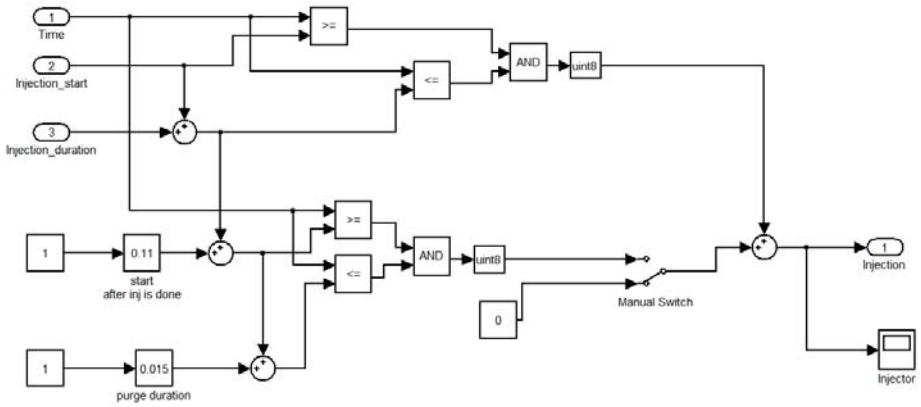

Figure C-1-2: Air Injector Block

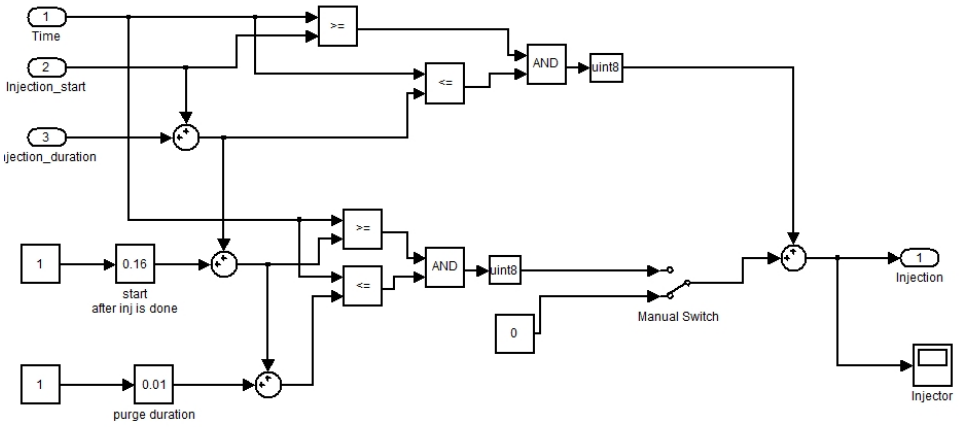

Figure C-1-3: Propane Injector Block

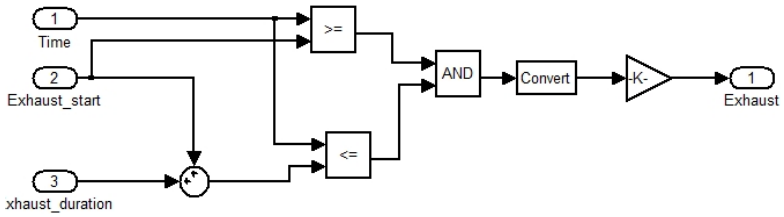

Figure C-1-4: Exhaust Block